



**NTNU – Trondheim**  
Norwegian University of  
Science and Technology

# An Experimental Study on the Application of Fish Oil as Fuel

**Bjørn Mikkel Rygh**

Marine Technology

Submission date: June 2015

Supervisor: Eilif Pedersen, IMT

Co-supervisor: Maximilian Malin, MARINTEK

Norwegian University of Science and Technology  
Department of Marine Technology





**MASTER THESIS IN MARINE MACHINERY**

**SPRING 2015**

**FOR**

**STUD. TECH. BJØRN MIKKEL RYGH**

**TITLE OF THESIS: An Experimental Study on the Application of Fish Oil as Fuel**

**Work description**

*As the earth's population and peoples standard of living increases, the global society is faced with an increasing energy demand. Fossil fuels have been a reliable source of energy in the past and will continue to be so in the future, but fossil energy sources are finite and new energy sources must be investigated to ensure energy security in the future.*

*It is therefore of great interest to study alternative fuels, and biofuels have shown to be a promising alternative. Biofuels have similar properties and energy content as fossil fuels and this makes them applicable in existing engine technology. These biologically derived fuels has the advantage of being produced from organic material and are hence renewable. Biofuels are also carbon neutral and their use will prevent further build-up of carbon dioxide in the atmosphere.*

*This master thesis will investigate the injection and combustion characteristics of two fish based bio oils and their blends with MGO. The results will be compared with pure MGO to see if fish oil is a possible alternative to the conventional marine fuels used today.*

**Scope of work:**

1. Assist in the work of assembling the combustion rig
2. Carry out a literature review on biofuels and earlier research done on biofuel testing.
  - Give an introduction on the topic of renewable energy and biofuels
  - Describe relevant fuel-, spray- and combustion characteristics
  - Describe research equipment and test methods
3. Perform fuel testing in the combustion rig
  - Test fuels according to fuel matrix and test procedure
  - Perform non-reactive and reactive tests
  - Perform test using different imaging techniques
4. Analyze the results
  - Analyze images to obtain penetration length, cone angle and lift-off length
  - Use radiation intensity to qualitatively investigate soot formation
  - Use pressure data to investigate rate of heat release and ignition delay
  - Present statistical evaluation of the data

The report shall be written in English and edited as a research report including literature survey, introduction to biofuels, test procedures, test results, discussion and conclusion including a proposal for further work.



It is supposed that Department of Marine Technology, NTNU, can use the results freely in its research work by referring to the students work.

The thesis should be submitted within 10.06.2015

Advisor: Associate Professor Eilif Pedersen

Co-advisor: PhD Candidate Maximilian Malin

Department of Marine Technology, 2015-02-10

---

Eilif Pedersen  
Associate Professor

# Preface

This master thesis is written in the spring semester of 2015 and represents the work of a full semester. It is written in its entirety by me and is my final proof of competency for the master's degree in Marine Technology at the Norwegian University of Science and Technology, NTNU. The thesis is an integrated part of my specialization in Marine Machinery and I would like to thank my academic supervisor, Associate Professor Eilif Pedersen, for providing helpful guidance and support.

Conducting the research and writing this report has been a very challenging and educational process and I have encountered many obstacles along the way. These obstacles has been solved in cooperation with several people and industry partners and I would also like to thank:

Maximilin Malin, PhD Candidate and co-supervisor, for motivation and daily supervision. I really appreciate all the help and your keen interest for my work as well as being a person to consult at all times.

Vladimir Krivopolianskii, Researcher at Marintek Sintef, for help with preparing the test bed and running experiments. Also thanks for the help with learning the Matlab analysis tool. Your earlier experience with similar research has been valuable.

Vilmar Æsøy, Associate Professor at Aalesund University College, for valuable ideas in preparing test procedures and discussion of results. Also thanks for the help with acquiring the fatty acid ethyl ester and the analysis of chemical composition of the fuels.

Per Magne Einang, Research Director at Marintek Sintef, for giving me an office at Marintek Sintef. The close proximity to the combustion rig has saved me a lot of time and the access to the knowledge hub of Marintek Sintef employees has proved valuable.

Roger Røstad, Head of Processing at ScanBio, for providing the crude fish oil as well as giving me a tour of their processing plant. This was informative and interesting.

L'Orange, for providing the single hole injection nozzle used in this study.

Last but not least, I would like to thank my family for moral support throughout the whole course of my education.

Trondheim, June 2015

*Bjørn Mikkel Rygh*

Bjørn Mikkel Rygh





# Summary

Two fish based bio oils in blends with MGO (Marine Gas Oil) have been tested in a constant volume combustion chamber (CVCC). The CVCC has optical access and a high-speed camera has captured images of the spray formation. These images have been analysed and penetration length, cone angle, lift-off length and combustion intensity has been determined. The intensity has been used for qualitative determination of soot formation. Pressure data has been recorded and used for analysis of heat release and ignition delay. Both combusting and non-combusting sprays have been analysed and the fuel has been injected at three injection pressures; 800 bar, 100 bar and 1400 bar. For each fuel, eight injections have been done at each test point and three different images techniques have been used to capture images. The results have been compared to the results of tests with pure MGO and the goal has been to find out if these bio oils can be used as an alternative to MGO in the future.

The two fish oils that have been tested are Fatty Acid Ethyl Ester (FAEE) and Crude Fish Oil (CFO). They have different depth of processing and significant differences in kinematic viscosity. FAEE has been transesterified and resembles MGO in fuel characteristics, whilst CFO is a viscous liquid and is currently being used as a dietary supplement for animals. FAEE has been tested in blends of 93% MGO/7% FAEE and 50/50% as well as pure. Due to the high viscosity of CFO, this oil has only been tested in 93% MGO/7% CFO and 50/50% blends. All fuel blends are by volume.

Both bio oils are oxygenated, and based on the results of this study, this has a positive effect on combustion efficiency. The combustion intensity, and hence the soot formation, is shown to decrease with increasing bio oil blend ratio. Especially for pure FAEE, the reduction was significant. Ignition delay is shown to be unaffected by blend ratio, but the results show a decreasing relation with increasing injection pressures. This is believed to be because of the increasing injection velocity and spray jet turbulence with corresponding better atomization at higher injection pressures.

The spray characteristics show a dependence on fuel viscosity and the results for FAEE show that increasing FAEE blend ratio causes longer spray penetration and narrower cone angles. This is as expected due to that higher viscosity causes a bigger pressure drop over the injector. This pressure drop affects the atomization process and results in larger fuel droplets with increasing viscosity. Bigger fuel droplets has a higher momentum, which is an important factor in spray development. The lift-off length is increasing with increasing viscosity for the same reason. Worse atomization causes worse air/fuel mixing and the fuel penetrates longer before an ignitable mixture is obtained. For the CFO blends, these spray characteristic relations are not as prominent and the results are more ambiguous and unclear. The reason for this is not evident and further studies has to be conducted.





# Sammendrag

To fiskebaserte bio-oljer har blitt innblandet i MGO (Marine Gas Oil) og testet i et konstant volum forbrenningskammer. Dette forbrenningskammeret har optisk tilgang og et høyhastighetskamera har fanget bilder av sprayformasjonen. Disse bildene har blitt analysert og penetrasjonslengde, spray vinkel, lift-off lengde og forbrenningsintensitet har blitt bestemt. Forbrenningsintensiteten har blitt brukt til kvalitativ bestemmelse av sot dannelse. Trykkdata fra forbrenningsprosessen har blitt registrert og brukt i analyser av varmeavgivelse og tenningsforsinkelse. Både reaktive og ikke-reaktive injeksjoner har blitt analysert og brenslene har blitt injisert ved tre ulike injeksjonstrykk; 800 bar, 1000 bar og 1400 bar. For hvert brensel har åtte injeksjoner blitt utført på hvert målepunkt og tre forskjellige bildeteknikker har blitt brukt til å visualisere injiseringsforløpet. Resultatene fra brenselblandningene har blitt sammenlignet med resultatene fra tilsvarende forsøk med ren MGO, og målet har vært å finne ut om disse bio-oljene kan brukes som et alternativ til MGO i fremtiden.

De to fiskeoljene som er testet er Fatty Acid Ethyl Ester (FAEE) og Crude Fish Oil (CFO). De har forskjellig grad av prosessering og stor forskjell i kinematisk viskositet. FAEE har blitt transesterifisert og har lignende drivstoffegenskaper som MGO, mens CFO er en viskøs væske. FAEE har blitt testet i blandinger av 93% MGO/7% FAEE og 50/50%, samt ren. På grunn av den høye viskositet til CFO, har denne oljen bare blitt testet i blandinger av 93% MGO/7% CFO og 50/50%. Alle drivstoffblandinger er basert på volumprosent.

Begge bio-oljene har oksygen bundet i molekylstrukturen, og basert på resultatene av denne studien har dette en positiv effekt på forbrenningsprosessen. Resultatene viser at forbrenningsintensiteten, og dermed sot dannelsen, avtar med økende bio-olje innblanding. Spesielt for ren FAEE var reduksjonen betydelig. Tenningsforsinkelsen virker å være upåvirket av blandingsforhold, men resultatene viser en avtagende trend med økende innsprøytningsstrykk. Dette er antatt å være på grunn av en bedre forstøvningseffekt ved høyere innsprøytningsstrykk på grunn av høyere injeksjonshastighet og større grad av turbulens under spray formasjonen.

Resultatene viser at spray karakteristikkene er avhengige av brenselets viskositet og resultatene for FAEE viser at økende mengde FAEE i blandingen forårsaker lenger spray penetrasjon og smalere spray vinkler. Dette er som forventet på grunn av at den høyere viskositeten fører til et større trykkfall over injektoren. Dette trykkfallet påvirker forstøvningsprosessen og resulterer i at høyere viskositet gir større dråper. Større brensel-dråper har et høyere bevegelsesmoment, som er en viktig faktor i spray formasjonen. Lift-off lengden øker med økende viskositet av samme grunn. Dårligere forstøvning forårsaker dårligere luft/brensel-blanding og brenselet trenger lengre inn i forbrenningskammeret før en antenbar blanding oppnås. Disse relasjonene i spray egenskaper er ikke så fremtredende for CFO blandningene der resultatene er mer tvetydige og uklare. Grunnen til dette er ikke innlysende, og videre studier må utføres.



# Contents

<b>Preface .....</b>	<b>iii</b>
<b>Summary .....</b>	<b>v</b>
<b>Sammendrag .....</b>	<b>vii</b>
<b>List of Figures.....</b>	<b>xii</b>
<b>List of Tables.....</b>	<b>xiii</b>
<b>List of Abbreviations .....</b>	<b>xiv</b>
<b>List of Symbols.....</b>	<b>xv</b>
<b>1. Introduction.....</b>	<b>1</b>
1.1 Background .....	1
1.1.1 CVCC Improvements.....	3
1.2 Structure of the Thesis .....	3
1.3 Motivation .....	4
<b>2. Alternative Energy and Biofuels.....</b>	<b>5</b>
2.1 Why Alternative Fuels.....	6
2.1.1 Environmental Concern.....	6
2.1.2 Depleting Fossil Resources .....	9
2.1.3 Energy Independence and Energy Security.....	9
2.2 Biofuels .....	10
2.2.1 1 <sup>st</sup> Generation.....	11
2.2.2 2 <sup>nd</sup> Generation .....	11
2.2.3 3 <sup>rd</sup> Generation .....	12
2.2.4 4 <sup>th</sup> Generation .....	13
2.3 The Biofuel Situation .....	14
2.3.1 Politics .....	14
2.3.2 Production .....	15
2.3.3 Consumption .....	16
2.3.4 Current Issues.....	17
<b>3. Important Characteristics.....</b>	<b>21</b>
3.1 Fuel Characteristics.....	21
3.1.1 Density.....	21
3.1.2 Kinematic Viscosity.....	22

3.1.3	Heating Value .....	23
3.1.4	Cetane Number/Cetane Index .....	23
3.1.5	Oxidation Stability .....	24
3.1.6	Acid Value .....	26
3.2	Spray Characteristics .....	27
3.2.1	Penetration Length.....	28
3.2.2	Cone Angle .....	29
3.2.3	Lift-Off Length .....	30
3.3	Combustion Characteristics .....	31
3.3.1	Radiation Intensity and Soot Formation .....	31
3.3.2	Rate of Heat Release .....	32
3.3.3	Ignition Delay.....	33
<b>4.</b>	<b>The Research Equipment and the Fuels .....</b>	<b>35</b>
4.1	Constant Volume Combustion Chamber .....	35
4.1.1	Experimental Setup .....	35
4.1.2	Working Principle .....	37
4.1.3	Gas Mixing .....	38
4.1.4	Subsystems .....	39
4.1.5	Limitations .....	40
4.1.6	Imaging Techniques.....	41
4.2	The Fuels.....	45
4.2.1	Marine Gas Oil.....	46
4.2.2	Crude Fish Oil .....	47
4.2.3	Fatty Acid Ethyl Ester.....	48
4.2.4	Fuel Analysis .....	50
<b>5.</b>	<b>Test and Analysis Procedures .....</b>	<b>55</b>
5.1	Test Procedures .....	55
5.1.2	Cold Shot .....	55
5.1.3	Hot Shot.....	56
5.1.4	Boundary Conditions .....	56
5.2	Image Analysis .....	59

<b>6. Results and Discussion .....</b>	<b>61</b>
6.1 Spray Characteristics .....	62
6.1.1 Penetration Length and Cone Angle .....	62
6.1.2 Additional Considerations on Spray Penetration and Cone Angle .....	66
6.1.3 Lift-Off Length .....	68
6.2 Combustion Characteristics .....	71
6.2.1 Radiation Intensity and Soot Formation .....	71
6.2.2 Notes on the Thermodynamic Analysis.....	74
6.2.3 Rate of Heat Release .....	75
6.2.4 Ignition Delay.....	79
<b>7. Conclusion .....</b>	<b>81</b>
7.1 Conclusion .....	81
7.2 Concluding Remarks .....	82
7.3 Suggestions for Further Work .....	82
<b>References.....</b>	<b>83</b>
<b>Appendix.....</b>	<b>I</b>

# List of Figures

Figure 1: Once a bird nesting area. Cat Island five years after the Deepwater Horizon accident ...	7
Figure 2: Total Annual Anthropogenic GHG emissions 1970 - 2010.....	8
Figure 3: The Carbon Cycle.....	9
Figure 4: Food vs Fuel.....	12
Figure 5: Carbon Sequestration .....	13
Figure 6: World Biofuel production in million tonnes oil equivalents.....	15
Figure 7: World Biofuel production in million tonnes oil equivalents.....	15
Figure 8: World energy consumption in million tonnes oil equivalents.....	16
Figure 9: Definition of Spray Characteristics.....	27
Figure 10: Radiation Spectrum of Diesel Combustion .....	31
Figure 11: Experimental Setup .....	36
Figure 12: Schematic flow plan of the combustion rig .....	36
Figure 13: Combustion rig working principle .....	37
Figure 14: Gas Mixing Arrangement .....	38
Figure 15: Typical Load Condition Curve.....	40
Figure 16: Direct Imaging Setup .....	41
Figure 17: Direct Imaging Technique .....	42
Figure 18: Shadowgraph Setup .....	42
Figure 19: Shadowgraph Principle.....	43
Figure 20: Shadowgraph Imaging Technique.....	43
Figure 21: Schlieren Setup.....	43
Figure 22: Schlieren Imaging Technique .....	44
Figure 23: Crude oil distillation .....	46
Figure 24: Crude Fish Oil .....	47
Figure 25: Fatty Acid Ethyl Ester.....	48
Figure 26: Transesterification Process .....	49
Figure 27: Volume Injection Curve.....	57
Figure 28: Energy Injection Curve .....	58
Figure 29: Raw Image Cold Shot.....	60
Figure 30: Cold Shot Analysis Output.....	60
Figure 31: Raw Image Hot Shot.....	60
Figure 32: Hot Shot Analysis Output .....	60
Figure 33: Penetration Lengths for all fuels .....	62
Figure 34: Cone Angles for all fuels.....	63
Figure 35: Penetration Length [mm] at 1.333 ms .....	64
Figure 36: Averaged Cone Angles [deg] .....	64
Figure 37: Cone Angle for MGO at Different Injection Pressures.....	65
Figure 38: Penetration Length for MGO at Different Injection Pressures .....	65
Figure 39: Penetration Length Hotshots .....	66
Figure 40: Cone Angle Hotshot .....	67

Figure 41: Lift-Off Length for all Fuels.....	68
Figure 42: Image Series of Combusting Spray.....	68
Figure 43: Averaged Lift-Off Length [mm] .....	69
Figure 44: Lift-Off Length for MGO at Different Injection Pressures.....	70
Figure 45: Radiation Intensity for all Fuels.....	71
Figure 46: Averaged Intensity [-].....	72
Figure 47: Radiation Intensity for MGO at Different Injection Pressures.....	73
Figure 48: Rate of Heat Release and Cumulative Heat Release.....	75
Figure 49: Combustion Efficiency.....	76
Figure 50: Combustion Phasing MFB 50%.....	77
Figure 51: Combustion Duration MFB 90%.....	77
Figure 52: Rate of Heat Release for MGO at Different Injection Pressures.....	78
Figure 53: Ignition Delay MFB 5% .....	79

## List of Tables

Table 1: Global fuel consumption, volumes of various fuels.....	17
Table 2: Density requirements.....	22
Table 3: Viscosity Requirements .....	22
Table 4: Cetane Number Requirements.....	24
Table 5: The Gas Mixing Process .....	38
Table 6: Key Parameters of the Fuel System.....	39
Table 7: Camera Settings.....	39
Table 8: Fuel Matrix.....	45
Table 9: Fatty Acid Composition of the Fish oils .....	50
Table 10: Elemental Composition .....	51
Table 11: Fuel Characteristics MGO/FAEE .....	51
Table 12: Fuel Characteristics MGO/CFO.....	51
Table 13: Test Procedure.....	55
Table 14: Boundary Conditions .....	56
Table 15: Injector Opening Times [ $\mu$ s] .....	58

# List of Abbreviations

---

	<i>Description</i>
ACEA	European Automobile Manufacturer's Association
ASTM	American Society for Testing and Materials
B5	5% biodiesel and 95% petroleum diesel blend
B7	7% biodiesel and 93% petroleum diesel blend
B100	Pure biodiesel
BTL	Biomass to Liquid
CFO	Crude Fish Oil
CH <sub>4</sub>	Methane
CI	Compression Ignition
CO	Carbon Monoxide
CO <sub>2</sub>	Carbon Dioxide
CVCC	Constant Volume Combustion Chamber
ECA	Emission Controlled Area
EGR	Exhaust Gas Recirculation
FAEE	Fatty Acid Ethyl Ester
GHG	Greenhouse Gas
GWP	Global Warming Potential
HHV	Higher Heating Value
H <sub>2</sub> O	Water
IMO	International Maritime Organization
KOH	Potassium Hydroxide
LHV	Lower Heating Value
MARPOL	Marine Pollution
MENA	Middle East and North Africa
MFB	Mass Fraction Burned
MGO	Marine Gas Oil
NaOH	Sodium Hydroxide
NO <sub>x</sub>	Nitrogen Oxides
N <sub>2</sub>	Nitrogen
N <sub>2</sub> O	Nitrous Oxide
O <sub>2</sub>	Oxygen
RGB	Red Green Blue
ROHR	Rate of Heat Release
SO <sub>x</sub>	Sulphur Oxides
T10	Distillation Temperature at 10% Recovery
T50	Distillation Temperature at 50% Recovery
T90	Distillation Temperature at 90% Recovery
UN	United Nations

---



# List of Symbols

<i>Symbol</i>	<i>Unit</i>	<i>Description</i>
A	[-]	Nozzle Geometry Constant
E	[J]	Activation Energy
F	[-]	Ignition Delay Constant
N	[-]	Ignition Delay Constant
R	[J/K]	Universal Gas Constant
S	[mm]	Penetration Length
T	[K]	Temperature
U	[J]	Internal Energy
V	[m <sup>3</sup> ]	Volume
W	[J]	Work
Q	[J]	Heat
$c_p$	[J/mol K]	Specific Heat at Constant Pressure
$c_v$	[J/mol K]	Specific Heat at Constant Volume
$d_o$	[m]	Injection Orifice Diameter
$d_{sac}$	[m]	Sac Hole Diameter
$l$	[m]	Length of Nozzle Hole
$m$	[kg]	Mass
$p$	[Pa]	Pressure
$p_{ch}$	[Pa]	Chamber Pressure
$p_{inj}$	[Pa]	Injection Pressure
$t$	[s]	Time
$t_{break}$	[s]	Breakup Time
$t_{id}$	[ms]	Ignition Delay
$\gamma$	[-]	Ratio of Specific Heats
$\rho_{ch}$	[kg/m <sup>3</sup> ]	Chamber Density
$\rho_l$	[kg/m <sup>3</sup> ]	Liquid Density



# Chapter 1

## Introduction

### 1.1 Background

The focus of this master thesis is to investigate fish oils potential as fuel for compression ignition engines. Two fish based oils will be tested in a Constant Volume Combustion Chamber (CVCC), and spray and combustion characteristics will be compared to those of MGO (Marine Gas Oil). The CVCC has optical access and it is hence possible to capture images of the injection and combustion processes. These images together with acquired pressure data will be analysed to obtain information used for comparison.

A problem with biofuels in the past is that they have been in direct competition with food production and this has caused heated debates. The fish oils used in this study are hence chosen with this in mind. The first fish oil is a product produced from farmed fish that has died or been killed for other reasons than human consumption. Norwegian rules and regulations prohibits the use of these products for human consumption and its current application is as a dietary supplement for animals not intended as food, including pets and animals in the fur industry. This oil is termed Crude Fish Oil (CFO) and it is a dark brown viscous liquid with a distinct smell of fish.

The second fish oil is a by-product from the omega fatty acid extraction. This oil has been subject to deeper processing and is a transparent liquid with a slight fish odour and similar viscosity as MGO. When looking at the chemical composition of this oil it is defined as biodiesel, but it is not prepared according to any biodiesel fuel specification and it fails on some of the requirements. This oil has been transesterified, which is the most common process of producing biodiesel from fatty oils. In the transesterification process the triglycerides in the CFO is broken down to fatty acid alkyl esters, which is the chemical name of biodiesel. Depending on the alcohol used in the process one ends up with either fatty acid ethyl ester (FAEE) or fatty acid methyl ester (FAME). The latter is the most common, but FAEE has been tested in this study.

Based on these three fuels, six fuel blends will be tested and they will be compared on spray characteristics and combustion characteristics. The spray characteristics includes spray penetration, cone angle and lift-off length, whilst the combustion characteristics includes rate of heat release, ignition delay and combustion intensity. The combustion intensity will be used to qualitatively determine the soot formation. The fuels will be injected at three different injection pressures and three different imaging techniques will be used to obtain images of the spray formation. The images will be used to determine the spray characteristics as well as the combustion intensity, whilst the acquired pressure data will be used to determine the rate of heat release and the ignition delay.

This work builds upon earlier research done in the field of fish oil studies at MARINTEK.

1. Combustion and Emission Characteristics of Fish Oil Fuel in a Heavy-Duty Diesel Engine [1].

This study was conducted at MARINTEK in 2012. The purpose of the study was to compare engine performance and emission characteristics from a diesel engine under modes of propulsion and generator operation when running both on pure MGO, pure FAEE and their 50% blend by volume. The main objective was to see the behaviour of gaseous, soot and particle matter emissions when shifting from conventional MGO to fish oil under different marine operating cycles.

The study was done using a diesel engine and the focus was on engine performance and emission characteristics of the FAEE. It was concluded that, when taking into account differences in density and heating value, FAEE gives close to identical engine performance compared to MGO as well as strong improvements in emissions of carbon monoxide, unburned hydrocarbons and soot particles. Only slight differences in emissions of NO<sub>x</sub> and CO<sub>2</sub> was observed.

As the first study proved that FAEE works as a fuel and shows good emission characteristics, the second study was aimed at studying the ignition and combustion processes closer.

2. Biodiesel Testing in a Constant Volume Combustion Rig [2].

This study was conducted at MARINTEK in 2014 and the purpose was to study ignition and combustion properties in a constant volume combustion chamber with optical access. Pressure data was used to evaluate rate of heat release and a high-speed camera captured images of the combustion process. The images was then visually analysed and spray and combustion characteristics was compared. The fuels that was tested was pure MGO, FAEE and a 50% blend of FAEE and CFO.

The results obtained from this study did not provide satisfying stability and a conclusion could not be drawn.

This master thesis seeks to take over where the second study left off. With a slightly different approach, more fuel blends and an improved test bed, the goal is to obtain results that makes it possible to see trends with high enough stability that it will be possible to conclude on whether these fish based bio oils are applicable as fuel or not.

### 1.1.1 CVCC Improvements

After this second study, the combustion rig, the test procedure and the analysis method has been improved.

#### 1.1.1.1 Analysis Tool

An image analysis tool has been developed in Matlab. This tool reads the raw images of the injection and combustion processes and writes all spray characteristics to a Microsoft Excel spreadsheet. More information is found in section 5.2. It is expected that this will give a more consistent image evaluation than the visual evaluation used earlier.

#### 1.1.1.2 Filling Process

The gas filling process is now fitted with a PID controller. This means that the process of filling the combustion rig with the gas mixture for the pre-combustion has been automated. Based on an operator-controlled set point, the rig is filled with the desired pressure. Earlier this was manually controlled and the PID controller will most likely give more stable test conditions. See Chapter 4 for further information.

#### 1.1.1.3 Injection Nozzle

The last study used a multi-hole injection nozzle and this complicated the evaluation of the spray formation because the developed sprays intersected each other. For this study, L'Orange has provided us with a single-hole injection nozzle. This nozzle is made for research purpose and will make the spray detection easier and more accurate.

#### 1.1.1.4 Number of Injections

For this study, eight injections are done at each test point compared to three injections in the earlier study. The data will be averaged and the increased number of injections will create a more accurate result.

## 1.2 Structure of the Thesis

*Chapter 1* is meant to explain why this master thesis is written, give a brief introduction to the topic of the thesis and to put it in context with preceding studies done on the same topic.

*Chapter 2* briefly explains alternative energy and biofuels. This chapter has been included to give the thesis a broader perspective, to highlight the importance of studying alternative fuel sources and to give the reader a deeper understanding of the core mechanisms driving research in this field. Fuel, energy and engines are general topics and apply to every industry, but were it is found suiting, the information is presented from a marine perspective.

*Chapter 3* deals with important characteristics. Fuel-, spray- and combustion characteristics are explained, what they depend on and the reasons for differences between fossil fuels and biofuels are discussed. This chapter presents the theory behind, and serves as the fundament for understanding, the different characteristics which makes up the basis of comparison in this study.

*Chapter 4* describes the research equipment, the working principles and the optical imaging techniques used to obtain the raw data. The fuels are described in more detail and the results of the fuel analysis is presented.

*Chapter 5* aims to explain the test procedure, define aspects related to the test environment and describe the analysis methods used to obtain the results.

*Chapter 6* presents the results of the study and plots of spray behaviour are discussed.

*Chapter 7* contains the conclusion as well as some concluding remarks and suggestions to further work.

Throughout this thesis, some equations are presented to help explain different aspects or simply to show how to calculate different parameters. All symbols used are listed under the symbols section and by referring to this, a deeper understanding of the equations will be gained.

### 1.3 Motivation

The diesel engine has been the preferred prime mover of the merchant fleet since it gradually started replacing the coal firing steam engines in the 1920's. When looking at emissions per tonne cargo kilometre, maritime transportation is by far the most environmentally friendly way of transporting goods, but the merchant fleet is still a huge source of pollutants that are causing global warming and in general are harming our planet. Up until recent years, the maritime transportation sector has consumed cheap, low quality fuel and has not been subject to particularly strict emission regulations. The introduction of global caps on emissions of sulphur dioxides and nitrogen oxides forces the industry into using more processed, cleaner fuels and to adopt exhaust gas cleaning systems. Within the next 5 to 10 years, the maritime air emission regulations will require further reduction of air emissions and the industry will be needing more clean-burning fuel. When taking into account that the fuels derived from crude oil are finite and will run out within foreseeable future, it is inherent that new sources of energy are investigated.

The bio oils that will be tested in this study are fish based and hence renewable. They are also oxygenated and will allow for emission reduction by improving the combustion process. Renewable and emission reducing are key words that attracts attention in times of increasing environmental awareness, and research in the field of biologically derived fuels is important. An increasing understanding of these fuels will enable efficient utilization of their energy and allow for sustainable energy production in the future.

The fishing industry in Norway is strong and if sustainable production and application of fish oil as fuel is found possible this would open new business opportunities and benefit Norwegian industry.

# Chapter 2

## Alternative Energy and Biofuels

Fossil fuel has been the main energy source since the industrial revolution in the late 18<sup>th</sup> century. The manufacturing processes went from hand production to mechanised production using steam power. To produce steam, coal was burned to heat water. Coal seemed like the ideal power source with its easy access and seemingly inexhaustible supply. From the mid-19<sup>th</sup> century, technology allowed for the production of petroleum, and it quickly gained foothold as a new fossil energy source. Initially kerosene, which was used for lighting and heating, was the main petroleum product consumed, but as the processing technology advanced, more petroleum products entered the market. These petroleum products, with their high energy content, quickly became the main energy source powering machines and transportation, producing electricity, heating houses and providing hot water [3].

Energy demand is closely linked to economic growth. With more countries evolving from a developing to an industrialized country, the global energy demand is rapidly rising [4]. With economic growth comes higher standards of living and an increase in demand for personal transportation and transportation of goods. To meet this increasing demand for energy, more fuel must be burned.

In the later years, depleting fossil energy sources and increasing environmental concern has shifted the focus towards renewable energy sources, and huge amounts of money are spent to fund research and development of technology that can ensure power generation based on renewable energy sources in the future.

## 2.1 Why Alternative Fuels

There are many factors related to the interest in alternative fuels, but it is in particular two main drivers that are responsible for the global focus on a sustainable future using renewable energy [5].

- I. Environmental concerns and local requirements
- II. Availability and cost of fossil fuels and energy security

### 2.1.1 Environmental Concern

The International Maritime Organization (IMO) develops and maintains a framework of rules and regulations for the maritime industry. In the MARPOL Convention Annex VI, IMO outlines regulations for prevention of air pollution from ships. In particular, SO<sub>x</sub> and NO<sub>x</sub> emissions are a big issue due to their acidic properties causing acid rain. This in turn has a huge potential for harming the environment through acidification.

The amount of SO<sub>x</sub> emitted to the air is directly linked to the amount of sulphur in the fuel. Since biofuel is sulphur free, their use will completely remove SO<sub>x</sub> emissions. However, multiple studies have reported an increase in NO<sub>x</sub> emissions when using biofuels, but with no SO<sub>x</sub> in the exhaust, NO<sub>x</sub> can be removed through post-combustion exhaust treatment. Stricter rules and regulations related to exhaust emissions and the introduction of Emission Controlled Areas (ECA), with particular strict emission regulations, forces the maritime industry to consider more environmental friendly alternatives to the conventional maritime fuels used today.

Accidents happen from time to time and with the Deepwater Horizon blowout fresh in mind it is clear that the environmental effects of an oil spill is devastation. This accident is considered the largest accidental marine oil spill in the history of the petroleum industry and the Gulf of Mexico still suffers extensive damage to marine and wildlife habitats [6]. Biofuels have a much lower risk of causing the same devastating effects on the environment when spilled. This is due to that biofuels consist of biological molecules that, to a much larger extent, are biodegradable compared to fossil fuels. This means that naturally occurring bacteria and other organisms are able to use biofuel molecules as energy sources and break them down to harmless by-products. Although large concentrated spills of biofuels has the same potential of killing small animals and plants, they will not make the environment uninhabitable for long periods of time [7]. Figure 1 shows one example of the environmental damage caused by the accident. This island is still uninhabitable five years after the accident.





*Figure 1: Once a bird nesting area. Cat Island five years after the Deepwater Horizon accident [6]*

#### 2.1.1.1 The Greenhouse Effect and the Carbon Cycle

Maybe a bigger cause of environmental concern is the greenhouse effect caused by greenhouse gas (GHG) emissions. Greenhouse gases is the designation of gases that, by absorbing radiation within the thermal infrared range, traps heat in the atmosphere and is the fundamental cause of global warming. The most important anthropogenic greenhouse gases is carbon dioxide (CO<sub>2</sub>), methane (CH<sub>4</sub>), nitrous oxide (N<sub>2</sub>O) and fluorinated gases [9]. Figure 2 shows the total global anthropogenic emissions of greenhouse gases adjusted for global warming potential with a 100-year perspective, GWP<sub>100</sub>. These adjustments are made so that the emission data can be compared. Since the ability to absorb energy and the lifetime of the different gases in the atmosphere are different, they are all calculated into CO<sub>2</sub>-equivalants.

The CO<sub>2</sub> emissions from burning fossil fuel is the biggest contributor to GHG emissions and global warming. In 2013, the shipping industry accounted for around 3% of the CO<sub>2</sub> emissions with approximately 1 billion tonnes of CO<sub>2</sub> emitted to the atmosphere [11]. However, with today's energy demand and choice of fuel, these emissions are not easy to do anything about without increasing efficiency and lowering fuel consumption. The products of an ideal combustion is nitrogen, water and carbon dioxide and the amount of emitted CO<sub>2</sub> is directly linked to the amount of carbon in the fuel. It is therefore inevitable to emit CO<sub>2</sub> when using carbon-based fuels.

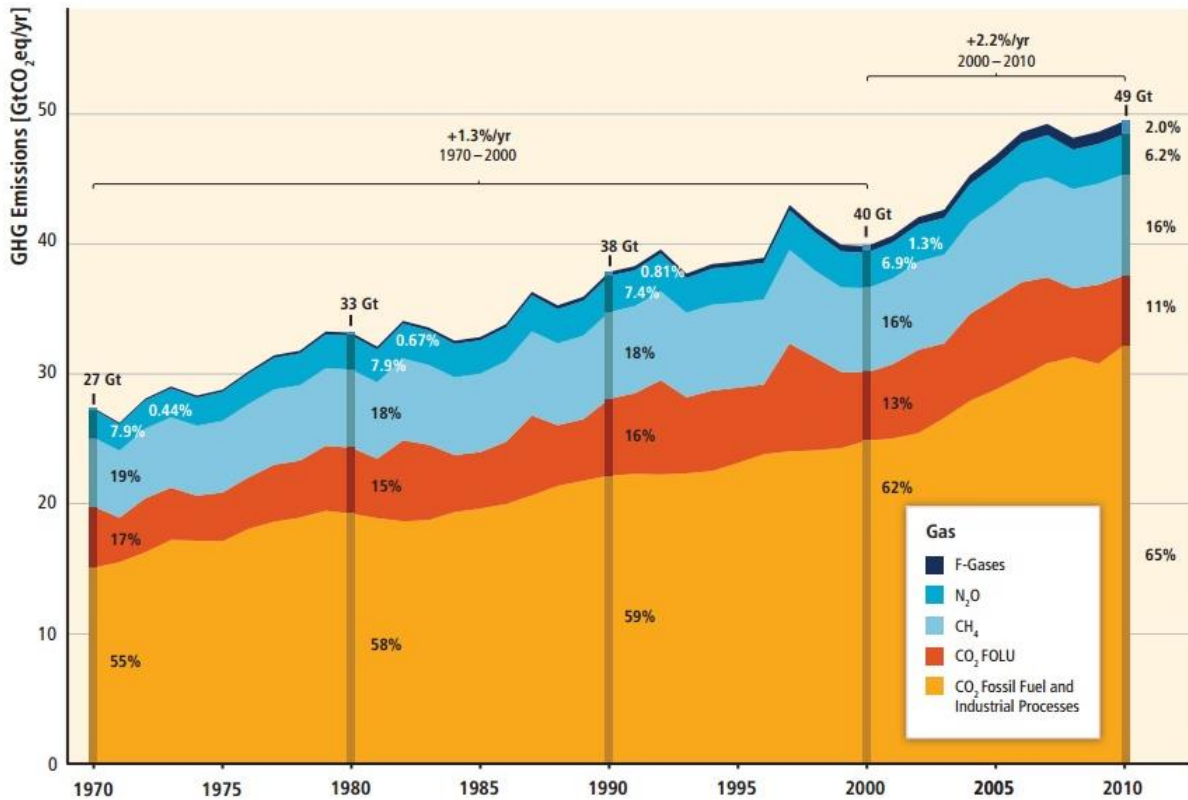


Figure 2: Total Annual Anthropogenic GHG emissions 1970 - 2010 [8]

The carbon that is bound in fossil fuels are considered part of the slow carbon cycle because it is essentially locked out, and not in contact with the atmosphere [12]. When fossil fuel is burned, the carbon is shifted to the fast carbon cycle and the emitted CO<sub>2</sub> is being added to the natural occurring CO<sub>2</sub>. When in addition large areas of forest are being cleared, the natural carbon cycle is not able to handle the extra amount of CO<sub>2</sub> and this leads to a build-up in the atmosphere.

There are many different types of alternative fuels; some are based on fossil energy sources and some on non-fossil energy sources. To prevent further build-up of CO<sub>2</sub> in the atmosphere without any measure of carbon sequestration, the energy source has to come from within the fast carbon cycle. This means to harvest the energy in non-fossil energy sources and produce biofuels from biomass. Through photosynthesis, plants take CO<sub>2</sub> out of the atmosphere, binds the carbon and emits the oxygen. As the plant grows, the carbon is used to produce biomass and when the plant is decomposing or burned, the carbon is again emitted to the atmosphere as CO<sub>2</sub>. This carbon cycle makes fuel from biomass carbon neutral, which means that no additional carbon is introduced to the environment [13]. Figure 3 shows a representation of the fast carbon cycle. The aspects involved are much more complex than outlined in this figure and its purpose is just to give a brief understanding of the basic principle.

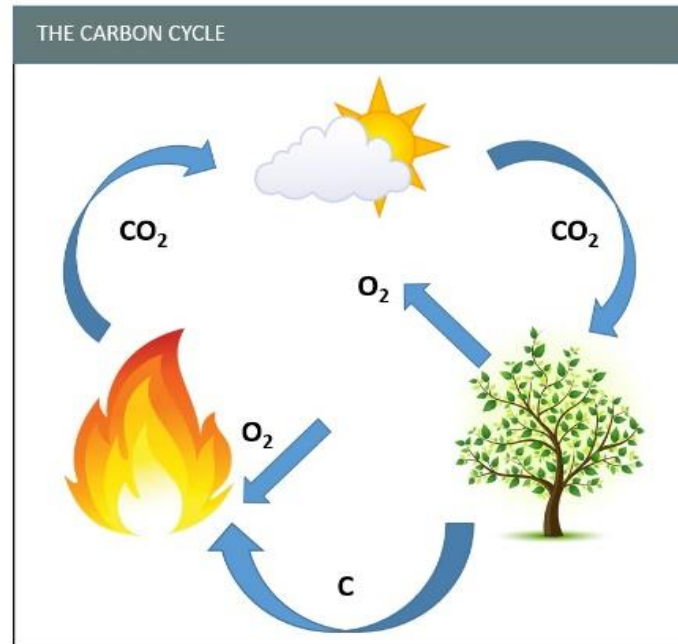


Figure 3: The Carbon Cycle

### 2.1.2 Depleting Fossil Resources

It is hard to tell how long the fossil energy sources will last. Better technology for petroleum recovery increases the exploitation rates and makes closed oil fields economically viable to reopen. This, together with new oil field discoveries makes it difficult to predict the actual lifetime of the oil industry, but one thing is certain; the fossil fuels are finite.

All the fossil fuel that is burned decreases the amount of fossil fuel that is left. Fossil fuel is not considered renewable since it takes millions of years to form, and hence, one day it will run out. Based on the current amount of proven reserves and the current production rate, it is estimated that the global supply of oil will run out in 53 years and the global supply of natural gas and coal will run out in 55 and 113 years respectively [14].

### 2.1.3 Energy Independence and Energy Security

Most countries in the world today are relying on import of petroleum products [15]. This dependency of foreign energy makes countries vulnerable to changes in the global petroleum export market. With local production of biofuels, the energy dependence can partially be reduced. It will however not be possible with today's technology and feedstocks to produce amounts even close to that needed to be energy independent, but most countries will be able to produce some amount of biofuel. This local production will stimulate domestic economy by supporting domestic industry, creating jobs and lowering import cost, which in turn will keep more money in the local market. [16].

Middle East and North Africa (MENA) accounts for 52% of the global oil reserves and 47% of the global natural gas reserves. Many of these countries are regarded as politically unstable

and historical precedents of oil disruptions from the region has been a cause of unstable oil prices in the past [17]. The importance of energy stability has been known for many decades, but the recent instability in MENA has brought the debate on energy stability back. The 2014 UN Climate Summit addressed the issue of dependency on fossil fuel and one of the action areas announced was sustainable energy with a shift in focus areas towards renewable energy sources [18]. *Sustainable Energy for All*, a global initiative led by the United Nations and the World Bank launched, during the conference, a new program called the Global Energy Efficiency Accelerator Platform. This program seeks to improve the global energy efficiency and promote renewable energy towards 2030 [19]. As this program has a global perspective with many industry-leading partners and supporters, its focus on renewable energy will ensure better energy security in the future.

## 2.2 Biofuels

Biofuels has been around in the form of wood since the first trees started growing, and liquid biofuels were exploited long before the first internal combustion engines were issued. The history is full of stories mentioning oil lamps as a source of light and an ancient oil lamp was in 1940 found in a cave that is believed to be inhabited 10 – 15 000 years ago. The first mass produced vehicle, the Ford model T, had an Otto cycle engine designed to run on ethanol [20] and when Dr. Rudolph Diesel in 1893 issued the compression ignition (CI) engine, it was his intention that the engine should be built so that it could be powered by vegetable oil. His vision was that farmers could make their own fuel in remote agricultural areas where petroleum products was inaccessible [21]. He did a lot of research on the topic but shortly after his death, a new class of petroleum fuel became available called *Diesel Fuel*. Diesel fuel and its high-energy content quickly became the fuel of choice and the design of the CI engine was changed to match the properties of the new fuel.

Due to the availability and the cost of diesel, vegetable oil was not given any attention except at some occasions during the 1920's when the shortage of oil pushed the prices up. Unfortunately, the new engine design could not run on vegetable oil due to the much higher viscosity. Many methods aimed at reducing the viscosity of vegetable oil, like blending with water and alcohol, was attempted without and great results. In 1937, a Belgian inventor claimed he had solved the viscosity problem. By using a process of breaking the oil molecules into smaller fatty acid alkyl esters, he managed to obtain a viscosity suitable for the new injection system. This method was called transesterification, and is the most common basis for all biodiesel production today [21]. More information regarding the transesterification process is found in section 4.2.3.1.

The definition of a biofuel is; *any fuel whose energy is obtained through a process of biological carbon fixation* [7]. Carbon fixation is a process that converts inorganic carbon to organic carbon compounds. This process can produce a variety of different organic compounds, but for it to become a biofuel, it must be possible to exploit the energy in the organic compound in a mechanical setting. In other words, biofuels are any hydrocarbon-based fuel that is produced from a living or once living material within a relative short timeframe. This stands in

contrast with fossil fuels, which takes millions of years to form. This definition also includes synthetic biofuels [7]. Synthetic fuels can be produced using the Fischer-Tropsch process that converts carbon monoxide and hydrogen into hydrocarbons. When using biomass as the feedstock the product will be synthetic biofuel and the process is called BTL – Biomass to Liquid.

Biofuel is based on renewable sources like, sugar, starch, animal fats and vegetable oil. There are different types of biofuels based on the process of production and type of source. The two main types of biofuel in production around the world today are ethanol and biodiesel. Ethanol is produced mainly through fermentation of sugars and starch, while biodiesel is mainly produced using transesterification, of animal fats and vegetable oils. Biofuels can be used in conventional engines in its pure form but blends with conventional fossil fuels are the most common. This is mainly due to that some properties of biofuel are not ideal for engine systems or the combustion process itself e.g. acidic level, cold weather operation and solvency properties, see section 2.3.4. Engine modifications must be made for long-term use of most pure biofuels [22]. As the knowledge and awareness on biofuels has improved over the years, different generations of biofuel has emerged.

### 2.2.1 1<sup>st</sup> Generation

The term first generation biofuels relates to biofuels produced directly from food crops. On a global scale, corn and wheat are the most widely used feedstock for producing ethanol, whilst biodiesel is produced mainly from soybean and rapeseeds [23]. The biomass source used is dependent upon what type of source that is available at different geographical locations. Some big issues with the first generation biofuels are that some biofuels produced this way can result in negative net energy gain. This means that they, during production, consumes more energy than what is available in the final product. Another big issue that got the world's attention was the *food vs fuel* debate illustrated by Figure 4. First generation biofuels are using organic materials, which can be used to feed an increasingly hungry world, to make fuel. As a result of the increasing demand for biofuel, a larger part of the feedstock are diverted to fuel production and this has been blamed for the rising food prices the latest years [24]. The problems associated with the first generation of biofuels gave rise to the next generation.

### 2.2.2 2<sup>nd</sup> Generation

To address the issues with the first generation, the process of producing second generation biofuels aims to make use of non-food crops as the main source of energy. Non-food crops implies wood, food waste, livestock feces and other types of biomass not suitable as food [23]. The aim for second generation biofuels is also to be more cost effective compared to fossil fuel. Even though prices are declining, technological challenges still hamper this cost effectiveness causing biofuels to be more expensive than conventional fossil fuels [25], [26]. Net energy gain is also something that is thought to be improved when the development of this industry is completed.



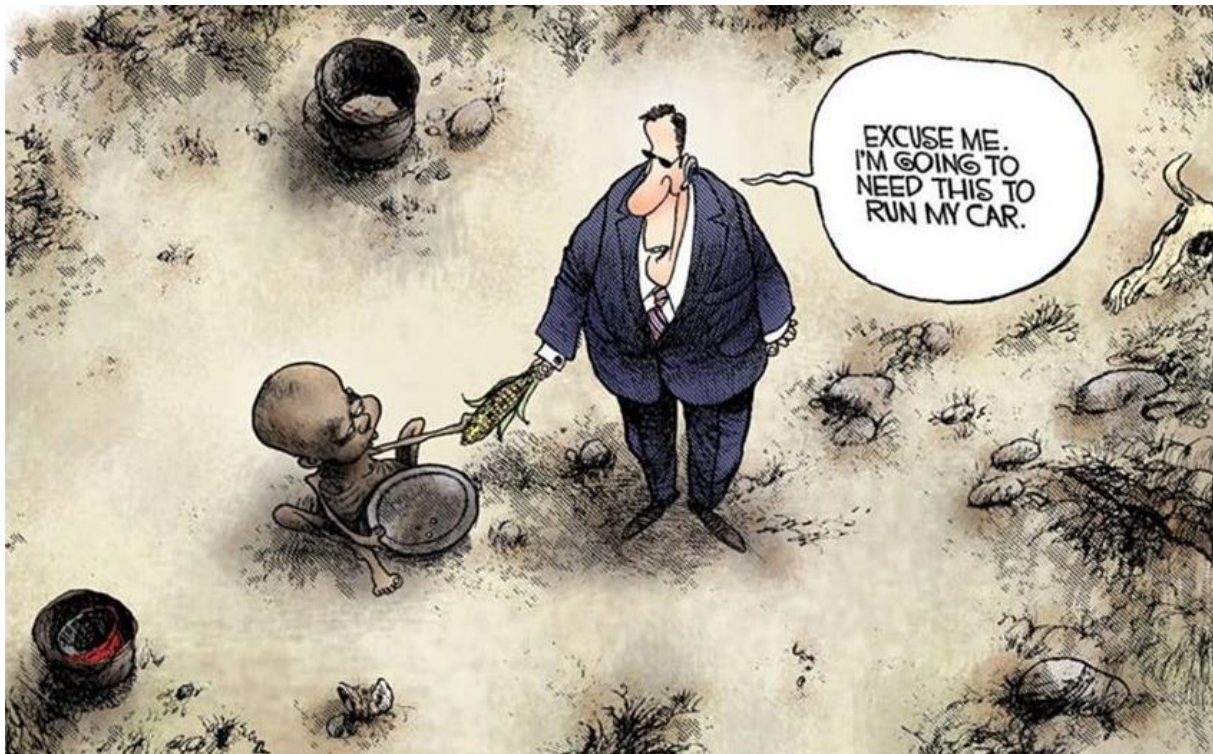


Figure 4: Food vs Fuel

### 2.2.3 3<sup>rd</sup> Generation

Before the second generation of biofuel production has been fully developed, a third generation of biofuels are being investigated. The third generation biofuels seek to make use of production areas not suitable or not needed for agricultural cultivation. This implies making use of the vast areas of oceans around the world. In particular, algae has been found to be a massive source of energy and can be grown in areas not competing with production of other food sources [24]. Algae does not need any freshwater, fertilizers or pesticides to grow and it grows faster than any plant on land. In addition, it contains up to 60-70% fermentable sugars and has a high oil yield [27]. In Norway, wild algae has been harvested for about 45 years and there is a worldwide market for algae products like, food, fertilizers and a range of products with pharmaceutical application. However, the algae utilization today is very low. With algae cultivation on an industrial scale, it is believed that this can significantly contribute to the world's supply of energy [27]. A study from Massey University, New Zealand concluded that to cultivate and produce biodiesel from microalgae is the only way to potentially completely displace liquid fuels derived from petroleum in the future [28]. In addition to biodiesel, algae can be used to manufacture a wide range of fuel including jet fuel and high-octane fuel for piston-engine aircrafts [24].

### 2.2.4 4<sup>th</sup> Generation

In the future, a fourth generation biofuels will take over. It aims to make use of the best parts of the previous generations, but where the previous generations seek carbon neutrality, the fourth generation aims to be carbon negative [24]. By capturing CO<sub>2</sub> at all stages of production using a process like oxy-fuel combustion, the CO<sub>2</sub> can be stored in closed oil and gas fields, saline aquifers or in discontinued mineshafts. This process is called carbon sequestration and Figure 5 shows the basic concept. This ensures a carbon negative production, meaning that the CO<sub>2</sub> emitted to the air is less than the CO<sub>2</sub> used in photosynthesis by the energy source [29].

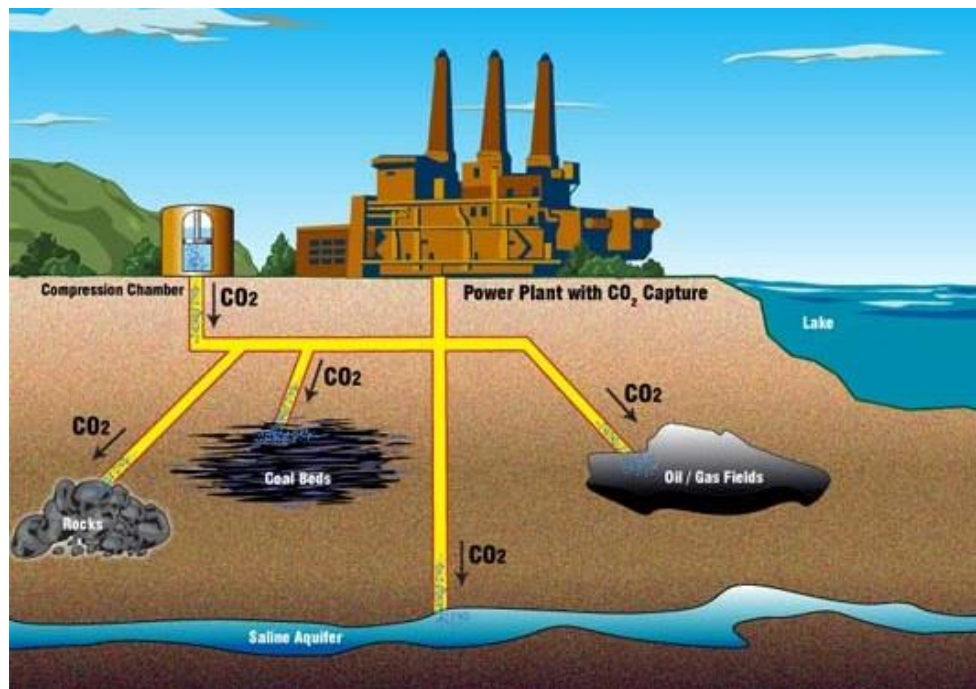


Figure 5: Carbon Sequestration

## 2.3 The Biofuel Situation

### 2.3.1 Politics

For biofuel to get a foothold and be a viable alternative to fossil fuels there has to be a political incentive for its application and in many countries there are. The European Union, under the Directive 2003/30/EC, established a goal of reaching a 5.75% share of renewable energy in the transport sector by 2010. In 2009 under the Directive 2009/28/EC, the goal was raised to a minimum of 10% for every member state by 2020 [30]. EU also has seven policy axes making up their biofuel strategy including stimulating demand, production and distribution, enhancing trade opportunities and supporting developing countries in research and development of the biofuel industry [31].

All commercial fuels are subject to quality controls. The required biodiesel specifications are specified in EN 14214 for Europe and in ASTM D6751 for the U.S. If the biodiesel meets the required specifications, the petroleum diesel specifications in Europe, EN590, currently allows for a maximum biodiesel blend of 7% by volume. Every vehicle with a CI engine produced by the members of the European Automobile Manufacturer's Association (ACEA) can today use B7 (7% biodiesel and 93% petroleum diesel) without it effecting the vehicle manufacturers warranty [32]. The ASTM International standard specification for diesel fuel oils, D975-14a, currently approves B5 for safe operation in any CI engine [33].

In Norway, biodiesel is the most common biofuel and there is injunctions on how much of the total amount of diesel sold that has to be biodiesel. In 2009, this amount was set to 2.5% but in 2010, the amount was raised to 5% [34]. The fuel distributors are free to choose how they want to obtain this, with selling low-level biodiesel blends, pure biodiesel or a combination of the two. At most petrol stations B7 is the diesel available and in some places it is possible to get B30 (30% biodiesel and 70% petroleum diesel) for special application.

Many other countries around the world has similar goals for mandated use of renewable energy. National legislations in Finland has targeted a 20% renewable energy usage by 2020 and U.S. has a goal of 20% by the end of 2022 [35]. In Brazil, a possible new legislation of raising the ethanol blend in gasoline from the present 25% to 27.5% is now investigated. Tests are being performed to make sure that this increased ethanol blend will be beneficial for engine performance and on emissions [36].



### 2.3.2 Production

The biofuel production today is dominated by two nations, U.S. and Brazil. The production consists mainly of ethanol and the total amount of produced biofuel in 2013 was 65.3 million tonnes oil equivalents. Of this, 43.5% was produced in the U.S. and 24.2% in Brazil. The total global biofuel production increased 6.1% from 2012 to 2013 [14].

Figure 6 shows the global biofuel production over a ten-year period and Figure 7 shows the ratio of produced biodiesel and ethanol. Over the last 10 years, the production of biofuel has increased with about 450% and with government goals of increasing the use of renewable energy in the future, it is safe to assume that the production rate will continue to grow.

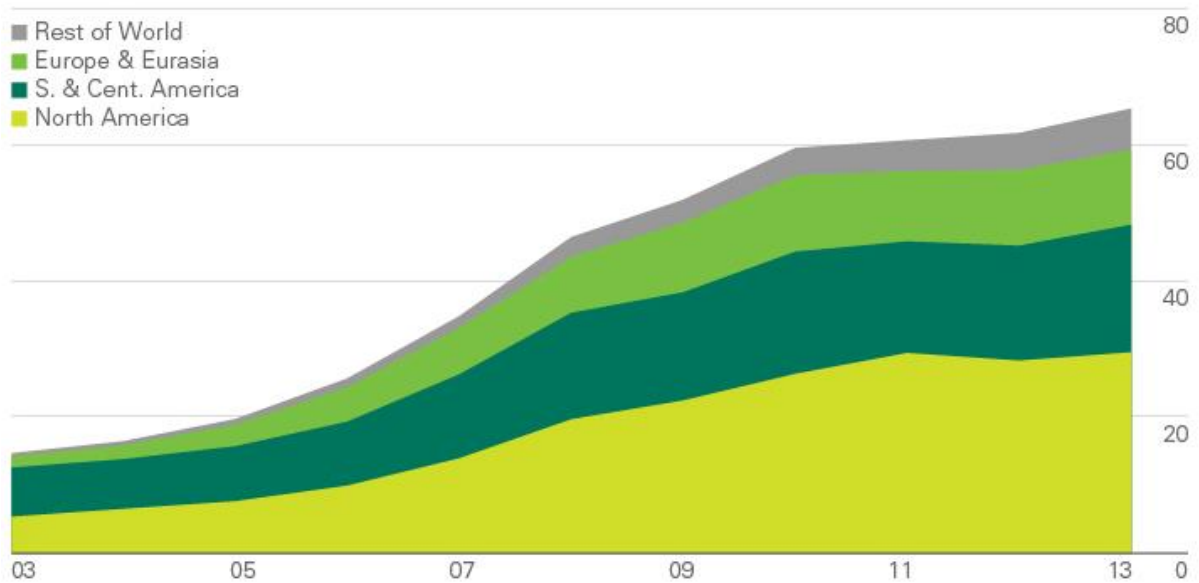


Figure 6: World Biofuel production in million tonnes oil equivalents [10]

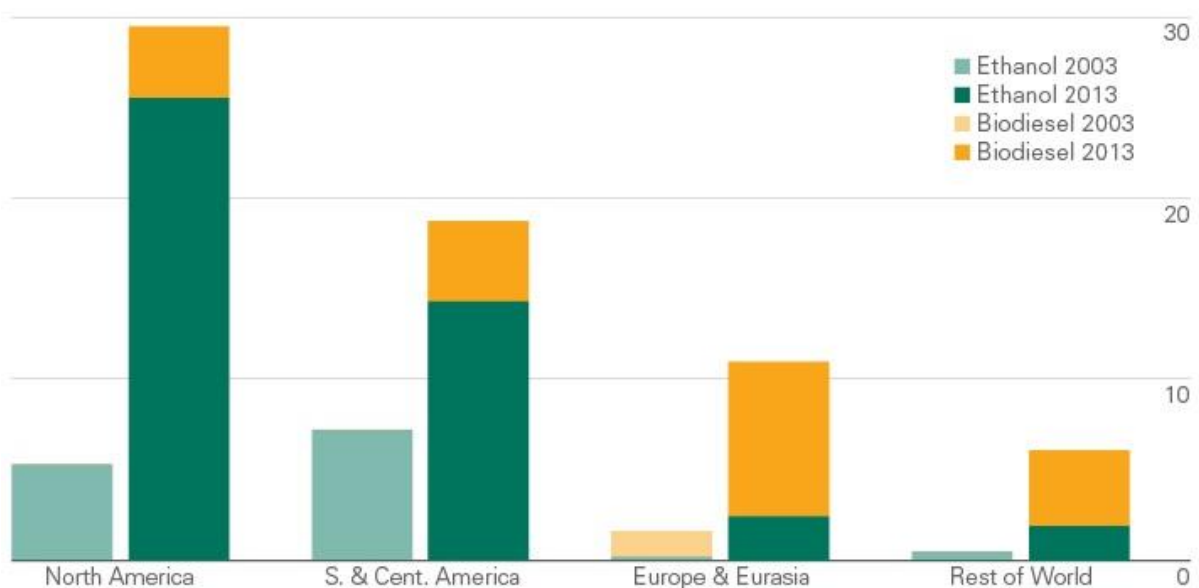


Figure 7: World Biofuel production in million tonnes oil equivalents [10]

### 2.3.3 Consumption

The biofuel consumption today is small compared to the fossil fuel consumption and biofuel is mainly used due to government legislations. In 2013, renewables in power generation and transport reached a record share of 2.7% of the total global energy consumption [14]. Figure 8 shows the total global energy consumption from 1988 to 2013. Biofuels are part of the renewables and is the energy source with lowest utilization.

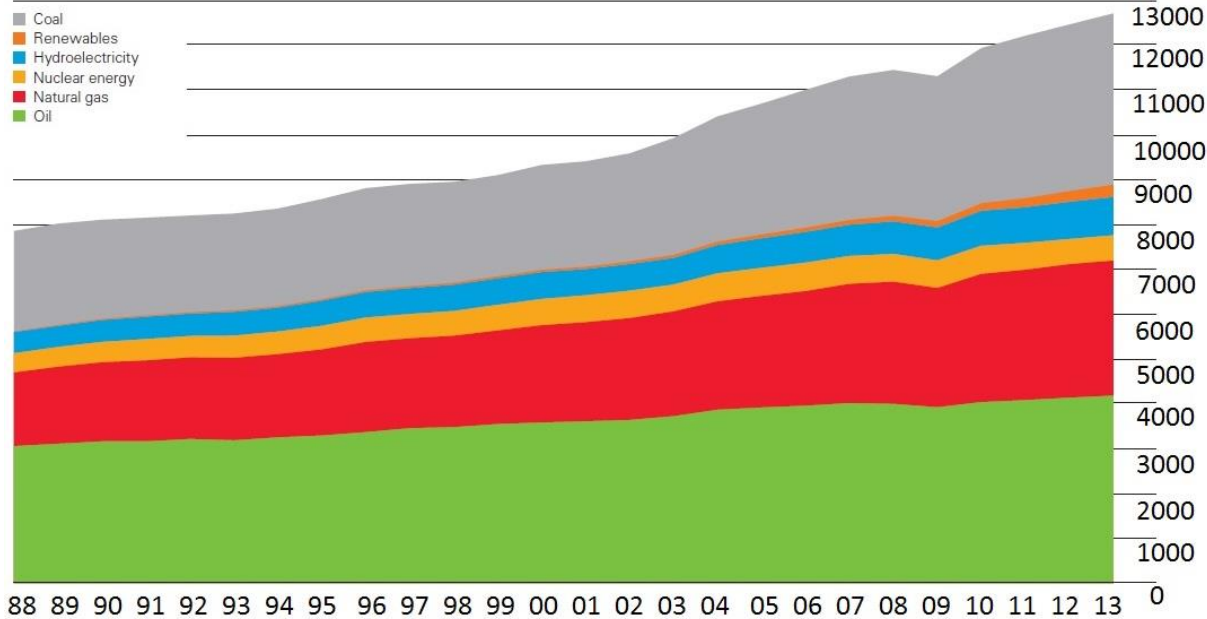


Figure 8: World energy consumption in million tonnes oil equivalents [14]

As of today, marine fuels are governed by fossil fuels, and renewable fuels have virtually no marine application. Table 1 shows the total fuel consumption of various fuels in 2010 as well as the share consumed by maritime transportation. There are many reasons for the situation being like this and there are some issues related to the use of alternative fuels in the marine sector. However, it is likely that the share of renewables used by ships will rise as the stricter emission regulations and national legislations forces the industry to adopt cleaner energy.

Table 1: Global fuel consumption, volumes of various fuels [3]

Fuel	2010 Total Consumption (million TOE/year)	Consumption for maritime Transportation (million TOE/year)
<b>Oil</b>	4.028	330 HFO/MDO: 280/50
<b>Natural Gas</b>	2858 of which LNG: 250 – 280	Very low (Approximately 40 vessels in 2013)
<b>LPG</b>	275	0
<b>Methanol</b>	23	0
<b>Ethanol</b>	58	0
<b>DME</b>	3-5	0
<b>Fischer-Tropsch</b>	15	0
<b>Biodiesel</b>	18-20	0
<b>Liquefied Biogas</b>	Very low	0
<b>Nuclear (Uranium)</b>	626	Very low
<b>Hydrogen</b>	Very low	0
<b>Rapeseed Oil</b>	5	0

#### 2.3.4 Current Issues

Returning to Table 1, we see that renewable fuels has not yet gotten a foothold as a suitable fuel for marine application. The maritime sector consumes huge amounts of fuel each year and the production of renewable fuels are just not large enough to sustain the fuel demand for large-scale application in shipping. There is in particular one big problem hindering the entry of renewable fuels in the maritime transportation sector, and that is the development of the required infrastructure. The ship owners will not consider using other fuels before a stable long-term supply can be guaranteed, and the fuel producers will not produce more fuel than the amount that is demanded [5]. The question is, who will take the first step and announce their cooperation and who will pay for the development of the required infrastructure. To see a solution to this problem, it may require governmental involvement.

In shipping today, around 70% of the fuel expenses are paid for by the charterer [37]. This means that it is unlikely that the ship owner will invest lots of money on engine technology that can accommodate the use of renewable fuels unless he otherwise will be prohibited to operate. Another aspect of this is the price of renewable fuel. As long as the price is higher than the price of fossil fuel, investments accommodating the use of renewable fuel will only lead to higher operating costs and the ships will suffer from a competitive disadvantage. However, due to the increasing pressure on the maritime transportation sector to lower the air emissions, the ship owners will be forced to invest in new technology to meet the stricter emission regulations. Different exhaust gas treatment systems are available, but renewable

fuels will be an alternative they have to consider and will in some cases be an economical viable solution.

The fuel-bound oxygen present in biofuels makes the molecules polar and this is a major concern when it comes to long-term storage and oxidation resistance. The polarity of the biofuel molecules makes them soluble in water and water will disperse in suspended droplets throughout the fuel. Because biofuels also are biodegradable and acts as a nutrient for micro-organisms, the presence of water will facilitates micro-organism growth. Over time, this can lead to formation of sludge-like matter, which clogs filters and degrades the fuel [38]. This biofuel property is great when considering fuel spills, but it is something you do not want inside a fuel tank. The fuel tanks on board ships are dimensioned with considerable safety margins and tanks are seldom run completely dry. This means that some fuel can stay in the tank for very long periods of time and this is hence an obstacle that must be solved before biofuels can be considered a serious alternative to marine petroleum fuels.

Old engine technology is not designed to facilitate biofuels and properties of the fuel makes their application difficult. This is the reason why mainly low-level biofuel blends are in use today. In the later years however, engine manufacturers have started to produce engines that can run on pure biofuels, but it will take many years before these new engines will be the dominating engine technology on the market. As long as biofuels are more expensive than fossil fuels, people will be hesitant to invest in new technology assuring safe biofuel usage.

It is possible to modify older engines to run safely on high-level biofuel blends. The modifications needed is similar for the different biofuels and the main modifications needed for biodiesel and ethanol will briefly be explained in the following.

### 2.3.4.1 Diesel Engine Modifications

#### *Rubber Seals and Lines*

High-level biodiesel blends degrades rubber materials. This will cause leaking with prolonged exposure and one has to ensure that the materials used in the fuel system is compatible with biodiesel [39].

#### *Fuel Filters*

Biodiesel has properties that make it act as a solvent on deposits in the fuel system. This will cause rapid clogging of fuel filters in the first period after switching to high-level biofuel blends. After the biodiesel has solved all the deposits in the fuel system, the fuel filter service intervals will return to normal [40].

#### *Cold Weather Operation*

Due to increased viscosity in cold temperatures, cold starting may be a problem when using high-level biodiesel blends. This can be solved with fitting a fuel heating system or to have a separate fuel tank with petroleum diesel for cold starting [41].

### *Oil Changes*

Field tests has shown that engines running on biodiesel tended to require more frequent oil changes due to more rapid oil dilution [41].

### 2.3.4.2 Gasoline Engine Modifications

#### *Fuel Filters*

Ethanol also acts as a solvent in the fuel system and the same fuel filter problems, as mentioned for biodiesel, may be encountered [41].

#### *Cold Weather Operation*

Ethanol blends have higher latent heat of evaporation than pure gasoline and thus worse cold start abilities in cold weather. This can be fixed with the same methods as for biodiesel [41].

#### *Compensation for Oxygen Content in Fuel*

The fuel-bound oxygen present in ethanol will affect the air-fuel ratio at which the engine is operating. Modern engines are fitted with lambda sensors and an engine management system that automatically changes the air-fuel ratio to achieve close to stoichiometric combustion. However, in some cases the oxygen content might be outside of the limits that the engine management system is able to compensate for and other measures must be considered. For older engines with carburetors, the oxygen content has to be compensated for by manually adjusting the air-fuel mixture [41].



# Chapter 3

## Important Characteristics

### 3.1 Fuel Characteristics

Fuel characteristics are very important and they are affecting most of the processes in an internal combustion engine. Standard fuel specifications has been developed to make sure that the fuel is of a specific quality, to ensure safe use and the same product from every supplier. Although biodiesel and petroleum diesel has chemical and thermodynamic properties that are quite similar, there are some differences, and this will influence the spray- and combustion characteristics as well as the emission characteristics.

When doing a comparison study on different fuels it is important to take into consideration differences in density, viscosity, energy content and so on. If this is neglected, it will not be possible to draw a conclusion that reflects the actual situation. There are many fuel characteristics, but the author has chosen to elaborate on the most important and the once chosen for the fuel analysis. The fuel analysis is discussed in section 4.2.4 and a summary of the different fuel specifications can be found in Appendix A.

#### 3.1.1 Density

The density is a measure of mass per volume. It can also be referred to as a measure of the specific energy in a fuel. The higher the density of a fuel, the higher the potential of stored chemical energy per unit of volume. The density is a parameter of great importance and it is affecting other fuel properties like heating value and cetane number [42]. ASTM D4052 is a standardized test to determine the density by a digital density meter [43]. Because the density of hydrocarbon based fuels are strongly temperature dependent, the standardized temperature at which the density is measured is 15°C. The accepted units are grams per millilitre (g/mL) or kilograms per cubic metre (kg/m<sup>3</sup>).

The density of biodiesel is influenced by the chemical composition and is increasing with decreasing carbon chain length and with increasing number of double bonds [44]. For petroleum diesel, the density varies depending on the refinery feedstock and variability in the diesel fuel boiling range [45]. The standard specifications for density of petroleum diesel, MGO and biodiesel is summarized in Table 2. The European standards specifies an acceptable density range, whilst the ASTM International standard has no regulation on density. ASTM argues that if the fuel complies with all the other specifications it will have a density in the desired range [42]. The density of biodiesel are, on a general basis, higher than the density of petroleum diesel.

Table 2: Density requirements

	<b>Petroleum Diesel</b>		<b>MGO</b>	<b>Biodiesel</b>	
<b>Standard</b>	EN 590	ASTM D975	ISO 8217 - DMA	EN 14214	ASTM D6751
<b>Density [kg/m<sup>3</sup>]</b>	820 - 845	-	Max 890	860 - 900	-

### 3.1.2 Kinematic Viscosity

Viscosity is a measure of a liquids resistance to flow due to internal friction. It is referred to as the thickness of the fluid and is of importance for fuel system design as well as for the combustion process itself. ASTM D445 is a standardized test to determine the viscosity by measuring the time for a volume of liquid to flow under gravity through a calibrated glass capillary viscometer [43]. The standard temperature at which viscosity is measured is 40°C and the unit is millimetres squared per second (mm<sup>2</sup>/s).

The viscosity increases with increasing carbon chain length and with increasing degree of saturation. Straight-chained fatty acids has lower viscosity than branched fatty acids. For the branched fatty acids, it is also affected by the double-bond configuration where cis configuration gives lower viscosity than trans configuration [46]. The viscosity affects pressure drop in the fuel lines and viscous fuels requires more pumping energy as well as wears components in the fuel system faster [42]. The viscosity is also affecting the atomization process of the fuel. Higher viscosity results in worse atomization and hence larger fuel droplets. This causes improper air/fuel mixing, poor combustion, increase in emissions and deposits inside the combustion chamber. It is therefore important to have a suitable viscosity to ensure stable operations.

Kinematic viscosity is the parameter specified in fuel specifications and, in contrast to dynamic viscosity, it takes the density,  $\rho$ , of the liquid into account. The relation between kinematic viscosity,  $\nu$ , and dynamic viscosity,  $\mu$ , is stated in Equation (1).

$$\nu = \frac{\mu}{\rho} \quad (1)$$

The standard specification for kinematic viscosity of petroleum diesel, MGO and biodiesel is summarized in Table 3.

Table 3: Viscosity Requirements

	<b>Petroleum Diesel</b>		<b>MGO</b>	<b>Biodiesel</b>	
<b>Standard</b>	EN 590	ASTM D975	ISO 8217 - DMA	EN 14214	ASTM D6751
<b>Kinematic Viscosity [mm<sup>2</sup>/s]</b>	2.0 – 4.5	1.9 – 4.1	2.0 – 6.0	3.5 – 5.0	1.9 – 6.0



### 3.1.3 Heating Value

The heating value of a fuel is the magnitude of the heat of reaction for the complete combustion of a unit mass of fuel at a standard temperature of 25°C [47]. This means the amount of heat that is released during a complete combustion i.e. the available energy in the fuel. A complete combustion of a hydrocarbon fuel is when all the carbon is converted to CO<sub>2</sub> and all the hydrogen is converted to H<sub>2</sub>O. The available energy is important for fuel consumption. To produce the same power output, it will be necessary to inject higher quantities of a low energy fuel than a fuel with high energy content.

ASTM D240 is a standardized test to determine the heating value of a liquid hydrocarbon fuel by using a bomb calorimeter. A sample of the fuel is placed in the bomb calorimeter along with sufficient amounts of cooling water to ensure that the water produced during combustion is condensed. When the combustion is complete, the temperature increase of the bomb and the water is measured. This temperature increase is then used to determine the gross heating value, or higher heating value (HHV), of the fuel [47]. The net heating value, or lower heating value (LHV), is determined with the produced water still in a gaseous phase. The heating value is usually expressed in joules per kilogram (J/kg) and the fuel specifications does not contain any limitations on this parameter.

The heating value of a fuel is affected positively by an increasing number of carbon atoms and an increasing ratio of carbon and hydrogen to oxygen and other components of the fuel [42]. It is also affected by the degree of saturation. A fuel containing carbon-carbon double or triple bonds has lower heating value than saturated fuels [48]. The heating value of biodiesel are lower than the heating value of petroleum diesel and MGO. This can be explained by both the presence of fuel bound oxygen and by the lower degree of saturation.

### 3.1.4 Cetane Number/Cetane Index

The cetane number is a measure of the ignition quality of a diesel fuel. Ideally, diesel fuel should ignite quickly after start of injection with a small area of pre-mixed combustion followed by diffusion combustion during injection. A fuel with low ignition quality has a long ignition delay and the risk of injecting the entire fuel charge before ignition increases. This will cause uncontrolled burning rates and a rapid pressure rise that can damage the engine as well as increasing emissions [42]. Blends of Cetane and Isocetane defines the cetane scale, where Cetane has the highest ignition quality and a cetane number of 100. Isocetane has the lowest ignition quality and a cetane number of 15. The cetane number of a fuel is determined by varying the compression ratio in a test engine to produce the same ignition delay with blends of the two reference fuels as for the fuel that the cetane number is to be determined [47].

By looking at the chemical structure of the reference fuels, it is possible to identify one important cetane number dependency. Both Cetane and Isocetane has the chemical formula C<sub>16</sub>H<sub>34</sub>, but whereas Cetane is a straight-chained hydrocarbon, Isocetane is highly branched [49]. This means that increased branching decreases the cetane number. The cetane number is also decreasing with decreasing carbon chain length and with decreasing degree of

saturation [42]. The standard specification for cetane number of petroleum diesel, MGO and biodiesel is summarized in Table 4.

Table 4: Cetane Number Requirements

<b>Standard</b>	<b>Petroleum Diesel</b>		<b>MGO</b>	<b>Biodiesel</b>	
	EN 590	ASTM D975	ISO 8217 - DMA	EN 14214	ASTM D6751
<b>Cetane Number (lower limit)</b>	51	40	40	51	47

Determination of the cetane number is a very expensive and tedious procedure and for this reason, there has been developed correlations to predict cetane number based on other fuel properties [47]. Cetane index is one of these correlations and in the standardized test method ASTM D4737, the cetane index is calculated based on density and the three distillation temperatures T10, T50 and T90. The distillation is done according to ASTM D86. For this study, the cetane index has been analysed and the precision is reported to be  $\pm 2$  cetane numbers for 65% of the evaluated fuels in the cetane number range of 32.5 to 56.5 [50]. Greater errors may be encountered outside of this cetane number range.

This method to predict the cetane number for biodiesel has however been criticised by several authors and some uncertainty in the test results have to be expected. Graboski and McCormick [51] claims that the cetane index is dependent upon the fuels aromaticity, and that it lacks significance for biodiesel since biodiesel has no aromatics. U.S. Department of Energy [52] states that biodiesel exhibits a boiling point rather than a distillation curve. This implies that biofuel has a very flat distillation curve, which makes the differentiation of the distillation temperatures inaccurate and the empirical relation not valid. Lapuerta et al. [53] has proposed a solution to this and has developed a biodiesel cetane index that, instead of being dependent upon the density and distillation temperatures, are dependent on density, carbon chain length and the number of double bonds. The precision of this correlation is not stated and, for now, no standard makes use of it.

### 3.1.5 Oxidation Stability

When talking about the stability of a fuel, it is normal to distinguish between thermal stability and oxidation stability [52]. Thermal stability refers to the chemical stability of the fuel at elevated temperatures and oxidation stability refers to the chemical resistance to react with oxygen. This is of great importance when the fuel is subject to long-term storing. For biodiesel, the oxidation stability is the biggest issue of the two and it has been reported to be the cause of increasing acid value, increasing viscosity and the formation of insoluble sediments, which compromise engine performance and the fuel system reliability [54].

As a rule of thumb, saturated fatty acid are stable and for each level of increasing number of double bonds, the oxidation stability goes down by a factor of 10 [52]. This means that a fatty acid with two carbon-carbon double bonds are 100 times less stable than a saturated fatty acid. The process of oxidative degradation is divided into primary and secondary oxidation and starts with a free radical attack on a site with a double bond. The free radical detaches a hydrogen atom from the fatty acid chain and an oxygen atom then reacts with the fatty acid to form the primary oxidation product hydroperoxide [54]. These hydroperoxides starts to accumulate, decompose and interact to form secondary oxidation products like aldehydes, short-chained carboxylic acids and polymers [54]. All in which contributes negatively to alter the fuel properties and degrade the fuel.

Oxidation stability can be tested according to different standards, but the EN 14112 accelerated Rancimat test is the most common due to the ease of use and the reproducibility of the test [55]. A sample of the fuel is put in a reaction tube and heated to 110°C while air is bubbled through the sample to accelerate the oxidation process. A flow of air passes over the sample and goes into a measuring vessel containing distilled water. As the oxidation process progresses the conductivity of the distilled water is continuously measured. The carboxylic acids that form during secondary oxidation are volatile and as soon as they starts to form, they are carried with the airflow into the distilled water. These acids changes the conductivity of the water. The time before a change in the conductivity is detected is called the induction time, and is a measure of the oxidation stability for biodiesel [56]. Both ASTM International and European biodiesel specifications has a minimum induction time limit of 8 hours.

Antioxidants is an anti-oxidising agent that is naturally present in most parent oils, but because of the biodiesel production process and preparation, the antioxidants are often removed [52]. These antioxidants can be reintroduced in the biodiesel to stabilize the fuel before storage. There are two main types of antioxidants that can be used as an additive; chain breakers and hydroperoxide decomposers [54]. The chain breakers works by having a hydrogen atom that is more easily detached than those of the fatty acids, and thus acts as an interrupter to prevent the formation of hydroperoxides. The hydroperoxide decomposers reacts with hydroperoxide and converts them into alcohols, thus preventing further reaction to form secondary oxidation products [57].

The oxidative degradation is accelerated with the presence of metals and free fatty acids. Metals, in particular copper, has been shown to have a catalytic effect on the induction time [58] and the free fatty acids are more prone to free radical attacks than their corresponding fatty acid alkyl ester [59]. Free fatty acids is a result of an incomplete transesterification process and they can be removed or neutralized to increase the oxidation stability. Metals can be deactivated by adding metal chelating additives [52]. Sunlight is also a potential oxidation catalyst through photo-oxidation, but fuel is rarely exposed to sunlight and this is easily avoided [59]. To minimize the risk of oxidative degradation, the fuel should be kept in low temperatures, protected from sunlight and in containers made of fluoroelastomers or other plastics compatible with biodiesel. It is also recommended to limit the amount of oxygen that is in direct contact with the fuel. Commercially, this is done by using a blanket of nitrogen in the headspace of the storage tanks [52].

### 3.1.6 Acid Value

The acid value, or acid number, of a fuel is a measure of the amount of acids in the fuel. For biodiesel, this means the concentration of free fatty acids and an elevated acid value is an indicator of a poor transesterification process [52]. It is also possible to map the oxidative degradation by monitoring the acid value. The concentration of the secondary oxidation product carboxylic acid can be detected and by tracing the acid value over time, it is possible to get a picture of the chemical changes in the fuel [60]. The acid value only reflects the concentration of acids and not their strength. For this reason, it is important to distinguish between acid value and pH value, which is a measure of the strength and hence the corrosive properties of the fuel. No correlation between acid value and corrosive tendencies is known [61].

The acid value is determined by the amount of potassium hydroxide (KOH) that is required to neutralize one gram of a fuel sample and has the unit milligram KOH per gram fuel (mg KOH/g). Different standard test method can be applied, but ASTM D974 has been chosen for this study. This methods measures the acidic concentration by dissolving the sample in a solution of toluene, naphtholbenzein and isopropyl alcohol. Potassium Hydroxide is then titrated into the solution and the colour of the solution is monitored [60]. When the solution is neutralized the colour changes and the amount of potassium hydroxide needed is recorded. The MGO standard as well as both ASTM International and European biodiesel specifications has a maximum acid value limit of 0.5 mg KOH/g.

## 3.2 Spray Characteristics

There are two main categories of spray characteristics: macroscopic characteristics and microscopic characteristics [62]. Microscopic characteristics involves droplet velocity, droplet distribution, droplet size, air-fuel ratio distribution etc. and to analyse these characteristics, sophisticated research equipment is needed. Macroscopic characteristics involves penetration length, cone angle and lift-off length. These characteristics are easier to quantify by analysing images of the actual spray and macroscopic spray characteristics is the focus of this study.

The fuel spray is gradually formed as the injection of fuel in the combustion chamber continuous. The fuel is injected as a liquid jet and immediately after leaving the nozzle hole, this jet is exposed to aerodynamic forces (friction and pressure) in the combustion chamber. These aerodynamic forces starts to decelerate the spray and turn the fuel jet into droplets [63]. The point where the liquid jet is turned into a mist of fuel droplets is defined as the break-up point and is usually between 10 - 30 mm from the nozzle hole [64]. This is however depending on injection pressures and nozzle length/diameter ratios [47]. As the fuel droplets propagates through the combustion chamber, the droplets at the spray-tip experience stronger drag forces than the droplets following in their wake. This results in higher deceleration at the spray-tip and a continuous replacement of fuel droplets as the spray penetration increases. The droplets with lowest kinetic energy and momentum are pushed out from the centre axis to forms the outer spray region [63]. The spray gets more diluted as it interacts with the entrained chamber gases and this results in a gradual transition from liquid in the centre to gas at the outer borders of the spray.

The spray characteristics can be defined in many different ways. Figure 9 shows the definitions used in this study.

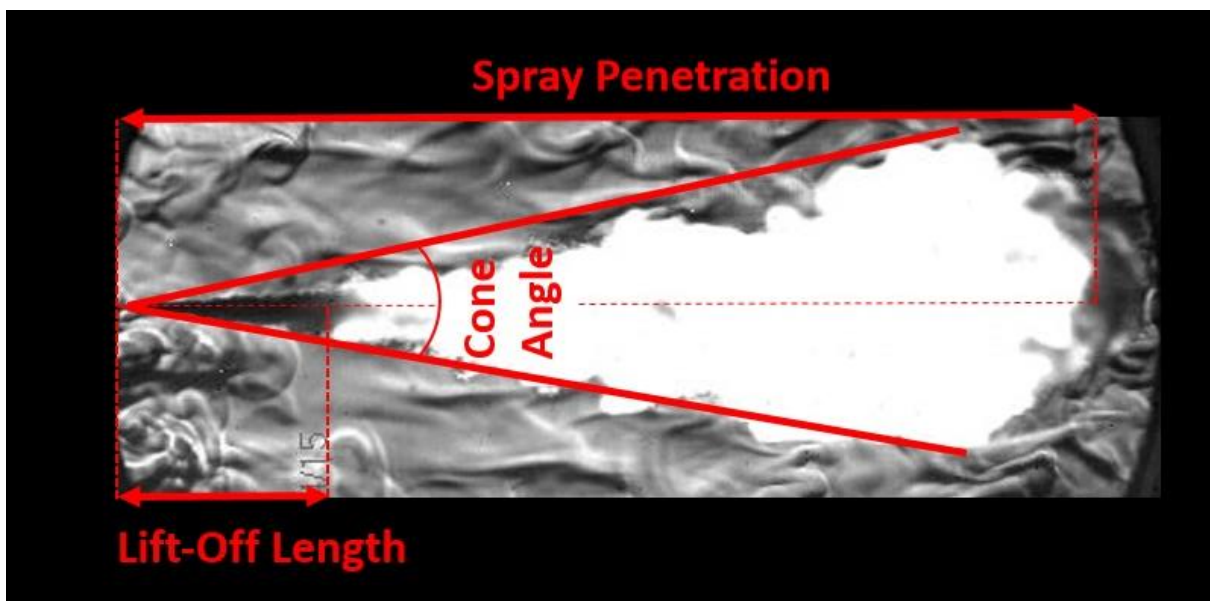


Figure 9: Definition of Spray Characteristics

### 3.2.1 Penetration Length

The penetration length is the total length of the spray along the axial injection direction. The penetration length is an important characteristic for combustion efficiency. If the penetration length is too long, the spray will wet the chamber walls and this has, in most cases, a negative impact on combustion efficiency and emission formation. Fuel that hits the wall will be affected by the quenching effect causing partial burning, increasing soot formation and emissions of unburned hydrocarbons. This is most prominent during cold starting conditions when the wall temperatures are low [63]. There are some examples of engine design where wall impingement has positive effects on the combustion process due to the ability to control evaporation rates and thus the combustion rate, M-combustion by MAN [65], but it is generally something that is unwanted. Too short penetration length results in underutilization of air and this has a negative effect on combustion efficiency [47].

The penetration length is mainly dependent upon injection pressure and chamber density [66]. Higher injection pressure means higher injection velocity and longer penetration, and the chamber density affects the resistance the fuel droplets are exposed to. Hence, higher chamber density means shorter penetration length. The viscosity of the injected fuel is reported to play an important role for the atomization process and thus has an indirect effect on the penetration length. Higher viscosity leads to worse atomization and bigger fuel droplets [67]. Bigger fuel droplets has higher momentum, which results in longer penetration.

The penetration length can be determined by two empirical equations established by Hiroyasu and Arai [64]. At start of injection, the injection velocity is much larger than the surrounding gas and the penetration length is described by an expression proportional to time, hence constant injection velocity, Equation (2). After the break-up, the fuel is decelerated and becomes proportional to the square root of time, Equation (3). Equation (4) is used to compute the brake-up time.

$$S(t) = 0.39 * \sqrt{\frac{2\Delta P}{\rho_l}} * t \quad \text{for } 0 < t < t_{break} \quad (2)$$

$$S(t) = 2.95 * \left(\frac{\Delta P}{\rho_{ch}}\right)^{\frac{1}{4}} * \sqrt{d_0 t} \quad \text{for } t \geq t_{break} \quad (3)$$

$$t_{break} = \frac{28.65 * \rho_l * d_0}{\sqrt{\rho_{ch} * \Delta P}} \quad (4)$$

$$\Delta P = p_{inj} - p_{ch}$$

### 3.2.2 Cone Angle

The cone angle is the angle between two lines intersecting the extreme values of the spray in radial direction. The cone angle is reported to be affected by chamber density and fuel viscosity, where higher viscosity gives narrower cone angles [67]. As the chamber density increases, the entrapped gas in the chamber exerts higher shear forces on the fuel droplets. This creates a radial component of the droplet velocity forcing the droplets to deviate from their initial axial path, resulting in larger cone angles. The cone angle is also affected by the continuous replacement of fuel droplets at the spray-tip because new droplets push their way through the middle of the spray and forces the preceding droplets outwards. Other factors influencing the atomization process, like injection pressure, chamber temperature and injection nozzle geometry will also have an influence on the cone angle due to the differences in droplet size and distribution.

Hiroyasu and Arai also investigated cone angles and developed the empirical relation in Equation (5). This equation gives the cone angle for sac hole nozzles with full needle lift [63] and the most influential parameter is the density ratio. The higher the gas density is in the combustion chamber the more resistance the fuel spray is exposed to. This increases the amount of replacement of fuel droplets at the spray-tip as well as the shear forces, forcing the droplets outwards.

$$\theta = 83.5 \left(\frac{l}{d_0}\right)^{-0.22} \left(\frac{d_0}{d_{sac}}\right)^{0.15} \left(\frac{\rho_{ch}}{\rho_l}\right)^{0.26} \quad (5)$$

A more general relation for the cone angle is given by Heywood [47], and is shown in Equation (6). Here A is a constant dependent upon a given nozzle geometry that can be determined by Equation (7).

$$\tan\left(\frac{\theta}{2}\right) = \frac{4\pi}{A} \sqrt{\left(\frac{\rho_{ch}}{\rho_l}\right)} \frac{\sqrt{3}}{6} \quad (6)$$

$$A = 3.0 + 0.28 \left(\frac{l}{d_0}\right) \quad (7)$$

### 3.2.3 Lift-Off Length

The flame lift-off is defined as the length between the fuel injector tip and the closest point of combustion during injection of fuel [68]. Different methods to determine this closest point of combustion is present in the literature. One common way, and the method used in this study, is to analyse images of the spray and to determine the closest point of combustion based on combustion intensity. The problem with this method is that the camera settings e.g. shutter time, frame rate and aperture setting plays a vital role in the level of captured intensity. It is hence very important to find the optimum camera settings and to hold these constant during the tests. The intensity of the combustion is determined by the soot formation, see section 3.3.1, and the visual flame is hence not necessarily the closest point of combustion, but rather the closest point of soot formation. Another method to determine the closest point of combustion is by looking at the chemiluminescence of hydroxyl (OH) radicals [69]. During combustion, there is a strong presence of these highly reactive and short-lived OH radicals in near-stoichiometric regions with high heat-release, and these conditions are expected at the lift-off length [68]. The OH radicals emit detectable light in the 310 nm range and the closest point to the injection tip with presence of light with this wavelength is then used to determine the lift-off length.

The lift-off length is dependent upon the ambient temperature and the chamber density and shows a non-linear decreasing relation as both ambient temperature and chamber density increases [68]. The injection pressure and hence the injection velocity is also affecting the lift-off length. This relation show a linearly decreasing lift-off length with increasing injection pressure [69]. All of the dependencies listed above is influencing the mixing process and hence the time it takes the fuel to mix with air to obtain an ignitable mixture. The viscosity of the fuel influences the atomization process, and thus the mixing process, and higher viscosity hence leads to longer lift-off length.



### 3.3 Combustion Characteristics

The combustion characteristics is related to the combustion process and different fuels will exhibit different characteristics based on their properties and chemical composition.

#### 3.3.1 Radiation Intensity and Soot Formation

One important characteristic of diesel combustion is its high luminosity caused by thermal radiation of soot particles [70]. During the combustion process, it is emitted electromagnetic radiation in ultraviolet, visible and infrared wavelength ranges and different reaction species emit either band radiation or continuous radiation [71]. See Figure 10.

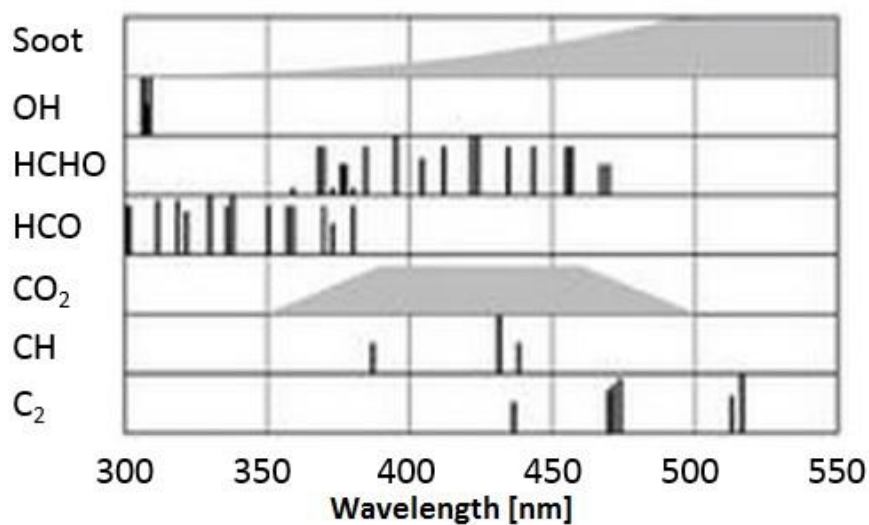


Figure 10: Radiation Spectrum of Diesel Combustion

Thermally excited soot has a continuous radiation spectrum within the visible wavelength range and satisfies Planck's law of radiation. Planck's law describes the electromagnetic radiation emitted by a black body in thermal equilibrium and says that the radiation intensity of a black body is dependent upon temperature [71]. Because of this, it will be important to keep the chamber temperature at start of injection as constant as possible during the tests. Although a perfectly black body does not exist, a body with a black surface like a soot particle gives good estimations on the radiation emitting behaviour [72]. Soot particles are very small, so even if there are temperature differences inside the combustion chamber it is safe to say that each individual soot particle is in thermal equilibrium. Since the soot luminosity dominates the visible wavelength range, it will be possible to qualitatively determine the sooting behaviour of the different fuels by comparing the total radiation intensity of the combustion process.

### 3.3.2 Rate of Heat Release

The rate of heat release (ROHR) is the rate at which the chemical energy in a fuel is converted to heat when the fuel is combusted, and it is calculated from the first law of thermodynamics for an open system [47]. Equation (8) shows the first law of thermodynamics where  $\Delta U$  is the change in internal energy,  $Q$  is the heat delivered to the system i.e. heat release, and  $W$  is the work done by the system.

$$\begin{aligned}\Delta U &= Q - W \\ Q &= W + \Delta U\end{aligned}\tag{8}$$

The net heat release is the gross heat release subtracted the heat transfer to the walls. Assuming that the combustion efficiency is 100 percent, normally it is above 98% for diesel fuel [47], then the gross heat release is equal to the chemically available heat that is released during the combustion:

$$\frac{dQ_{net}}{dt} = \frac{dQ_{chemical}}{dt} - \frac{dQ_{heat\ transfer}}{dt} = p \frac{dV}{dt} + \frac{dU}{dt}\tag{9}$$

Assuming that the ideal gas law applies, the internal energy is a function of the absolute temperature,  $dU = mc_v dT$ :

$$\frac{dQ_{net}}{dt} = p \frac{dV}{dt} + mc_v \frac{dT}{dt}\tag{10}$$

By assuming that  $m$ ,  $R$  and  $V$  are constant, the ideal gas law states that:

$$\frac{1}{p} \frac{dp}{dt} = \frac{1}{T} \frac{dT}{dt}\tag{11}$$

Equation (11) can be used to eliminate  $\frac{dT}{dt}$  from Equation (10) and since the volume of the CVCC is constant,  $\frac{dV}{dt}$  is zero:

$$\frac{dQ_{net}}{dt} = \frac{mTc_v}{p} \frac{dp}{dt}\tag{12}$$

By rewrite the ideal gas law,

$$\frac{mT}{p} = \frac{V}{R}\tag{13}$$

Make use of the relation,

$$\frac{c_v}{R} = \frac{c_v}{c_p - c_v} = \frac{c_v}{c_v \left( \frac{c_p}{c_v} - 1 \right)} = \frac{1}{\gamma - 1} \quad (14)$$

And substitutes Equation (13) and (14) into Equation (12), the formula used to calculate the ROHR in this study is found:

$$\frac{dQ_{net}}{dt} = \frac{1}{\gamma - 1} V \frac{dp}{dt} \quad (15)$$

### 3.3.3 Ignition Delay

Ignition delay is an important characteristic for the design of the injection system and for the tuning of the injection timing. The ignition delay is defined as the time between start of injection and start of combustion [73]. The start of injection can be determined by a needle-lift indicator as the point where the needle lifts of its seat. The start of combustion is more difficult to determine. Since diesel engines are designed to make use of the diesel fuels auto ignition properties, there are no ignition signal that can be used to trace the start of combustion. For this reason, the start of combustion is usually found by analysing the slope of the heat release curve or calculated based on mass fraction burned (MFB) [47].

In this study the ignition delay will be calculated with the MFB method. Based on the heat release, the ignition delay is determined by the combustion duration before a fixed percentage of the mass of fuel has burned. In literature, the ignition delay definitions when using this method are ranging from MFB 1-10% and as long as it is kept constant for all fuels, it does not really matter. For this study, MFB 5% has been chosen. An additional option to obtain the ignition delay is by visually evaluating the images of the combustion process and search for the first image with visual combustion. This optical approach is however highly dependent upon the frame rate of the camera and the interpretation of the images and are hence inaccurate . It can in best case be used to validate the MFB calculations, but this has not been done in this study.

The ignition delay consists of physical delay and chemical delay and both of these delay periods occurs simultaneously. The physical delay represents the atomization, vaporization and the mixing of air and fuel, whilst the chemical delay is the chemical reactions happening before the point of ignition [73]. The ignition delay is strongly dependent upon the chamber temperature and pressure, which is important for the vaporization needed to obtain an ignitable mixture of air and fuel. The combustion quality of the fuel also plays a vital role and the ignition delay is decreasing with increasing cetane number.

Over the years, many semi-empirical equations based on the Arrhenius equation has been developed to predict the ignition delay. The Arrhenius equation was proposed by Svante Arrhenius in 1889 and is a formula that takes into account the temperature dependence of

chemical reaction rates [74]. Equation (16) is a general ignition delay equation where F and N are constants, p and T are chamber pressure and temperature. E and R are the activation energy and the universal gas constant.

$$t_{id} = Fp^{-N} \exp\left(\frac{E}{RT}\right) \quad (16)$$

## Chapter 4

# The Research Equipment and the Fuels

### 4.1 Constant Volume Combustion Chamber

The CVCC is located in the engine laboratory at MARINTEK, Trondheim. It is a handy tool when studying the combustion properties of various fuels and can also be used to study different injector and spark plug technologies. The use of a CVCC in combustion research provides the possibilities to isolate the injection and combustion processes from all the influential sub processes happening in an engine. The optical access makes it possible to see inside the combustion chamber and this facilitates the use of a high-speed camera and the implementation of image analysing tools to achieve a better understanding of the injection and the combustion processes.

#### 4.1.1 Experimental Setup

The CVCC is mounted on a rail system, which facilitating precise alignment of the optical items for the different imaging techniques, see section 4.1.6. The chamber has optical access through two windows with a diameter of 15 cm and the rig is equipped with a high-speed camera to capture still photos of the spray development. Figure 11 shows a picture of the experimental setup and a CAD drawing of the test bed can be found in Appendix B.

The rig has a common rail fuel injection system with a maximum pressure of 1800 bar, a spark plug, air and gas inlet valves and an exhaust outlet valve. A fan is installed to ensure a homogeneous gas distribution inside the vessel. The combustion rig is computer controlled, and pressure sensors record data, which then is used in further analysis. See Figure 12 for the flow plan of the combustion rig.

The CVCC is designed for a maximum vessel pressure and temperature of 100 bar and 1800 K and hence, it is possible to replicate pressure and temperature environments of a CI engine. The inner diameter of the combustion chamber is 25 cm and it has a volume of 5 dm<sup>3</sup>.

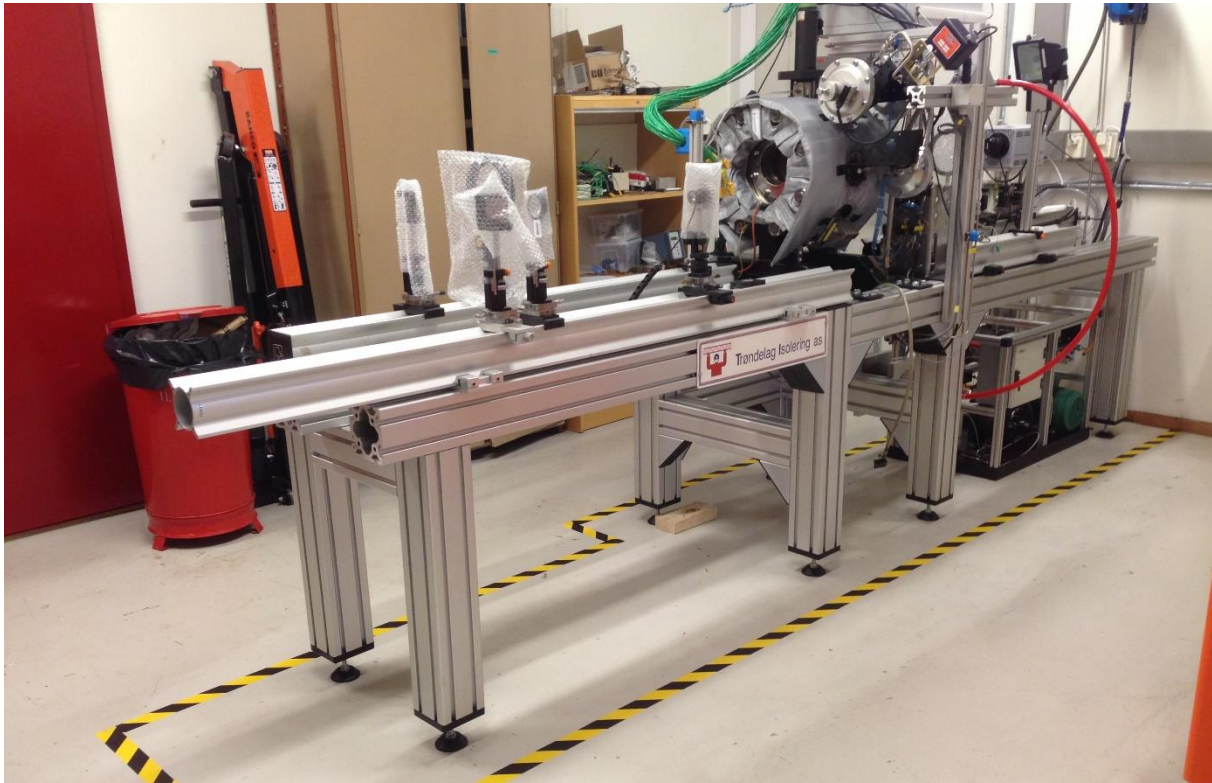


Figure 11: Experimental Setup

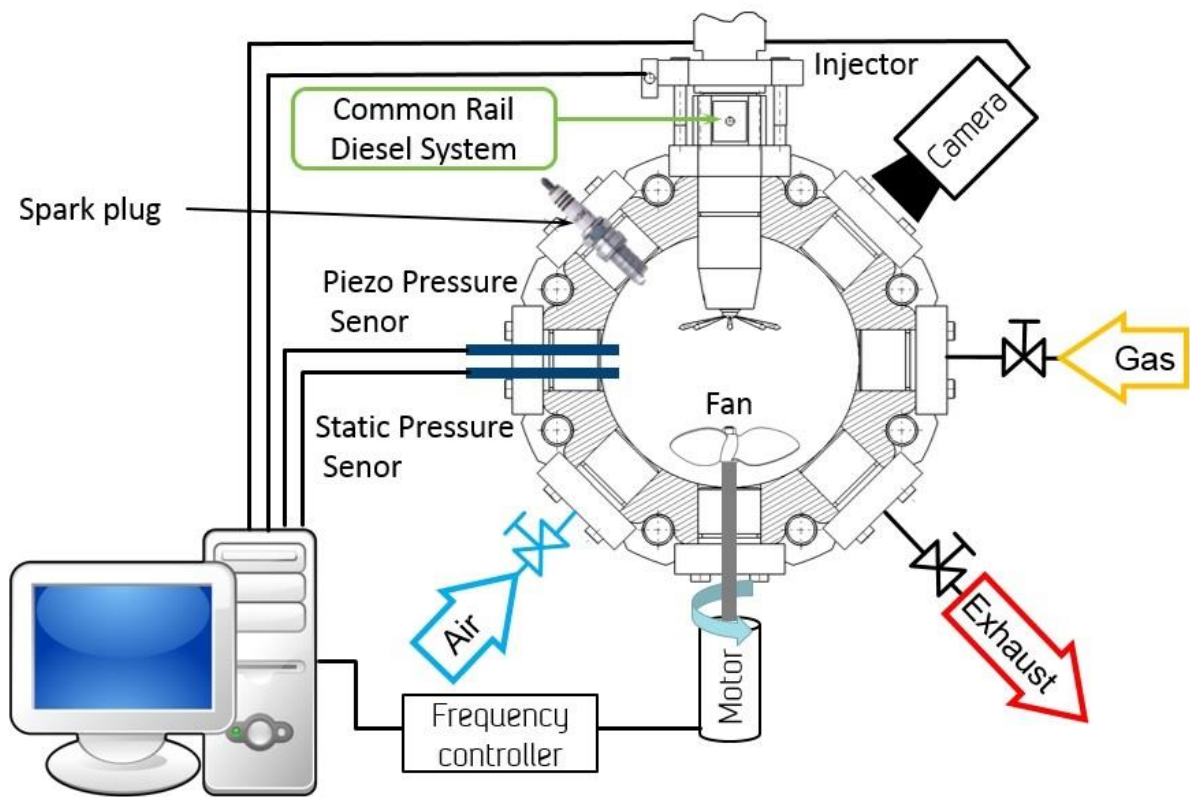


Figure 12: Schematic flow plan of the combustion rig

### 4.1.2 Working Principle

Figure 13 shows the working principle of the combustion rig. Since the CVCC has a constant volume and no moving parts to compress the charge air, the environment is prepared by igniting a gas mixture inside the chamber. The rig is filled with 10 bars of an ignitable gas mixture, see section 4.1.3, and it is ignited with the spark plug. This process of preparing the test environment, and to obtain test conditions where auto ignition of diesel fuels are possible is called the pre-combustion. Just after the pre-combustion, the temperature is too high for the environment to simulate an actual engine and one has to wait for heat losses to reduce the chamber conditions. When the conditions are as desired, the fuel is injected, and the main combustion occurs. The gas composition inside the chamber after pre-combustion can be controlled to simulate different working environments e.g. use of EGR (Exhaust Gas Recirculation).

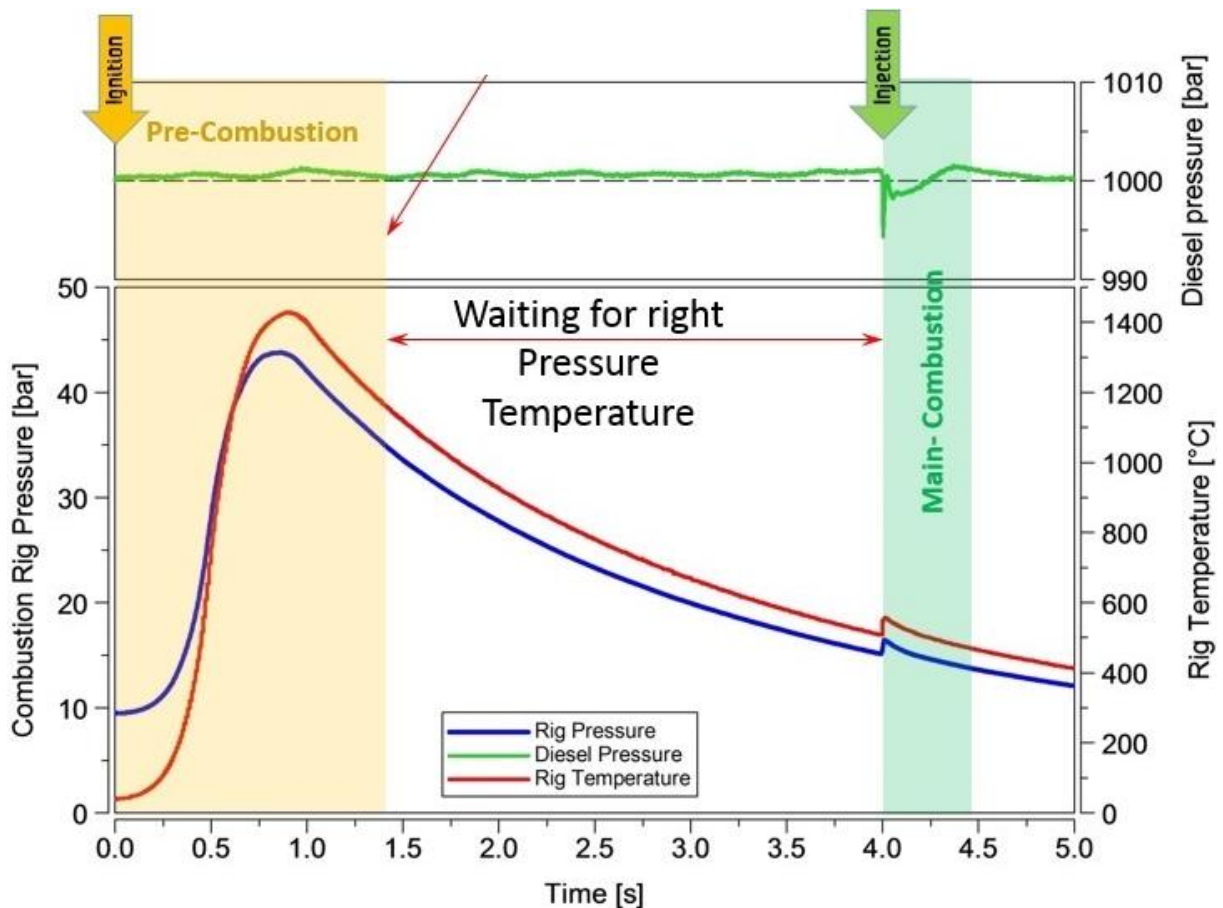


Figure 13: Combustion rig working principle [75]



### 4.1.3 Gas Mixing

The gas used as fuel for the pre-combustion is a mixture of CO, N<sub>2</sub> and O<sub>2</sub>. These gases are mixed based on partial pressures to obtain an ignitable mixture that, after pre-combustion, has 21 percent oxygen content to mimic air. Figure 14 shows the mixing arrangement.

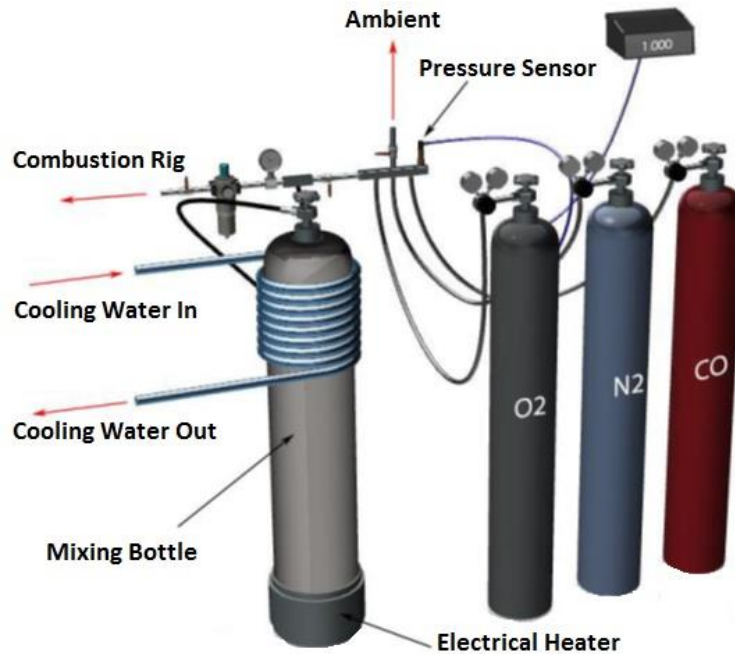


Figure 14: Gas Mixing Arrangement

The mixing process starts with one bar of ambient pressure. The mixing bottle is filled with 9.2 bars of carbon monoxide, 17.9 bar of nitrogen and 11.9 bars of oxygen. At the end of the mixing process, the pressure in the mixing bottle is 40 bars, which is sufficient for approximately 30 shots. The filling process is summarized in Table 5. The mixing bottle is rated for a maximum pressure of 300 bars, but since the bottle contains an ignitable gas mixture, the maximum mixing pressure is set to 40 bars for safety reasons in case of flashbacks or backfires. This makes sure that the mixing bottle is capable of sustaining the pressure increase, due to a sudden combustion of its entire content, without exploding. To obtain an as homogenous mixture as possible, the bottle is heated at the bottom and cooled at the top. This creates circulation inside the bottle and ensures a good gas mixing.

Table 5: The Gas Mixing Process

Gas	Partial Pressure [bar]	Cumulative Pressure [bar]
Air	1	1
CO	9.2	10.2
N <sub>2</sub>	17.9	28.1
O <sub>2</sub>	11.9	40



## 4.1.4 Subsystems

### 4.1.4.1 Fuel system

Table 6 shows the key parameters of the fuel system. The fuel system is equipped with fuel lines capable of handling the properties of biofuel.

Table 6: Key Parameters of the Fuel System

<i>Description</i>	<i>Value</i>	<i>Units</i>
<i>Maximum pump pressure</i>	1800	<i>bar</i>
<i>Maximum piping pressure</i>	2500	<i>bar</i>
<i>Fuel temperature condition</i>	288 - 333	<i>K</i>

The injector used in this study is an L'Orange VUO-G298uV120 made for medium speed application and it is fitted with a single hole injection nozzle with a orifice diameter of 35 mm.

Between the tests of different fuels, the fuel system is completely emptied and when a new fuel is introduced the fuel filter is changed. To make sure that all of the old fuel is flushed out of the system, the first couple of thousand injections after a fuel change are done in a canister and this fuel is removed before the start of testing.

### 4.1.4.2 Control System

The CVCC is computer controlled from a separate control room. One computer is used to run an in-house designed LabView interface for controlling the filling of gas, the flushing of exhaust and the initiation of the combustion sequence. This interface also allows for adjusting all the relevant operating parameters. A second computer is used to control the high-speed camera and to adjust all the camera settings. The ignition signal from LabView is used to trigger the recording of the high-speed camera.

### 4.1.4.3 High-Speed Camera

The high-speed camera is a Photron Fastcam APX RS and a KG1 coloured glass 315-725 nm band-pass filter has been applied. When using images for comparison it is very important to keep all the settings related to the image acquisition constant. Table 7 shows the camera settings.

Table 7: Camera Settings

<i>Setting</i>	<i>Value</i>	<i>Unit</i>
<i>Frame Rate</i>	15000	Pictures/second
<i>Resolution</i>	256x496	Pixels
<i>Aperture</i>	f/5.6	[-]
<i>Shutter Speed for Direct and Schlieren</i>	1/500000	seconds
<i>Shutter Speed for Shadowgraph</i>	1/50000	seconds

## 4.1.5 Limitations

### 4.1.5.1 Load Condition

The maximum vessel pressure of the CVCC is limiting the simulated load condition due to the rapid pressure increase during pre-combustion. The load condition is related to the charge air density, which in the CVCC, since the volume is constant, is represented by the density of the gas mixture. If the amount of gas that the CVCC is filled with is increased to simulate a higher load conditions, you risk overshooting the design pressure of the vessel during pre-combustion. Figure 15 shows a typical load condition curve for a medium speed one stage turbocharged CI engine. A break mean effective pressure (BMEP) of 50 bars corresponds to engine idling and at this load condition, the charge air density is 16.8 kg/m<sup>3</sup> at time of injection. Due to the rapid pressure increase during pre-combustion, the density limitation of the CVCC is 12 kg/m<sup>3</sup> and this corresponds to very low load. The rapid pressure increase can be reduced by igniting a leaner gas mixture, but the current ignition system is not able to do that and work on finding a more powerful ignition system is currently being conducted.

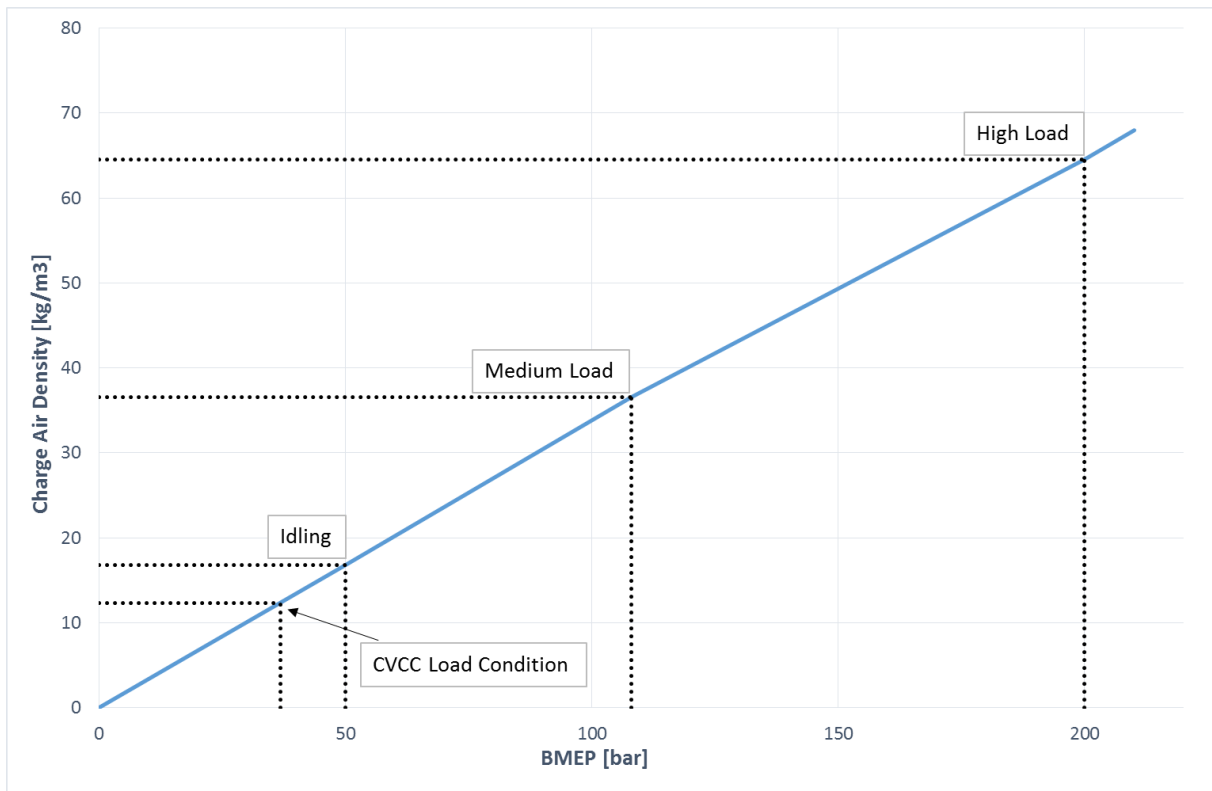


Figure 15: Typical Load Condition Curve

### 4.1.5.2 Window Diameter

Since this study rely on the analysis of images to determine spray characteristics, it is important that the spray is confined within the diameter of the window. If the penetration length of the spray is too long and it exits the visible area, the camera will not capture all the information and this may be a potential error source in this study.

### 4.1.6 Imaging Techniques

Three different imaging techniques has been used to capture images; direct imaging, shadowgraph imaging and schlieren imaging. The direct imaging technique is just ordinary photos of the combustion process and is used to determine the radiation intensity of the combustion. The shadowgraph technique and the schlieren technique is used to visualize the density field inside the CVCC during the injection and combustion process. The two latter visualization techniques makes it possible to determine the liquid and the gas phase of the injected fuel, and reveals some information about the air-fuel mixing process.

Both the shadowgraph and the schlieren techniques are based on that light rays refract when they travel through a medium with changing refraction index. The Gladstone – Dale formula, Equation (17), links the refraction index of a gas directly to the density of the gas, and hence is it possible to visualize density variations inside the CVCC by utilizing this light refraction.

$$n - 1 = k\rho \quad (17)$$

Here  $n$  is the refraction index,  $k$  is the Gladstone – Dale constant and  $\rho$  is the density.

The way these techniques work is by directing a beam of light through a lens to make the light rays parallel to each other. This beam of parallel light rays then goes through a test section before a second lens refocuses it. As the light rays travel through the test section, some of the light rays are deflected by the varying density field inside the CVCC and hits the second lens at an angle. The light that went through undeflected hits the lens, still parallel, and is focused in one point whilst the deflected light, which comes at an angle and hence sees a different lens, is focused somewhere else.

#### 4.1.6.1 Direct Imaging

The direct imaging technique has the easiest setup, see Figure 16. No back illumination is used so the background is completely black and only the light developed by the combustion process is captured by the camera. No details can be seen in the photos, but they are good for studying the radiation intensity of the combustion. Figure 17 shows an injection captured with direct imaging.

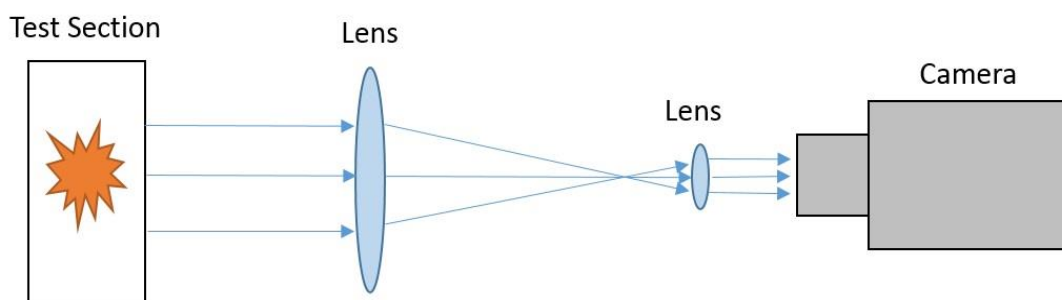


Figure 16: Direct Imaging Setup

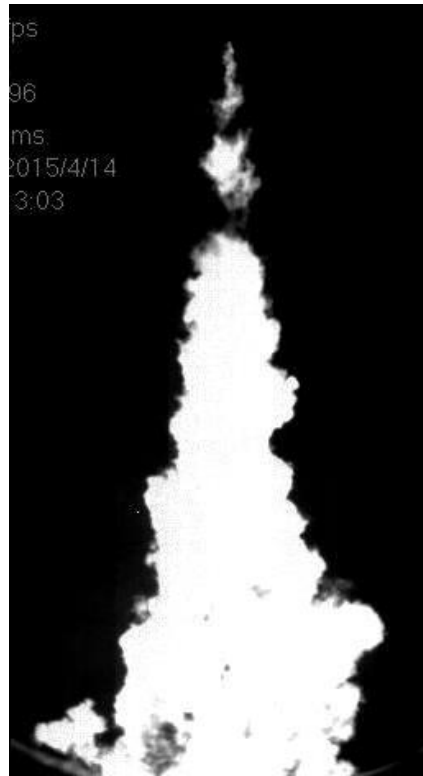


Figure 17: Direct Imaging Technique

#### 4.1.6.2 Shadowgraph

The shadowgraph technique is the simplest density visualization method and makes use of the deflection of light by producing an image with varying brightness. Figure 18 shows the setup.

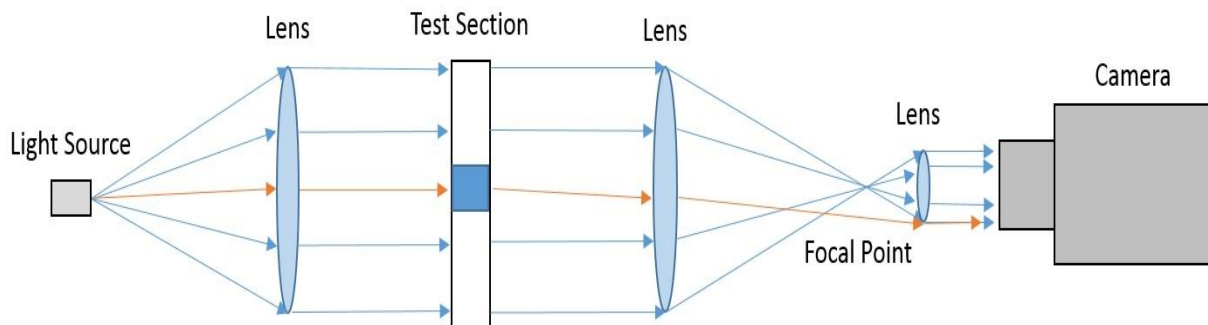


Figure 18: Shadowgraph Setup

Due to that some light has been deflected, some areas on the image will appear dark and some areas, where the deflected light hit, will get twice the light intensity and appear bright. See Figure 19. In this way, the areas of higher density is made visible as dark shadows with a contrasting brighter field next to it [76]. Figure 20 shows an injection of a non-combusting spray captured using the shadowgraph technique.

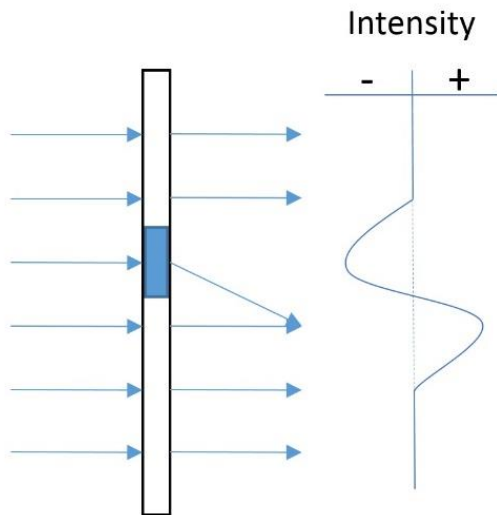


Figure 19: Shadowgraph Principle



Figure 20: Shadowgraph Imaging Technique

The shadowgraph technique tracks light ray displacement, due to refraction, and the image intensity is sensitive to the second derivative of the density distribution, perpendicular to the light propagation direction [77].

#### 4.1.6.3 Schlieren

The schlieren technique is based on the same principle as the shadowgraph and the setup in front of the test section is identical. The only difference between the techniques is that when using schlieren you are blocking light rays. The most common way to produce a schlieren image is by placing a knife-edge, typically a razor blade, in the focal plane to block the deflected light, and some part of the undeflected light to produce a contrast. See Figure 21. The light rays that pass by the knife-edge and hit the camera lens create an image of the density field [76].

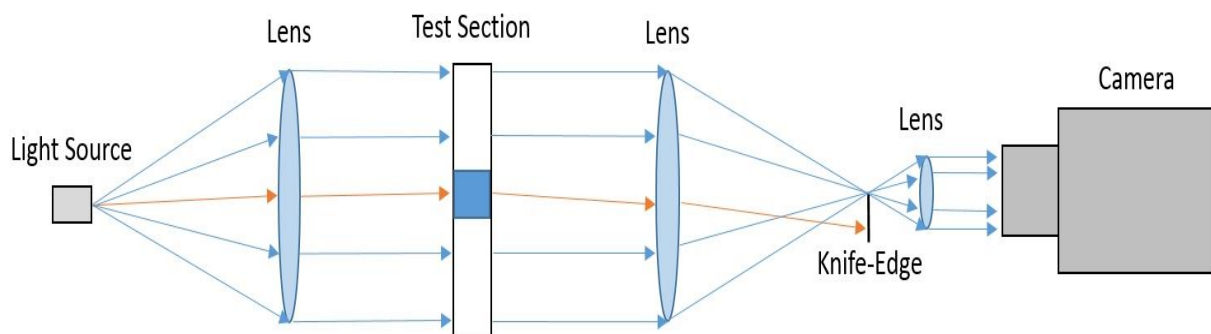


Figure 21: Schlieren Setup

The schlieren technique is more flexible when it comes to detailed imaging of the density field. The image shows density variations perpendicular to the knife-edge orientation and by orienting the knife-edge either horizontal or vertical, one can visualize density gradients in different directions. If radial density gradients is of interest one has to use a circular knife-edge. One additional choice is available and that is to block the undeflected light rays instead of the deflected ones. This is done by blocking only the light rays that travels through the focal point. The choice of which light rays to block, determines if one has brightfield schlieren or darkfield schlieren. In brightfield schlieren imaging, the density variations will appear dark on a bright background whilst for darkfield, the density variations is shown bright at a dark background.

The schlieren technique tracks angular displacement of the light rays, due to refraction, and the image intensity is sensitive to the first derivative of the density distribution, perpendicular to the light propagation direction [77]. Figure 22 shows a combustng spray captured with the schlieren technique.

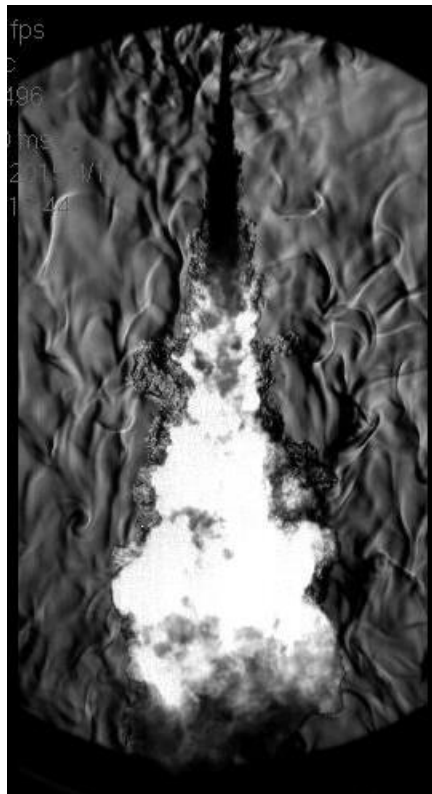


Figure 22: Schlieren Imaging Technique

## 4.2 The Fuels

In this study, the three fuels MGO, FAEE and CFO has been used in different blends, see Table 8 for the fuel matrix. The main differences between CFO and FAEE lies in the depth of processing and hence the properties of the fuels. MGO is a conventional petroleum based marine fuel.

	<i>Fuel 1</i>	<i>Fuel 2</i>	<i>Fuel 3</i>	<i>Fuel 4</i>	<i>Fuel 5</i>	<i>Fuel 6</i>
<i>MGO</i>	100%		50%	50%	93%	93%
<i>FAEE</i>		100%		50%	7%	
<i>CFO</i>			50%			7%

Table 8: Fuel Matrix

Fuel 1 is pure MGO and will serve as a basis for comparison as well as the base for the fuel blends. Fuel 2 is pure FAEE and fuel 3 is a 50% blend of MGO and CFO. Due to the viscosity of the CFO the blend ratio is set to 50% to lower the viscosity to a level where it is possible to inject the fuel properly through the injection nozzle. Fuel 4 will serve as a comparison to fuel 3. Fuel 5 is B7 and is chosen due to that this currently is the maximum biodiesel blend allowed by the EN590 diesel specification. Fuel 6 will serve as a comparison to fuel 5.

### 4.2.1 Marine Gas Oil

There are different types of marine petroleum fuels and the terminology can be a bit confusing. However, two basic fuel types can be used to roughly describe the fuels used in the marine industry; residual and distillate [78]. In addition, there are intermediate fuels, which is a blend of residual and distillate fuels. MGO is a distillate fuel and the fuel used in this study has fuel grade DMA (Distillate Marine fuel A) which means that it has properties that resembles number 2 fuel oil or normal petroleum diesel. The fuel specifications that applies for MGO of fuel grade DMA is ISO 8217-DMA, which is built upon the EN590 diesel specification [79]. MGO is made through the process of crude oil refining.

Crude oil is a complex substance of organic liquids containing a mixture of different hydrocarbon compounds and impurities [80]. The crude oil is processed in a refinery, where impurities are removed and the oil is broken down to different useful petroleum products by distillation. The distillation utilizes the different boiling points of the different components in the crude oil. When the crude oil is heated and the temperature increases, the different components evaporates. When the gases rises inside the distillation tower, they are cooled and condenses according to their boiling point. The different petroleum products are separated according to ranges in boiling point, and hence ranges in carbon chain lengths, due to the different temperature zones inside the tower [81]. See Figure 23. This process is called fractional distillation and is the most common way to refine petroleum products. To meet the demand for lighter products, the heavier residual products are often upgraded. This can be done by further distilling the residual products in vacuum and by various types of cracking, where long chained carbohydrates are broken down into lighter products [80].

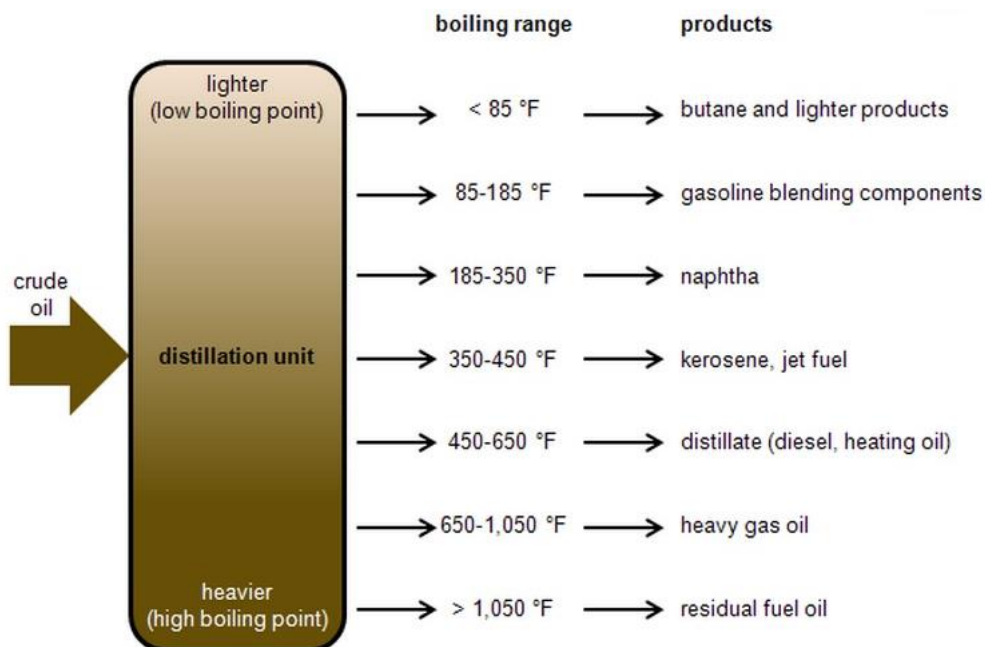


Figure 23: Crude oil distillation [81]



#### 4.2.2 Crude Fish Oil

The crude fish oil (CFO), Figure 24, is a dark brown viscous fatty oil with a distinct smell of fish and is produced from category two aquatic products. Category two aquatic products are farmed fish that has died or been killed for other reasons than human consumption. This oil is currently being used as a dietary supplement for animals not intended for meat production like pets and fur producing animals. The oil has been supplied by Scanbio, a company specialized in production of fish oil and fish meal located at Bjugn, Sør-Trøndelag.



*Figure 24: Crude Fish Oil*

The CFO is produced through a number of steps. First, the biomass is heated to release the oil from the fat depots in the fish. Large fish has to be hashed into smaller pieces before heating to ensure uniform processing. Steam cooking is the preferred way of heating due to the limited amount of water that mixes with the fish mass. To separate the liquids from the solids, the heated fish mass is either pressed, centrifuged or run through a combination of both. After the separation, the products are called press liquor and press cake. The press cake is dehumidified and minced into fish meal. The press liquor consists of oil, sludge and water and has to go through some further purification. First, the press liquor is reheated and sent through a horizontal centrifuge to remove the solids in the sludge. Then it is sent through a vertical centrifuge to separate the oil from the water. The oil is then polished in a special separator to remove any impurities that may still be in the oil to ensure good storage stability. Further processing is not necessary, but the stability of the final product can be further enhanced through heat bleaching and deodorization. The typical yield of this process is 100 kg oil and 200 kg fishmeal for every tonne of raw fish whilst the remaining 700 kg is mainly water. The yield is however dependent on the type of fish used and its oil content [82].

### 4.2.3 Fatty Acid Ethyl Ester

The fatty acid ethyl ester (FAEE) used in this study has been supplied by Marine Ingredients AS. The product is a by-product of the omega fatty acid extraction at their processing plant. The FAEE is a transparent liquid with just a slight fish odor and with a similar viscosity as MGO. See Figure 25. To transform the CFO into FAEE, the process of transesterification is utilized.



*Figure 25: Fatty Acid Ethyl Ester*

#### 4.2.3.1 Transesterification

Transesterification is a chemical process that can be used to produce biodiesel from fatty oils. The process consists of reacting the fatty oil with an alcohol and a catalyst. The most commonly used alcohols for this process is ethanol and methanol. As a catalyst, one can use either an enzyme, an acid or a base, but research recommends using a base catalyst like Sodium Hydroxide (NaOH) or Potassium Hydroxide (KOH), because the reaction time then is faster [83]. Dependent upon the kind of alcohol used, different products are produced. By using ethanol, one ends up with fatty acid ethyl ester and by using methanol the product is fatty acid methyl ester. Both of these products are characterised as biodiesel although their properties are slightly different. Methanol is the most common alcohol used due to its lower price.

Fatty oils contains triglycerides, which is esters that consists of one glycerol molecule and three fatty acid molecules. In the transesterification process, the fatty acid molecules breaks of the glycerol molecule and each of the fatty acid molecules bonds with one alcohol molecule to form a fatty acid alkyl ester [84]. This means that there has to be at least a 3:1 molar ratio of alcohol:fatty oil for a complete reaction to occur. However, the transesterification process

is an equilibrium reaction and hence, an excess of alcohol should be used to ensure that the reaction is pushed towards the products [83]. The process can roughly be divided into three stages. First, one fatty acid molecule breaks of the triglyceride molecule and, together with an alcohol molecule, forms an fatty acid alkyl ester. The remainder is now a diglyceride molecule. Secondly, another fatty acid breaks of to form a fatty acid alkyl ester, leaving a monoglyceride molecule. In the third step, the last fatty acid molecule breaks of and the remainder becomes a single glycerol molecule [84]. During the process, glycerol is hence being formed as a by-product. Glycerol can easily be separated from the biodiesel by letting it settle out due to density differences. Glycerol has a wide range of applications and can be sold separate. The excess alcohol is separated and reused, but is left until the biodiesel and the glycerol is removed because of the danger of reversing the process [85]. Figure 26 shows the chemical reaction of the transesterification process.

The efficiency of this process is high and every product has high value and wide application. As an example, for every 1000 kg of pure triglyceride, 107.5 kg of methanol is needed to produce 1004.5 kg of biodiesel and 103 kg of glycerol [85].

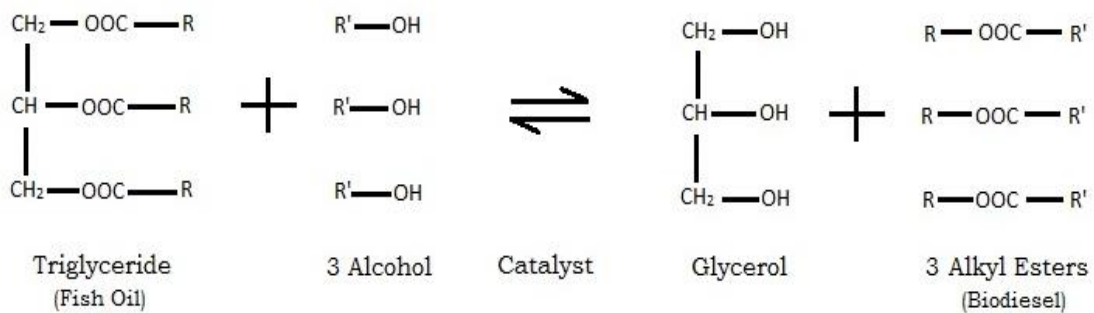


Figure 26: Transesterification Process

#### 4.2.4 Fuel Analysis

To better analyse the results from this study, it is important to know the chemical composition and the different characteristics of the fuels. To obtain this information, the different fuels was sent to analysis. The fuel characteristics was established be Petrotest AS and Independent Inspection Services AB, whilst the chemical composition was established in the laboratory at Marine Ingredients AS.

##### 4.2.4.1 Chemical Composition

The chemical composition of the fuels are presented in Table 9 and Table 10.

Table 9: Fatty Acid Composition of the Fish oils

Fatty Acid	Chemical Structure A:B*	Weight %	
		CFO	FAEE
<b>Myristic</b>	C14:0	2.75	18.97
<b>Palmitic</b>	C16:0	8.84	31.30
<b>Palmitoleic</b>	C16:1	4.34	23.46
<b>Hexadecatetraoic</b>	C16:4	-	4.50
<b>Stearic</b>	C18:0	2.5	2.30
<b>Oleic</b>	C18:1	42.03	9.07
<b>Linoleic</b>	C18:2	13.09	0.95
<b>Linolenic</b>	C18:3	4.93	1.11
<b>Stearidonic</b>	C18:4	0.84	2.40
<b>Arachidic</b>	C20:0	0.33	-
<b>Eicosenoic</b>	C20:1	4.79	-
<b>Eicosadienoic</b>	C20:2	1.43	-
<b>Eicosatetraenoic</b>	C20:4	1.56	0.43
<b>Eicosanoic</b>	C20:5	2.73	5.05
<b>Behenic</b>	C22:0	0.38	-
<b>Erucic</b>	C22:1	3.62	-
<b>Docosapentaenoic</b>	C22:5	1.46	-
<b>Docosahexaenoic</b>	C22:6	3.99	0.47
<b>Tetracosenoic</b>	C24:1	0.39	-
<b>Weight% Chain Length Range C14 - C16</b>		15.9	78.2
<b>Weight% Chain Length Range C18 - C20</b>		74.2	21.3
<b>Weight% Chain Length Range C22 - C24</b>		9.90	0.50
<b>Weight% Saturated Fatty Acids</b>		14.8	52.6
<b>Weight% Mono Unsaturated Fatty Acids</b>		55.2	32.5
<b>Weight% Poly Unsaturated Fatty Acids</b>		30.0	14.9

\*A – Carbon Chain Length, B – Number of Double Bonds

The most obvious difference in fatty acid composition lies in that FAEE mainly consists of fatty acids with short carbon chain lengths, whilst CFO has a more spread distribution with Oleic and Linoleic as main components.

Table 10: Elemental Composition

	MGO	FAEE	CFO
Weight% Carbon	86.32	75.58	76.87
Weight% Hydrogen	13.63	11.98	11.90
Weight% Oxygen	0	12.44	11.23
Weight% Sulphur	0.050	0	0

The elemental composition is as expected with presence of fuel bound oxygen in the bio oils and no sulphur.

#### 4.2.4.2 Fuel Characteristics

Table 11 and Table 12 presents the results of the fuel characteristic analysis. The results for MGO is taken from the analysis done for the first study discussed in the introduction. The reason for this is the high cost of the analysis and that MGO is subject to fuel standards that ensures close to constant fuel characteristics.

Table 11: Fuel Characteristics MGO and FAEE

	Test Standard	MGO	FAEE	50/50% MGO - FAEE	93/7% MGO - FAEE
Density [kg/m <sup>3</sup> ]	EN 12185	849	874.8	862.5	852.7
Viscosity [mm <sup>2</sup> /s]	ASTM D445	3.16	3.84	3.55	3.37
Cetane Index	ASTM D4737	48	56	49.9	49,4
Acid Number [mg KOH/g]	ASTM D664	-	0.1	0.1	0.1
LHV [MJ/kg]	ASTM D240	42.74	37.54	-	-
Oxidation Stability [Hours]	EN 14112	-	>0.5	-	-

Table 12: Fuel Characteristics MGO and CFO

	Test Standard	MGO	CFO	50/50% MGO - CFO	93/7% MGO - CFO
Density [kg/m <sup>3</sup> ]	EN 12185	849	921,9	890.7	857.5
Viscosity [mm <sup>2</sup> /s]	ASTM D445	3.16	31,5	10.5	3.91
Cetane Index	ASTM D976	-	36,4	44.3	50.7
Acid Number [mg KOH/g]	ASTM D664	-	>0.1	>0.1	1
LHV [MJ/kg]	ASTM D240	42.74	37.19	-	-
Oxidation Stability [Hours]	EN 14112	-	3.8	-	-

The dependencies of chemical composition on the fuel characteristics was discussed in section 3.1. By comparing the fuel characteristics with the chemical composition in Table 9 it is possible to identify some contradictions and unexpected relations. These will be discussed briefly in the following.

### *Density*

The density is dependent upon carbon chain length and number of double bonds with the relation, decreasing density with increasing chain length and decreasing number of double bonds. FAEE has a higher percentage of fatty acids with shorter carbon chain length, which should indicate a higher density than CFO. On the other hand, FAEE also has a higher percentage of saturated fatty acids. It is clear from the fuel analysis that CFO has a much higher density than FAEE, which indicates that the amount of saturated fatty acids has a bigger impact on the density than the carbon chain length.

### *Viscosity*

The viscosity is dependent upon carbon chain length and number of double bonds with the relation, increasing viscosity with increasing chain length and decreasing number of double bonds. CFO has a higher percentage of fatty acids with longer chain length, whilst FAEE has a higher percentage of saturated fatty acids. Again, the chemical composition is contradictory, but the viscosity of CFO is much higher and this indicates that the carbon chain length has the biggest impact on viscosity. In addition, the viscosity is dependent on whether the fatty acid composition is mainly straight chained or branched. The fatty acids Oleic and Linoleic, which are the main components of CFO, are both branched and hence results in higher viscosity. Myristic and Palmitic, which makes up close to the same weight percentage in FAEE, are both straight chained and this can contribute to explaining the big difference in viscosity. Due to the big difference in viscosity of MGO and CFO, the viscosity of their 50/50% blend is lower than expected.

### *Cetane Index*

The cetane index is dependent upon carbon chain length and number of double bonds with the relation, increasing cetane index with increasing chain length and decreasing number of double bonds. The chemical dependency follows the same trend as for the density and again the number of double bonds seems to be the factor with highest impact. When it comes to the cetane index, the results may be inaccurate. The laboratory reported difficulties with the distilling of CFO and had to stop the distilling at T60 due to turbulent boiling and extensive smoke formation. The cetane index is therefore calculated with a two variable equation using density and T50 (ASTM D976). For the FAEE the distillation was successful but, as discussed in section 3.1.4, it showed a very flat distillation curve. This makes it hard and inaccurate to determine the three distillation temperatures needed for the four variable equation (ASTM D4737). That the cetane index for the 50/50% and 93/7% blend of MGO and FAEE is almost identical is unexpected regarding the differences in cetane index for the pure fuels. This confirms the criticism this method of determining the cetane index for biofuels has been subject to.

*Oxidation Stability*

The results of the oxidation stability shows that the biofuels are unstable. This was expected, but the magnitude of instability was unexpected and it is the author's assumption that this is mainly due to that the biofuels that are tested in this study is not prepared according to any fuel standard because their current main application is not as fuel. The FAEE has an oxidation stability of less than half an hour and a colour change was observed during the FAEE testing in the CVCC. During the course of a couple of days, the FAEE turned from transparent to light yellow indicating a chemical change.





## Test and Analysis Procedures

### 5.1 Test Procedures

Each fuel has been injected at three injection pressures; 800 bars, 1000 bars and 1400 bars except from both 93/7% blends that only has been injected at 1000 bars due to the similarities to pure MGO. Cold shots and hot shots has been performed for every injection pressure with three different imaging techniques. See Table 13. For all fuels, eight injections were done at each injection pressure to get a basis for statistical evaluation as well as to limit the risk of drawing conclusions based on faulty experiments.

Table 13: Test Procedure

	<b>Injection Pressure [Bar]</b>			<b>Test</b>	<b>Imaging Technique</b>	<b>Injections</b>
<b>Fuel #</b>	800	1000	1400	Cold Shot	Shadowgraph	24
				Hot Shot	Schlieren	24
				Hot shot	Direct Imaging	24

#### 5.1.2 Cold Shot

A cold shot refers to a fuel injection in a test environment without any pre-combustion. This means that the temperature inside the CVCC is too low for auto ignition to occur. During a cold shot, only the injection properties of the fuel is studied and spray characteristics like penetration length and cone angle is of greatest importance. Cold shots can be captured using either shadowgraph or schlieren imaging techniques, however, in this study the shadowgraph technique has been used. The way the control system is set up, the injection of fuel follows the ignition of the gas mixture for the pre-combustion and they are linked in the combustion sequence. For this reason, the rig is filled with nitrogen instead of the ignitable gas mixture to obtain the correct rig pressure. Nitrogen is an inert gas and it is hence not ignited when the ignition signal is sent to the spark plug.

### 5.1.3 Hot Shot

A hot shot refers to a fuel injection in a test environment with pre-combustion. The pre-combustion raises the temperature inside the CVCC to a point where the injected fuel auto ignites. In this study, the hot shots has been combined with both shadowgraph and schlieren imaging techniques to capture all the relevant information. The hot shots are used to determine lift-off length and intensity. In addition, pressure data during combustion is collected to analysis heat release and ignition delay.

### 5.1.4 Boundary Conditions

To make sure that that the tests where done according to the planned procedure, a measurement protocols was established before each test. One measurement protocol covered the test of one fuel at the three injection pressures using one imaging technique. In total, three measurement protocols covered the complete test of one fuel.

The measurement protocols contains all the important boundary conditions of the test and an example of a measurement protocol is found in Appendix C.

#### 5.1.4.1 Test Environment

Pressure, temperature and density conditions are influencing the spray development and the combustion characteristics. To be able to compare the different fuels it is hence important to inject the fuels in the same test environment. This is addressed by filling the CVCC with a constant 10 bars of gas mixture before the pre-combustion and by keeping a constant point of injection of 3 seconds after pre-combustion for all tests. This will give constant injection conditions if the pre-combustion and the heat transfer processes are stable. The processes are however not stable and improvements on insulation and the implementation of internal electrical heating to reduce the temperature differences is being conducted in a parallel master thesis. For optimal experiment precision, the point of injection should be temperature controlled, but this is not the case at the moment. For the cold shots, 10 bars of nitrogen was filled. Based on the averaged data from the tests, the boundary conditions are listed in Table 14.

*Table 14: Boundary Conditions*

<i>Environment Condition</i>	<i>Averaged Value</i>
<i>Pressure before pre-combustion [Bar]</i>	$10 \pm 0.1$
<i>Pressure at Injection [Bar]</i>	$19.5 \pm 0.5$
<i>Temperature at Injection [°C]</i>	$530 \pm 11$
<i>Density during experiment [kg/m<sup>3</sup>]</i>	$12 \pm 0.2$

### 5.1.4.2 Injector Opening Time

If the opening time of the injector is held constant during the test of the different fuels this will, due to differences in fuel characteristics, give an unfair evaluation basis. For this reason, it was necessary to perform a delivery test on the injector.

A delivery test is used to determine the quantity of fuel that is delivered in one injection at different injector opening times and injection pressures. This quantity varies based on fuel characteristics like viscosity, density, bulk modulus etc. The test is performed by injecting multiple injections in a container and weigh it to establish the injected mass. The delivery test was performed at injection pressures of 800, 1000 and 1400 bar and with injector opening time of 300, 350, 400, 500 and 800 microseconds. Based on injection pressure and opening time, it was injected between 1000 and 4000 injections and an average weight per injection was calculated. By making use of the fuels density the injected mass was converted to injected volume and the injection curve, Figure 27, were plotted.

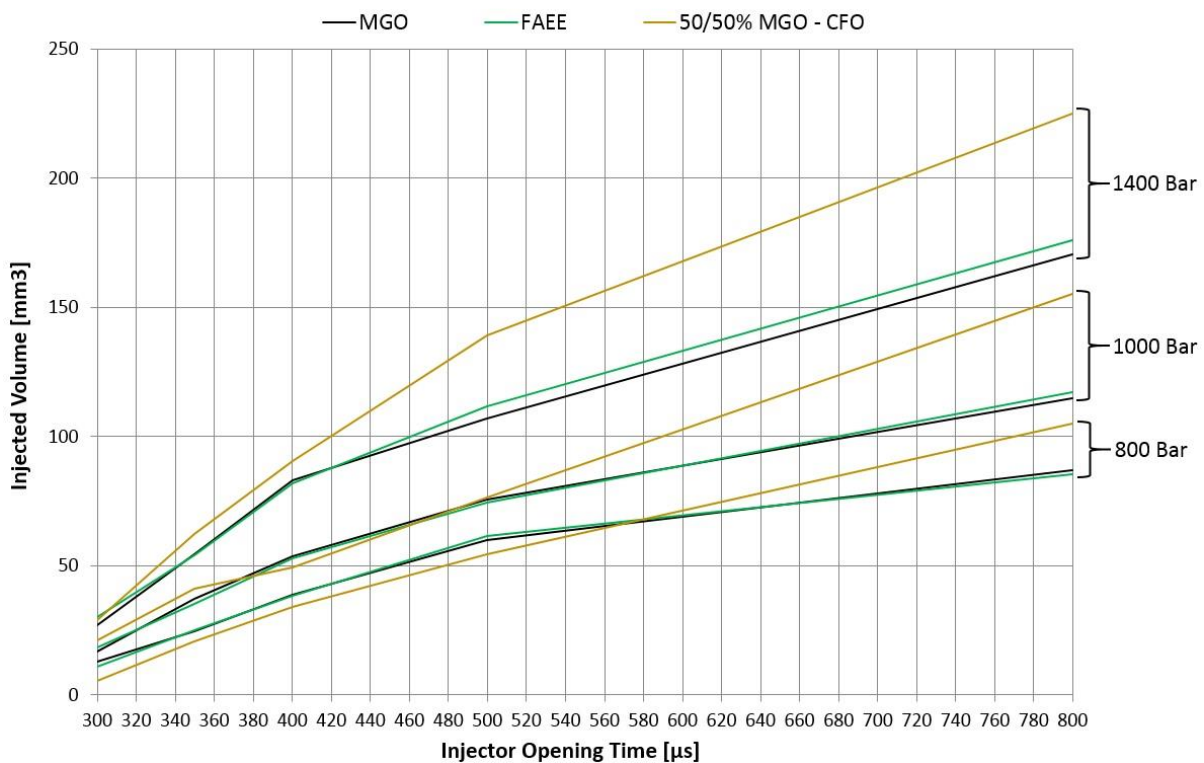


Figure 27: Volume Injection Curve

To establish the optimal injection conditions, the results of MGO testing with different injected volumes were analysed. With the current setup there is a trade off that has to be accounted for between the thermodynamic analysis and the image analysis. For the thermodynamic analysis, it is easier to see differences between the fuels when more fuel is injected. The problem with injecting more fuel is that it penetrates out of the diameter of the window, discussed in section 4.1.5, and information is lost. The injected volume that gave the most consistent results was 83 mm<sup>3</sup> and this was set as the boundary condition.

However, the best way of evaluating different fuels is by comparing them based on energy. By making use of the fuels heating value the injected energy curves were plotted, Figure 28. For MGO, 83 mm<sup>3</sup> corresponds to 3011 Joules and the injector opening times for the other fuels was calculated to give the same amount of injected energy. Due to the extensive time consumption of these test they have only been performed for MGO, FAEE and the 50/50% blend of MGO and CFO. The opening time for pure FAEE at 800 bar injection pressure and for the other blends has been established by linear regression over the respective curve segment. The injector opening times are summarized in Table 15 where the opening times has been rounded to the nearest 10<sup>th</sup> micro second due to limitations on the injector.

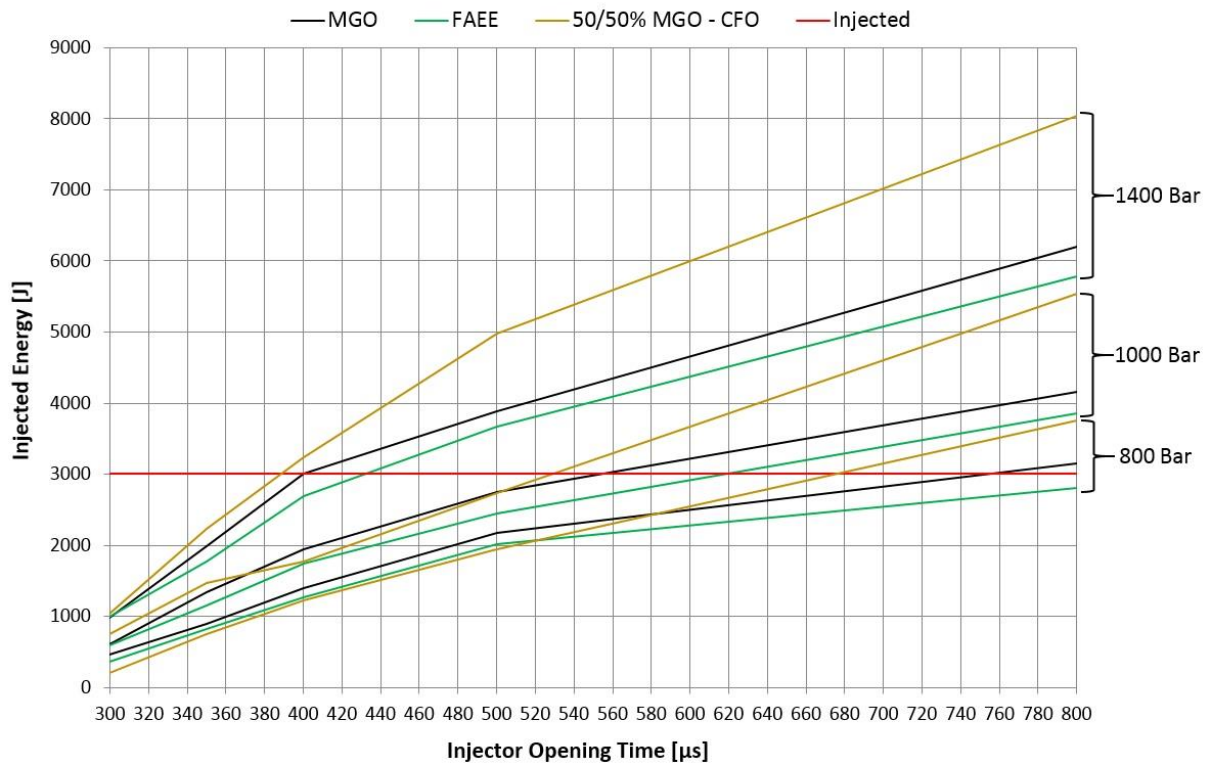


Figure 28: Energy Injection Curve

Table 15: Injector Opening Times [μs]

Injection Pressure [Bar]	MGO	FAEE	50/50% MGO - FAEE	93/7% MGO - FAEE	50/50% MGO - CFO	93/7% MGO - CFO
800	760	880	820	770	660	750
1000	560	620	590	560	530	560
1400	400	430	420	400	390	400

## 5.2 Image Analysis

As discussed in section 3.2, it is possible to predict spray characteristics by empirical equation. However, in this study the spray characteristics have been determined by analysing images of the actual spray. The image analysis is done using a Matlab script produced by MARINTEK. The script reads the raw images captured by the high-speed camera and assigns each pixel in the picture a value between zero and one according to its intensity. Zero being black and one being white. Based on a threshold value the script converts the initial grey scale images into a black and white images. In this study, the threshold has been kept constant at 0.5, which means that every pixel with a value equal to or above this is given a value of one and every pixel with values below this is turned to zero.

The camera is triggered by the injection signal and due to some latency in the system, the first image in each image series has no spray development. This image is subtracted from all the other images to delete any background noise. The spray characteristics are found by searching for the edges in the extremities of the spray to produce vectors for further calculation. These edges are determined using the Canny edge detection method, which basically means that the script is searching for the points where the pixel values turn from one to zero or from zero to one. Figure 29 shows a raw image of a cold shot and Figure 30 shows an intensity scaled output of the analysed image.

For the intensity scaling the script goes back to the grey scale pixel values and, instead of converting the pixels to either black or white, a RGB (Red Green Blue) colour model extension is applied. This means that each pixel is given a value between 0 and 255 according to their initial grey scale pixel values and a colour map of the spray is plotted. For the cold shots, the liquid phase is given the highest intensity, whilst the more diluted edges of the spray are shown with less intensity. The opposite intensity scaling is used for the hotshots, where the combusted region and the soot formation is of higher interest. Figure 31 shows a raw image of a combusting spray using the direct imaging technique and Figure 32 shows the output of the Matlab analysis. The total spray intensity is found by summing the intensity values in each pixel. All the spray data is written to an Excel spreadsheet for further analysis and plotting of spray behaviour.

To convert number of pixels into a measure of distance, a ruler is placed inside the CVCC and an image is analysed to obtain the pixel to millimetre scale ratio. With the current setup, this scale ratio is 3.65.

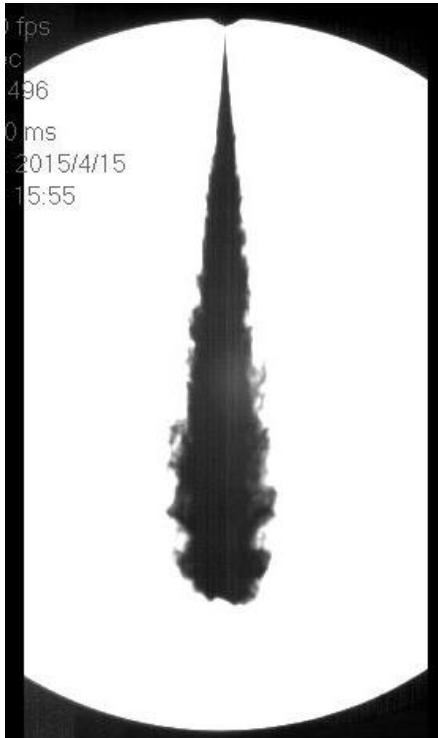


Figure 29: Raw Image Cold Shot

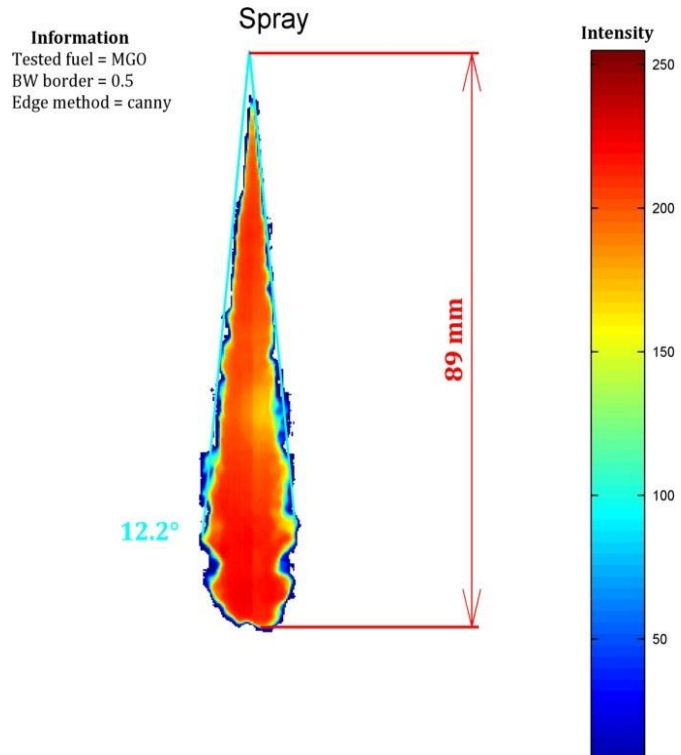


Figure 30: Cold Shot Analysis Output

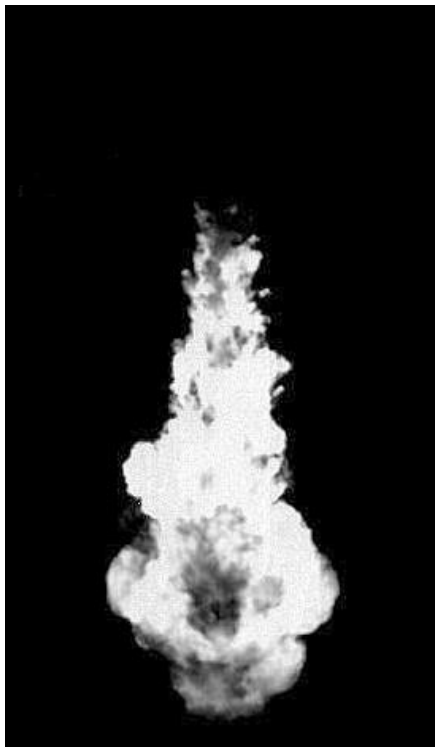


Figure 31: Raw Image Hot Shot

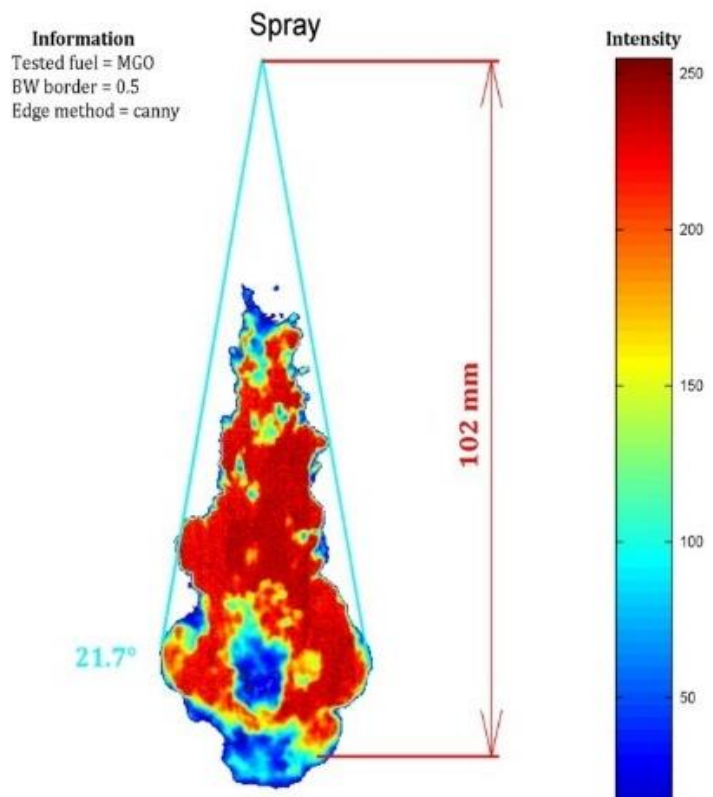


Figure 32: Hot Shot Analysis Output

## Chapter 6

# Results and Discussion

In the following, the results of the study is presented. Due to the huge amount of data and similar trends for all fuels across the different injection pressures, only the results for 1000 bar injection pressure will be presented. The influence of different injection pressures will be discussed by presenting plots comparing the injection of pure MGO. In addition, only the results obtained from the imaging technique that is best suited for the different characteristics will be used to discuss the spray characteristics. Image series covering the spray development of all fuels at 1000 bar injection pressure is found in Appendix D and an image series of MGO at the different injection pressures can be found in Appendix E. Both image series are from the Schlieren imaging technique since they are the most detailed. The rest of the results from the image analysis are presented in Appendix F.

All the results from the analysis of spray characteristic are adjusted for ignition delay. This means that all fuels are shifted to an averaged ignition delay. This makes the fuels individual spray development easier to compare and the trends more clear. Ignition delay is discussed in a separate section.

## 6.1 Spray Characteristics

### 6.1.1 Penetration Length and Cone Angle

The penetration length and the cone angles are linked and are hence discussed together. In this study, the viscosity and injection pressure are the factors with most influence since chamber density, chamber temperature and injection nozzle geometry are all kept constant.

The results are based on cold shots. During hot shots, there are a high degree of turbulence in the extremities of the spray due to the temperature differences caused by the combustion. This turbulence may influence the spray development and make it more random. By comparing them based on non-reactive shots, the influence of different fuel characteristics on the spray development is isolated, which makes the results more stable.

The penetration length and the cone angle is linked through jet theory. Based on conservation of momentum, the jet theory states that longer penetration corresponds to narrower cone angles and vice versa. This is due to that fuel droplets with higher momentum penetrates longer and is less affected by shear forces and other influences forcing the droplets outwards. The jet theory is linked to viscosity through the atomization process. Theory argues that increasing viscosity causes worse atomization due to bigger pressure drop across the injection nozzle with corresponding lower turbulence at the orifice exit and a reduction in spray jet instability. Worse atomization creates bigger fuel droplets, and it is expected that a trend based on viscosity can be observed in the results. This relation between viscosity, penetration length and cone angles has been reported in other studies [86], [87], [88].

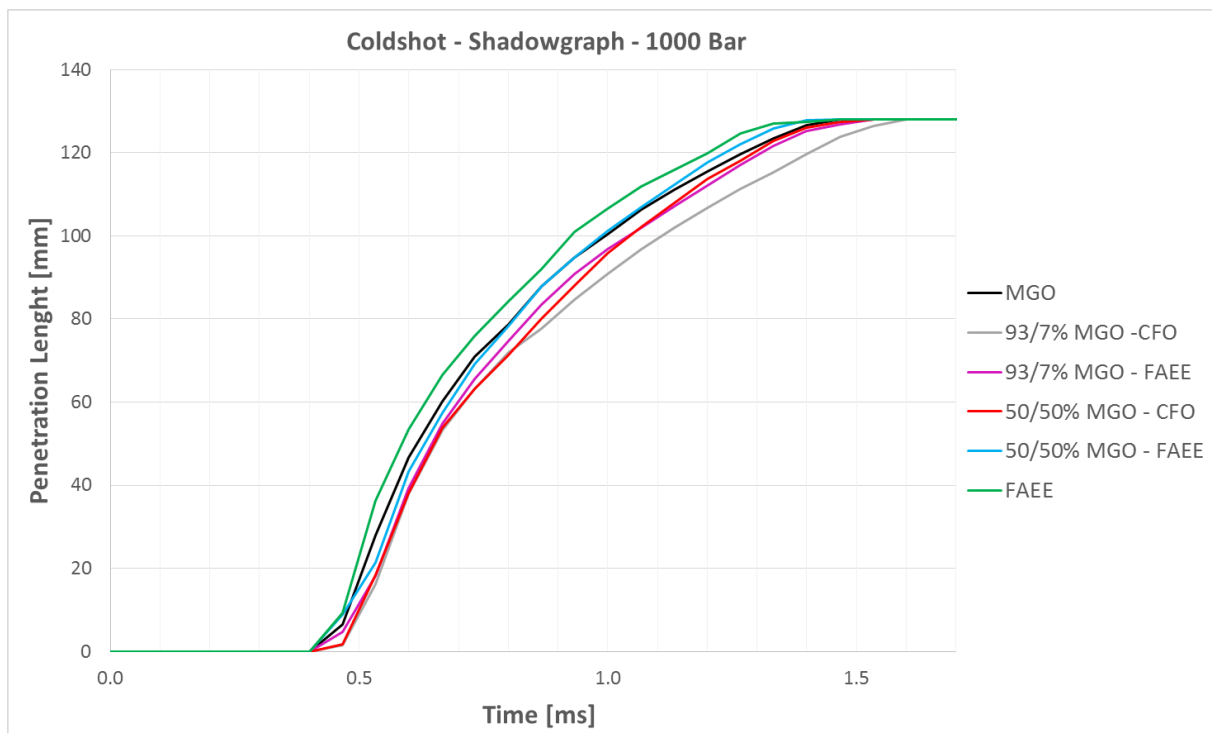


Figure 33: Penetration Lengths for all fuels



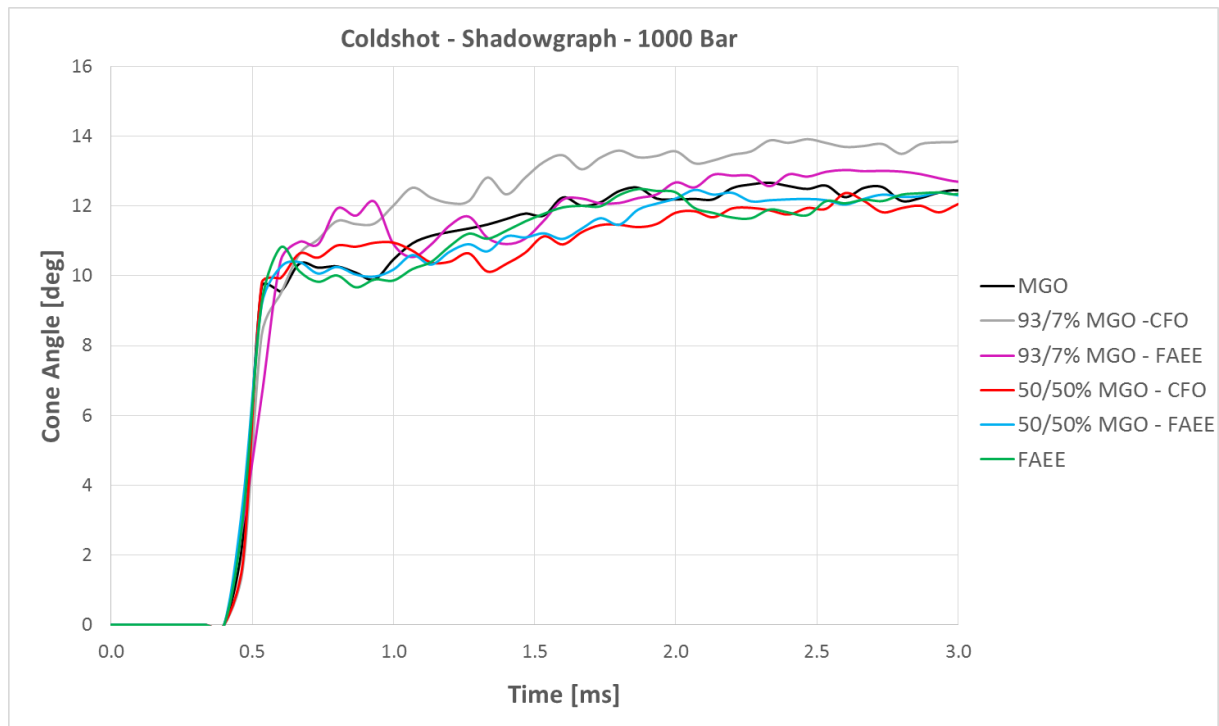


Figure 34: Cone Angles for all fuels

Figure 33 shows the penetrations lengths recorded for the different fuels and Figure 34 shows the corresponding cone angles. The results are not as expected. There are hardly any relation based on viscosity and neither when leaving the viscosity and atomization process out, by only comparing the fuels based on their development at different time steps. The only fuel that fits the jet theory is the 93/7% blend of MGO and CFO with shortest penetration and biggest cone angle. However, when seen in relation to the other fuels its behaviour is in conflict with the theory based on viscosity and it looks more to be a coincidence due to problems with the chamber density boundary condition.

The results are hard to explain and the spray unfortunately penetrates out of the window. It may be that it would have been easier to see a trend if the hole spray was visible, though this is unlikely. By looking at the cone angles, the spray shape is fully developed before it exits the visible area, but it would anyway have been interesting to see if there were a difference. The only thing that might explain the results is to study the statistics.

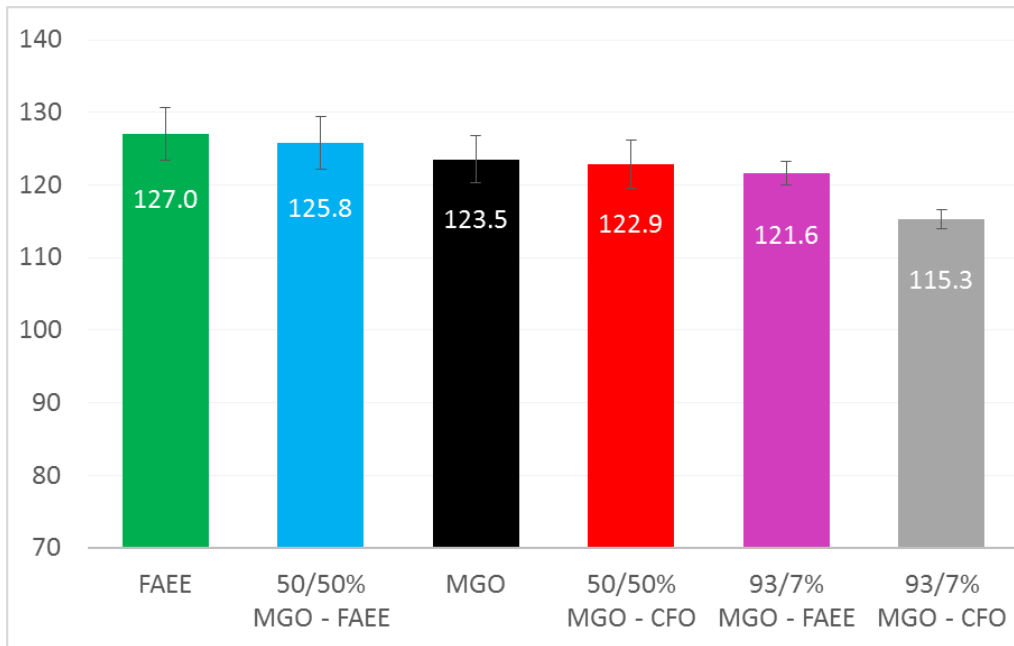


Figure 35: Penetration Length [mm] at 1.333 ms

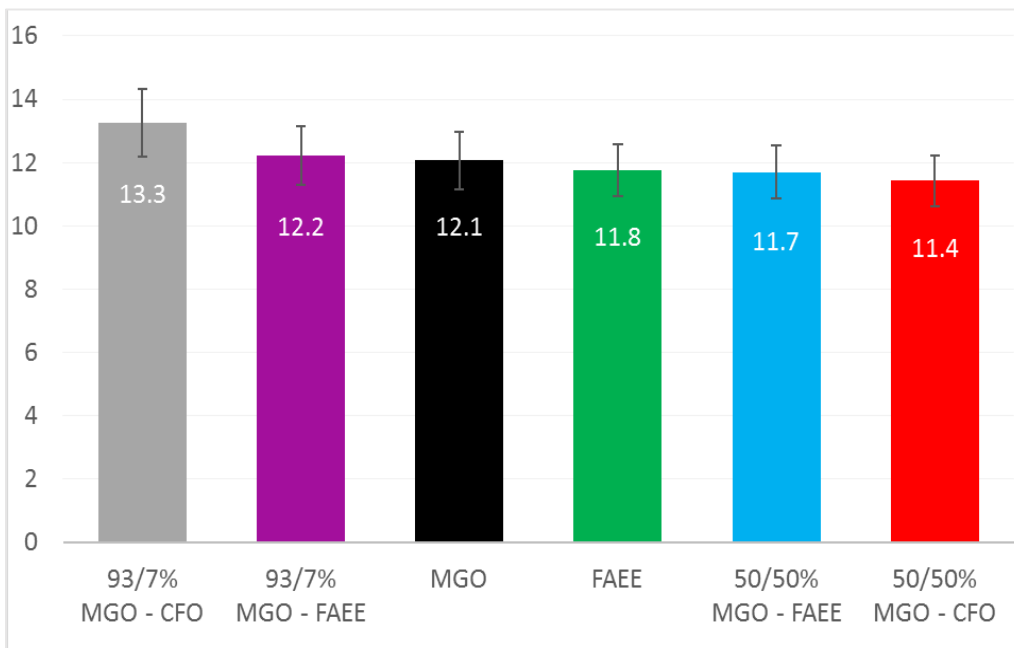


Figure 36: Averaged Cone Angles [deg]

Figure 35 show the penetration length of the different fuels just before they penetrate out of the visible area and Figure 36 shows the averaged cone angle in the fully developed region between 1.0 – 3.0 ms. The error bars are representing the standard deviation of the results. No clear relation can be seen here either, but since the error bars are intersecting each other for most of the fuels the differences between them is within the error of the experiment. Thus, the only thing that can be stated is that all fuels are exhibiting similar behaviour.

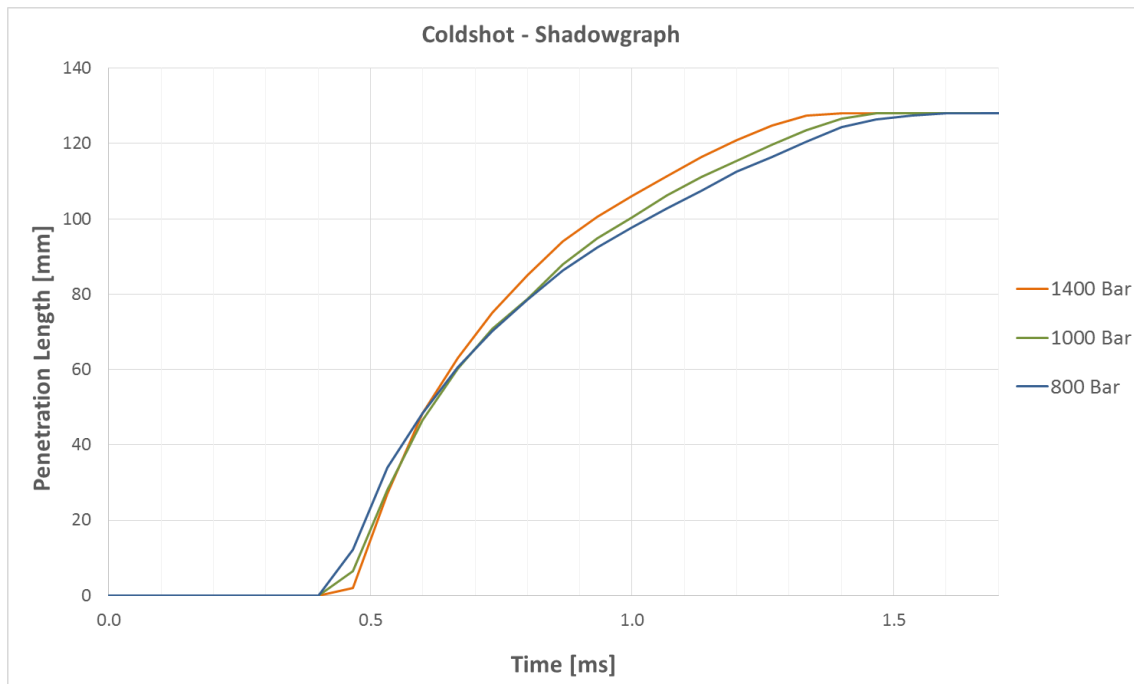


Figure 38: Penetration Length for MGO at Different Injection Pressures

Figure 38 and Figure 37 shows the penetration length and cone angles for MGO at different injection pressures. The cone angles increases with increasing injection pressure, due to better atomization. The smaller fuel droplets with less momentum are more affected by resistance in the chamber and are forced outwards. The penetration length is increasing with increasing injection pressure due to the increasing injection velocity and the increasing velocity overcomes the effect of better atomization and less momentum. These relations are found for all fuels and is in accordance with findings of other authors [87], [88].

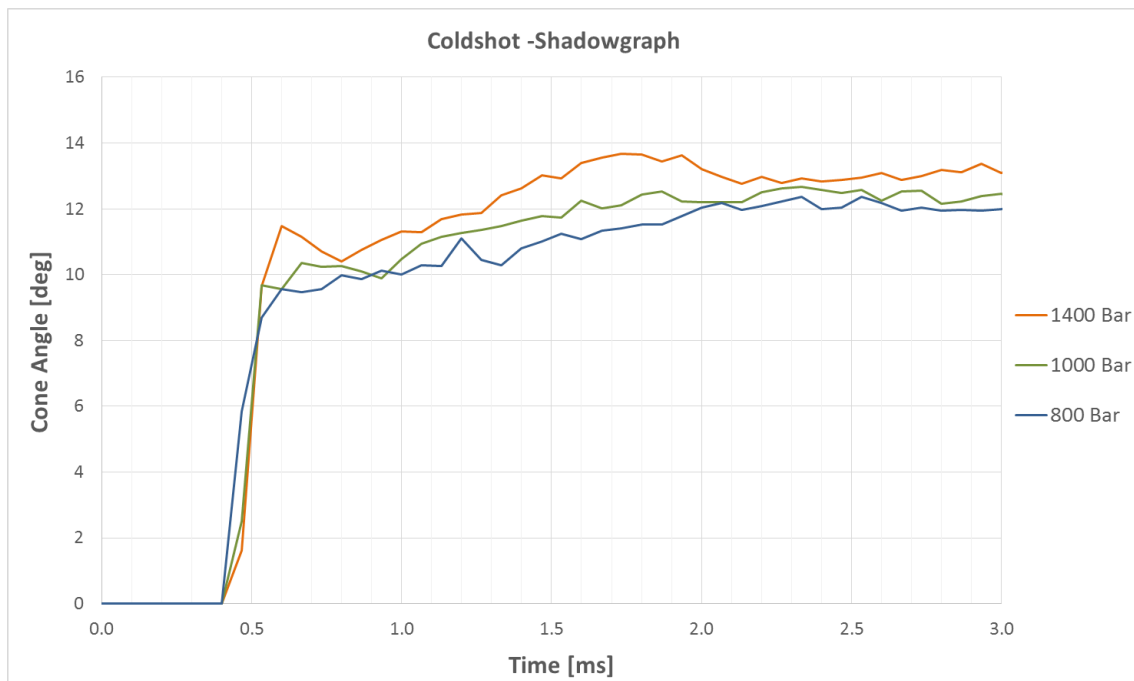


Figure 37: Cone Angle for MGO at Different Injection Pressures

### 6.1.2 Additional Considerations on Spray Penetration and Cone Angle

The chamber density has an important influence on the cone angles due to the resistance the spray meets. The chamber density used in this study is very low and it might be that it is too low to really see a difference based on fuel characteristics. The small differences that can be observed might be due to instability in the boundary conditions rather than fuel characteristics.

It was expected that for penetration length and cone angle, the cold shots would give a clearer picture because of the stable spray development of a non-reactive spray. However, the results for the hot shots gives bigger differences between the fuels and paints a somewhat clearer picture. At least for the MGO, FAEE and their blend it is possible to see a trend indicating longer penetration and narrower cone angles with increasing fuel viscosity.

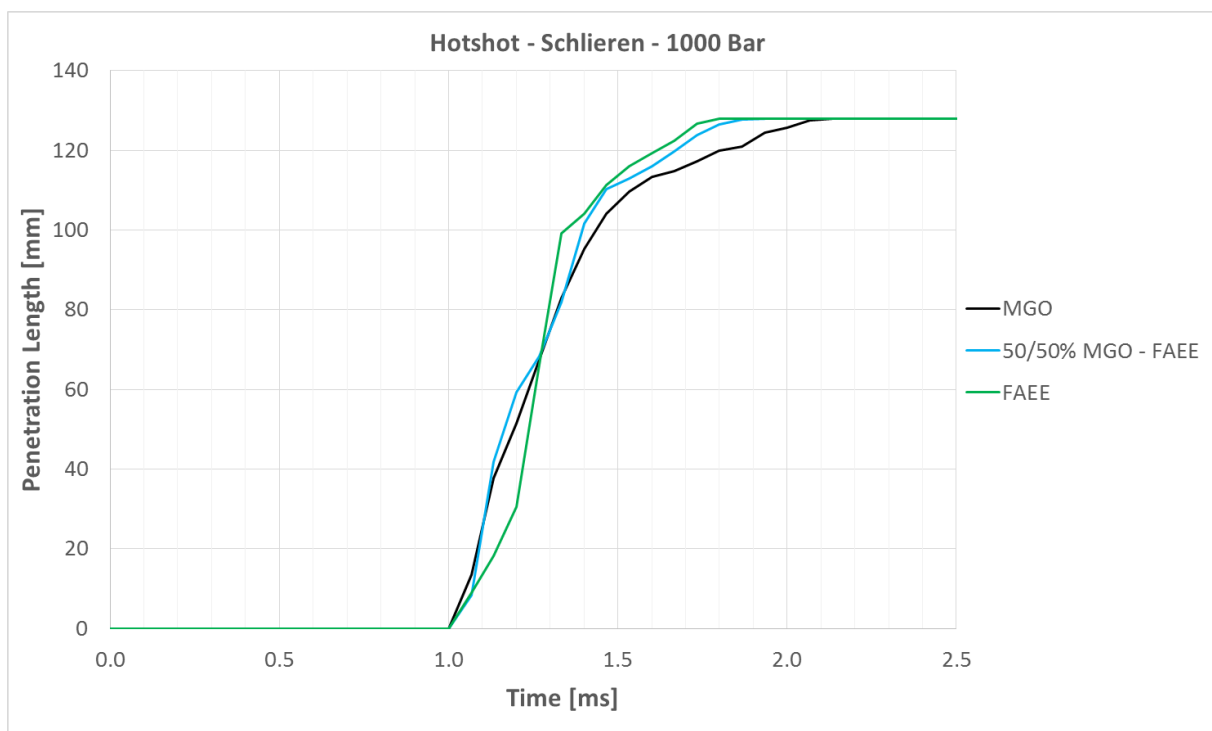


Figure 39: Penetration Length Hotshots

Figure 39 shows the penetration length for the hot shots using the schlieren imaging technique. Only MGO, FAEE and their 50/50% blends are shown here because they fit the model best and makes it possible to explain the expected results. A plot including all blends can be found in Appendix F. By looking at the cone angles in Figure 40 it can be seen that the spray shape has stabilized around 1.5 ms. The penetration length after 1.5 ms shows the difference that was expected and reported by others. The higher viscosity of FAEE makes it penetrate the longest, followed by the 50/50% blend and pure MGO.

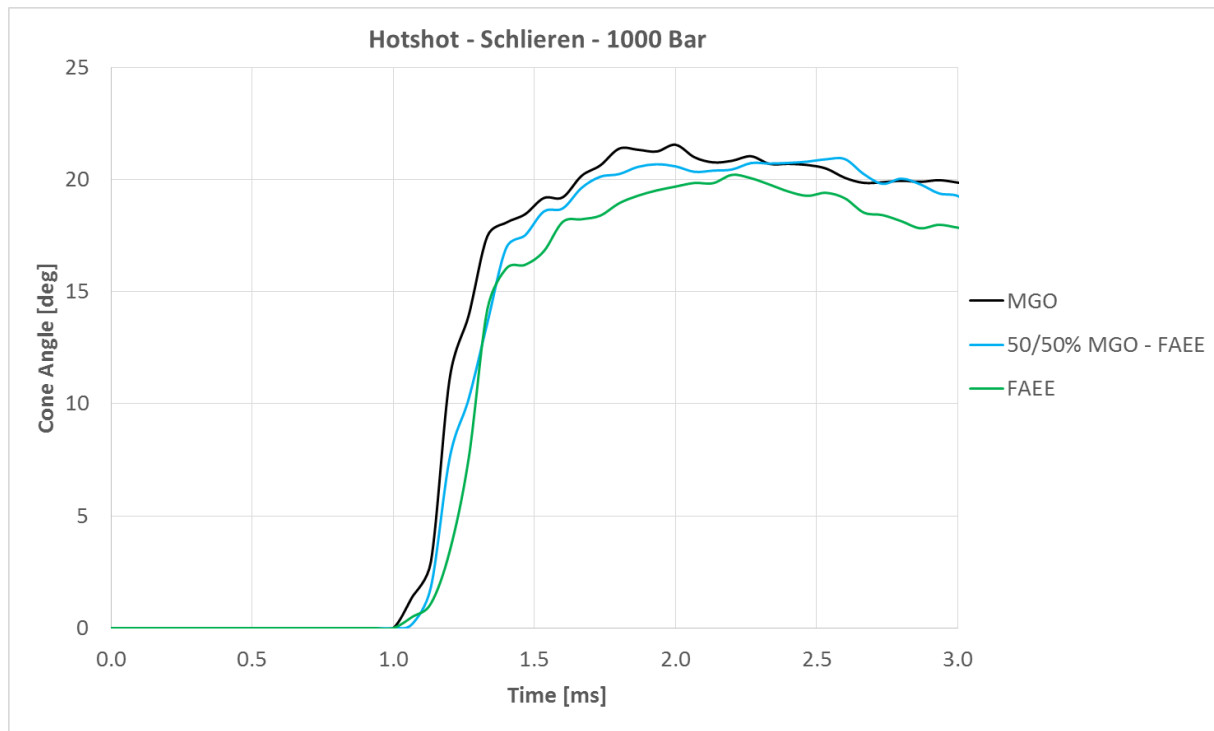


Figure 40: Cone Angle Hotshot

Figure 40 shows the cone angles for hot shots using the schlieren imaging techniques. The same trend as for the penetration can be seen, as well as their correlation through jet theory. Longer penetration corresponds to narrower cone angles.

There would be interesting to see how the results would have been if tests with non-reactive sprays in a hot environment was performed. This can be done by electrically heating the combustion rig and inject the fuel in an environment with no oxygen, or with a pre-combustion of a gas mixture which after pre-combustion has no oxygen left for the main combustion. These tests will capture the impact of the vaporization process on the cone angle and probably give better results than the cold shots provided in this study.

### 6.1.3 Lift-Off Length

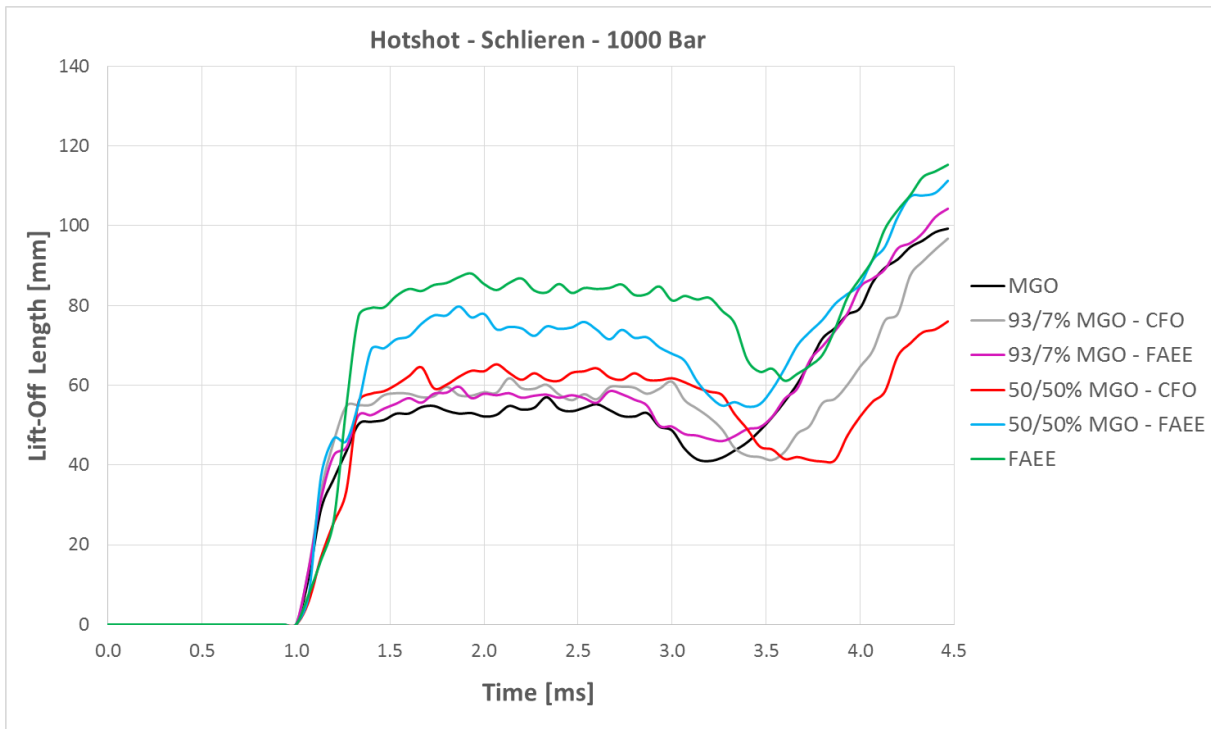


Figure 41: Lift-Off Length for all Fuels

Figure 41 shows the lift-off length for the tested fuels and shows typical lift-off length behaviour for all fuels. After ignition, the lift-off length is rising steeply before it levels out during injection. After the opening signal to the injector is terminated, the needle needs some time to close and the fuel that leaves the injection nozzle during this period has a lower velocity and hence penetrates shorter before it is burned. This is indicated by the area around 3.5 ms where the lift-off length is reduced before it again increases as the rest of the fuel in the chamber is burned. Figure 42 is an example of an image series showing this development.

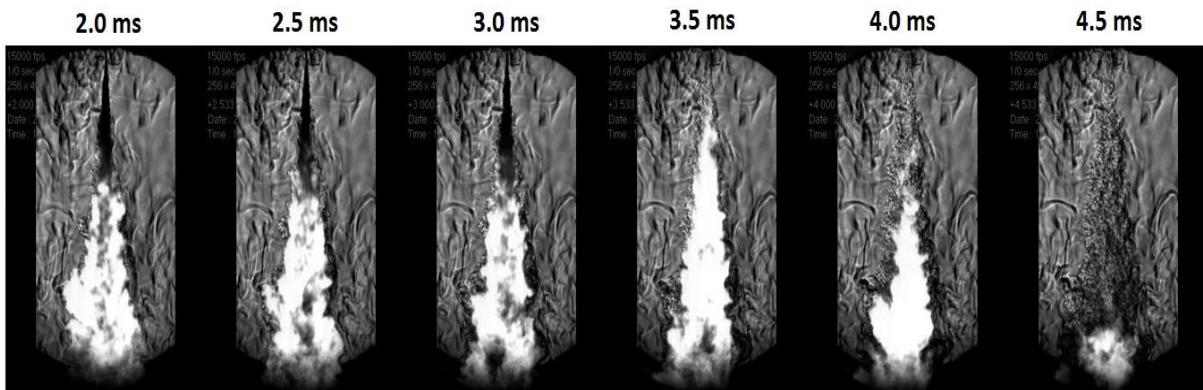


Figure 42: Image Series of Combusting Spray

The interesting region is between 1.5 ms and 3.0 ms. In this region the lift-off length is more or less stable for all fuels and the distance from the nozzle tells us the distance the fuel has had for mixing. The equivalence ratio at the lift-off length is decreasing as the lift-off length increases because more ambient oxygen has time to entrain the spray jet [89]. Low equivalence ratios help to suppress soot formation and the lift-off length relation can be seen in the results of the intensity analysis in section 6.2.1.

Of all the parameters influencing the lift-off length, as discussed in section 3.2.3, the viscosity is the only one not kept constant. It is possible to see a clear trend indicating longer lift-off length with increasing viscosity for MGO, FAEE and their blends. The CFO blends do not follow this trend, which indicates that other factors are influencing the results. The 50/50% blend of MGO and CFO has approximately three times higher viscosity than the other fuels and it was expected to show significantly longer lift-off length. It is possible that the viscosity of this fuel is too high and that the increased pressure drop across the injection nozzle causes the injection velocity to decline to a point where the ignitable air-fuel mixture occur earlier with a similar effect as when the injection needle is closing. The 93/7% blend of MGO and CFO has a slightly higher viscosity than FAEE and it was expected to have a similar lift-off length. It can be argued that a fuel with lower cetane index should have a longer lift-off length due to the increased ignition delay, but no trend can be found by comparing cetane index for the CFO blends either. Further investigation of the CFO must be carried out to find the causes for it to deviate from the expectations at to get a clearer picture of its behaviour.

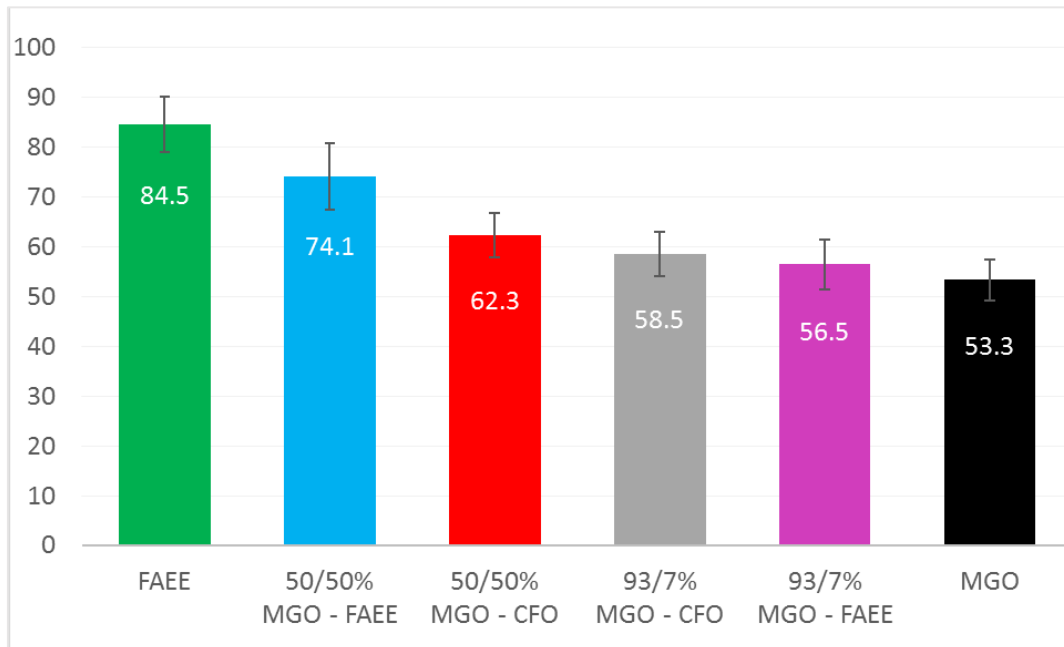


Figure 43: Averaged Lift-Off Length [mm]

Figure 43 shows the averaged lift-off length in the region between 1.5 ms and 3.0 ms. With the current camera frame rate this corresponds to 23 measurement points and the error bars indicates the averaged standard deviation over these points. The same trend can be seen here. However, the error bars are intersecting each other for some of the fuels and the only thing that can be said for certain is that FAEE and it 50% blend with MGO has the longest lift-off length. The other fuels exhibit more or less the same lift-off length behaviour.

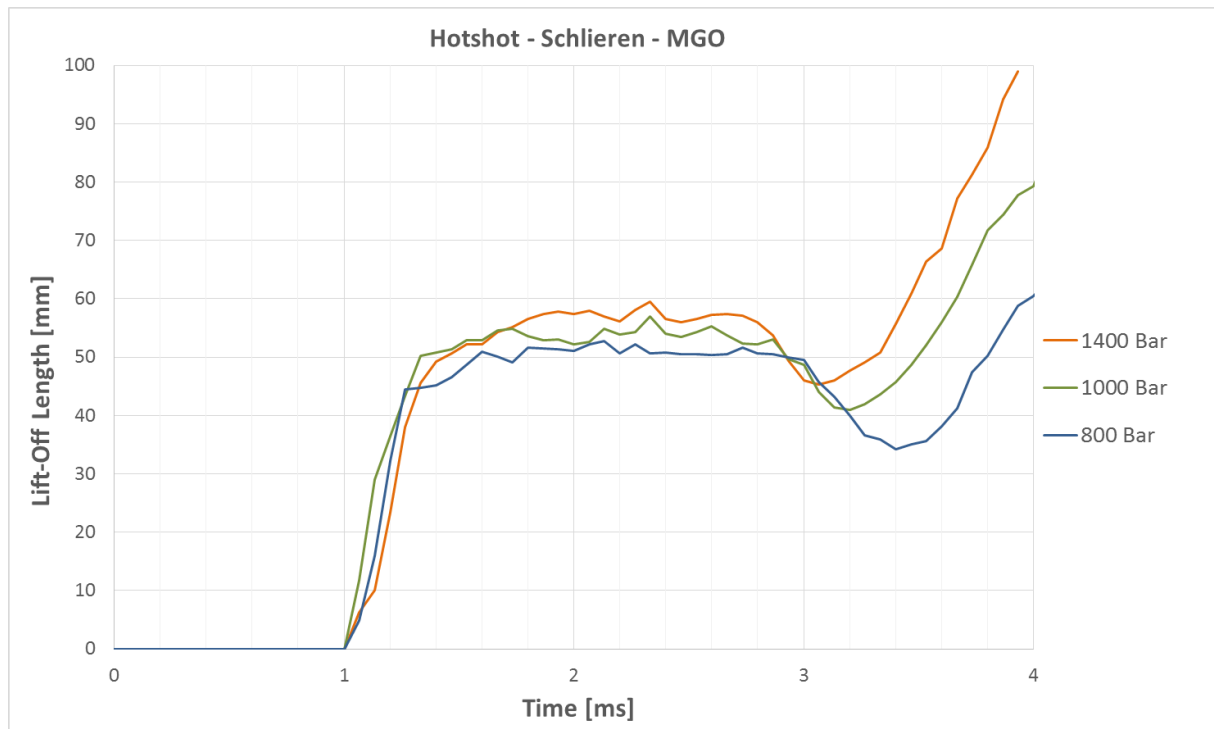


Figure 44: Lift-Off Length for MGO at Different Injection Pressures

Figure 44 shows the lift-off length for MGO at the three injection pressures. 1400 bar corresponds to the longest lift-off length due to the increased injection velocity. The increased injection velocity means that the spray penetrates longer before it reaches an ignitable mixture of fuel and air. A left-shift towards the end with increasing injection pressure can also be seen. This is because the combustion duration becomes shorter as the injection pressure increases. Due to the better atomization process, the fuel burns faster and the trend is the same for all fuels.



## 6.2 Combustion Characteristics

### 6.2.1 Radiation Intensity and Soot Formation

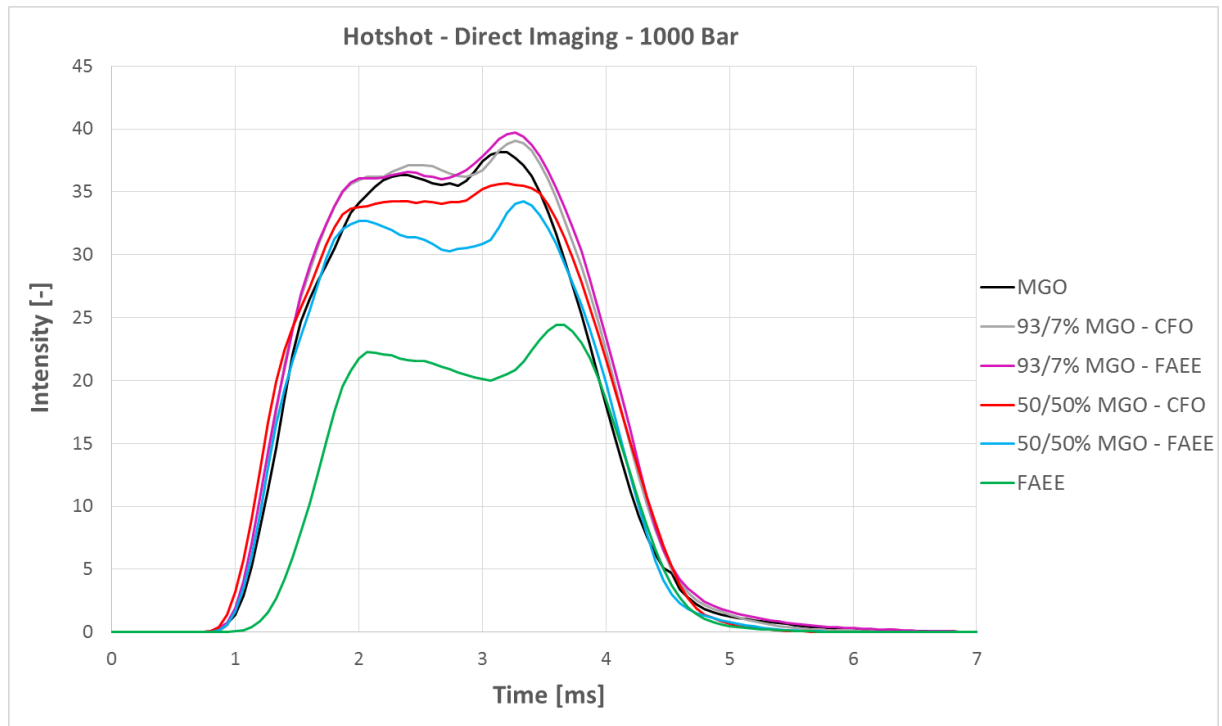


Figure 45: Radiation Intensity for all Fuels

The results from the analysis of combustion radiation intensity is shown in Figure 45. Theory argues that the presence of fuel bound oxygen improves the mixing process causing a more complete combustion with less soot formation. As discussed in section 3.3.1, the radiation intensity is linked to the formation of soot, and the results are as expected with a clear trend of decreasing radiation intensity with increasing oxygen content. These results are in accordance with [1], [90], [84] and [91], which all are reporting lower soot emissions when burning oxygenated fuels.

The shape of the curves can be seen in relation to the lift-off length. Both the increased amount of oxygen in the fuel and the increased amount of ambient oxygen that has time to entrain the spray jet as the lift-off length increases helps to suppress the soot formation. This extra oxygen and its effect on the combustion efficiency is the root cause of the lower soot formation for the fish oils and their blends. The increase in intensity around 3.5 ms comes from the same reason as for the decreasing lift-off length in this region. As the flame retracts towards the injection nozzle, the flame area gets bigger and more intensity is recorded.

The one fuel that really separates from the others are the pure FAEE. It may look like FAEE has a longer ignition delay then the other fuels due to the right shift of its intensity curve, but for this plot the ignition delay is accounted for. The difference in slope and peak intensity is

because of the improved combustion process, causing less soot. Another observation is that it is no linear relation between blend ratio and sooting tendency as may be expected. The blends show intensity curves that are more similar to MGO except from differences in peak intensity, and it looks as if the blends inherits more of the sooting tendency of MGO then those of the fish oils.

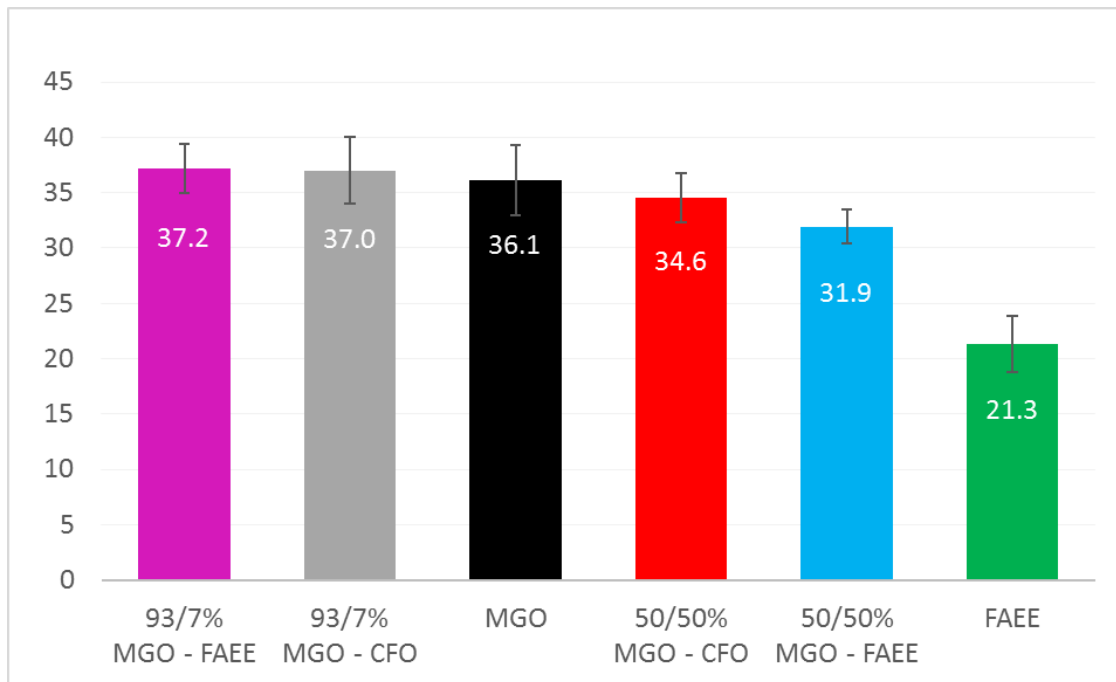


Figure 46: Averaged Intensity [-]

Figure 46 shows the averaged intensity in the region between 2.0 – 3.5 ms with error bars indicating the standard deviation. That the 93/7% blends show higher sooting tendency than MGO is a mystery, which the author has no explanation for. It was expected that it would be hard to detect a difference, but that they would exhibit higher sooting tendency is unexpected. By looking at the error bars, it is clear that difference is within the standard deviation of the test and this is probably the explanation.

The other fuels show a clear trend and agrees with theory, but also here, the error bars are intersecting and it is dangerous to say anything for certain. Pure FAEE stands out and shows significantly less soot formation than the other fuels and this correlates well with [1] who tested the same fuel in an engine and measured the soot emissions.

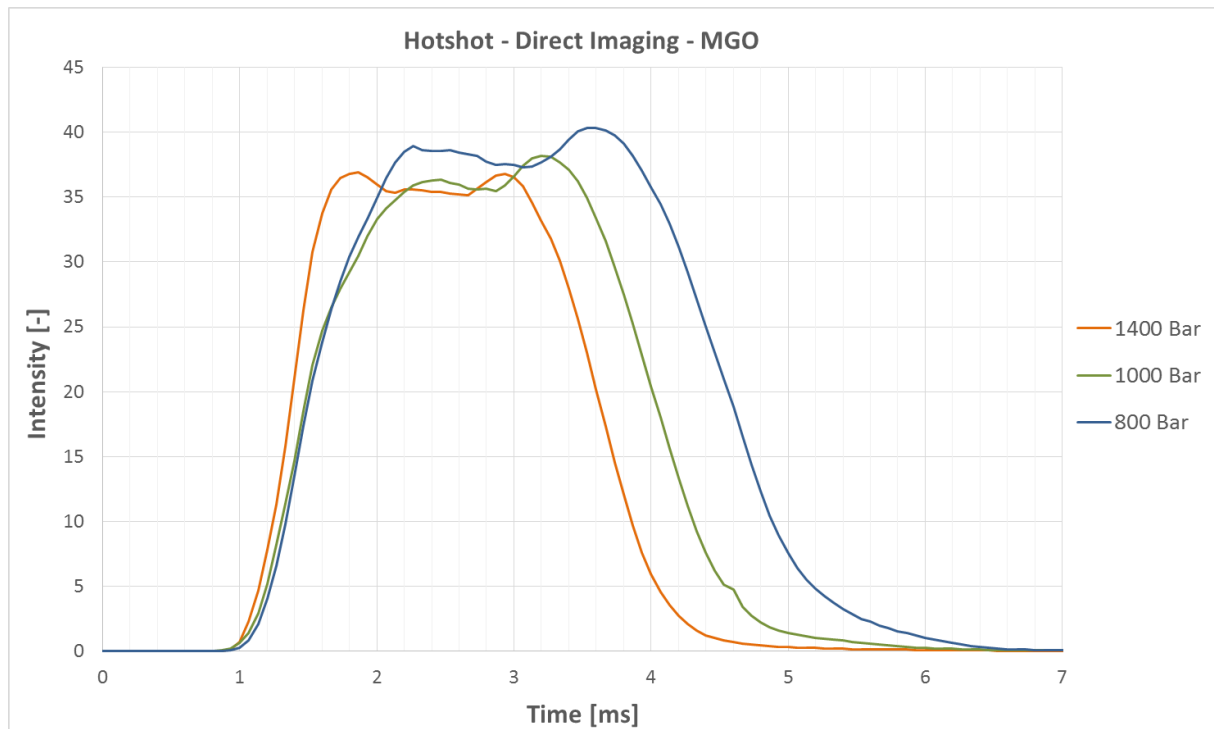


Figure 47: Radiation Intensity for MGO at Different Injection Pressures

Figure 47 shows the intensity for MGO at the three injection pressures. Here we see a trend indicating lower soot formation with increasing injection pressure. This is as expected due to better atomization, better air-fuel mixing and a more complete combustion process with higher combustion efficiency. As for the lift-off length, the intensity gets a left-shift with increasing injection pressure due to shorter combustion duration.

### 6.2.2 Notes on the Thermodynamic Analysis

In the following sections the results from the thermodynamic analysis will be presented. The timescale of these results are a bit shifted compared to the results from the image analysis. When comparing the heat release to the images, it is a noticeable delay in the pressure acquisition. By looking at the image series in Appendix D, it can be noted that none of the fuels show a combustion duration of more than approximately 4 ms for 1000 bar injection pressure. Neither do they show end of combustion later than approximately 5 ms. Figure 48 show the heat release at 1000 bar injection pressure. It can be seen that for all fuels the peak heat release is at approximately 5 ms, which cannot be the case. A peak heat release after all the fuel has burned is obviously not possible and the time scales are clearly not correlated.

The author has no good explanation for this, but a theory might be that since the volume of the CVCC is so big compared to the volume of fuel that is injected it takes some time before the pressure sensor notice a pressure increase. It might also be that there are some delay in the communication between the sensor and the computer. The fact that the spray penetrates out of the window and some information is lost in the images is ruled out as the reason. By calculating the MFB at the time corresponding to end of injection in the pictures, one ends up with approximately 10%. A MFB of 10% when the entire fuel charge has been delivered is clearly not realistic. If the penetration length was so long that most of the fuel charge ended up wetting the wall and not combust, the MFB 10% might have been plausible. This is however not the case either. The combustion efficiency shows normal tendencies with values within the expected range.

These differences in the time scale between the image analysis and the thermodynamic analysis is however not a big problem. Since this is a qualitative study, the axis values are less important than the behaviour of the fuels in relation to each other. The only problem is that this makes it hard to compare the results from the images with the thermodynamic data. This timescale issue should be looked into and solved in further studies due to the extra insight this comparison can provide.

### 6.2.3 Rate of Heat Release

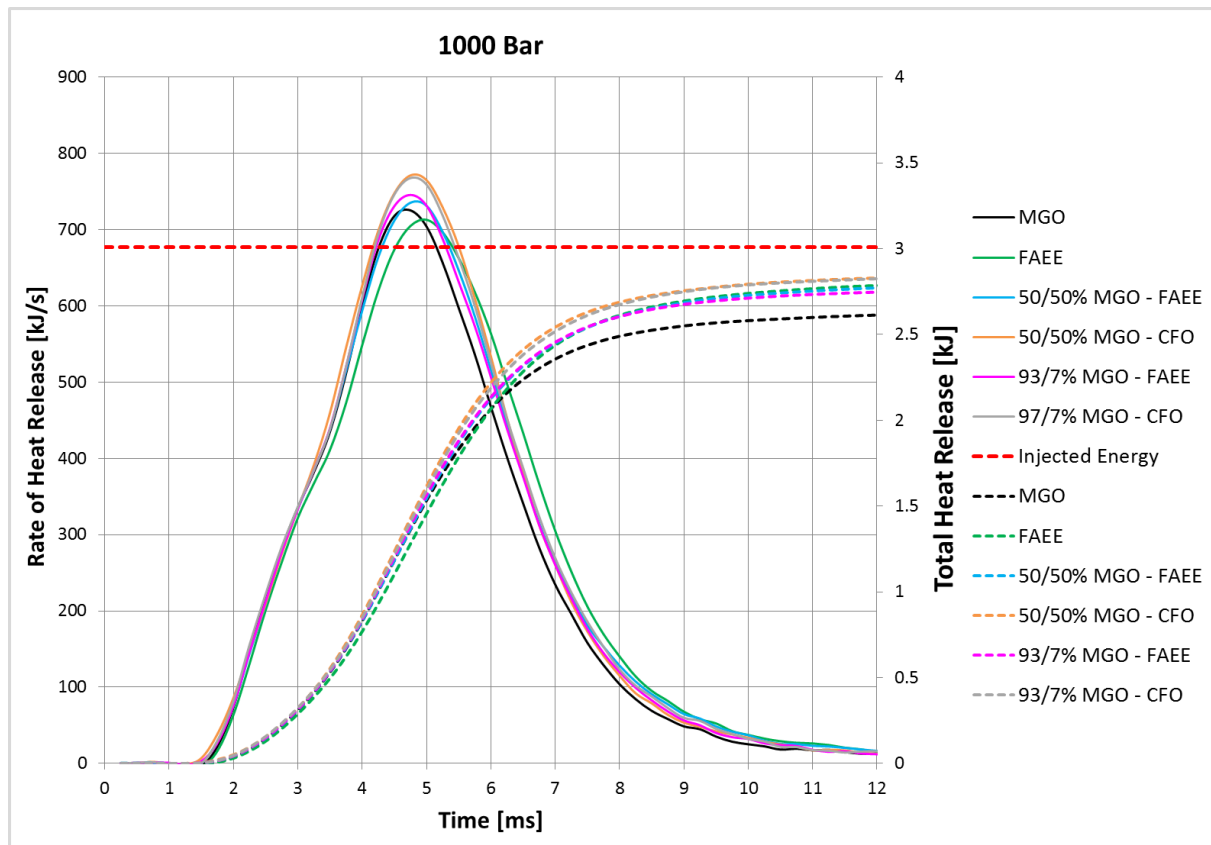


Figure 48: Rate of Heat Release and Cumulative Heat Release

Figure 48 show the rate of heat release as well as the cumulative heat release distribution for all the fuels at 1000 bar injection pressure. Diesel combustion typically show three combustion phases, premixed combustion, diffusion combustion and late/post combustion. The premixed combustion is instant and occurs in areas within the flammability limits, and hence corresponds to a rapid heat release. The next phase is diffusion combustion where the fuel mixing happens at the flame front just before it burns. This regime is also called rate-controlled combustion and corresponds to controlled heat release. The late combustion follows diffusion combustion and happens at the end of the combustion process when the last fuel is burned. Due to the large volume of the CVCC, pressure dampening and time delays, these regimes is not as prominent as expected due to the low load condition.

By looking closely at the curves at 3 ms it is possible to observe a small dent in the curve where the slope declines before it again inclines. This is the point that separates the premixed combustion from the diffusion combustion.

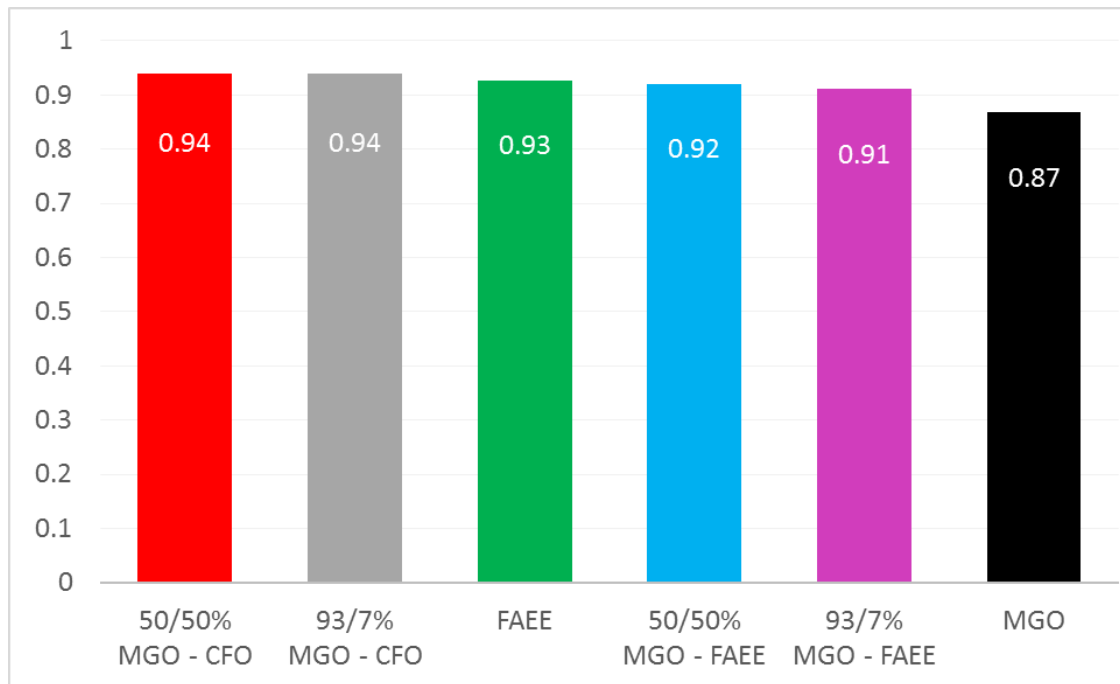


Figure 49: Combustion Efficiency

All fuels exhibit similar heat release and this is as expected since the same energy content is injected. The small differences that can be observed is mainly due to differences in combustion efficiency and by looking at the cumulative heat release, they are easier to distinguish. Figure 49 show the combustion efficiency for the tested fuels and it is a clear trend indicating increased combustion efficiency when fuel bound oxygen is present in the fuel. This is as expected and, when combusting oxygenated fuels, this seems to be a well established consensus reported by many authors.

Why the CFO blends have such a high combustion efficiency is however not entirely clear since they have a lower oxygen content and a shorter lift-off length than FAEE. By referring to the injector curves, Figure 27 and Figure 28, it is clear that the increased viscosity of the CFO makes the injected quantity deviate significantly from the other fuels. The slope of the 50/50% blend of MGO and CFO is steeper than for MGO and FAEE. This means that any inaccuracy in the injector or in the injection signal will have a bigger influence on the injected quantity of the CFO blends compared to the other fuels. It may also be cycle-to-cycle variations of the injections and this has not been investigated. If this is the case and a larger quantity has been injected, this would explain the results. The calculation is based on an injected energy content of 3011 Joules and if the actual injected energy content is higher, this will result in a better, yet wrong, indication of combustion efficiency.

Figure 50 and Figure 51 show the combustion phasing and the combustion duration for the fuels and they only further emphasises that there are no big differences in the heat release. The only thing worth noting is the differences between the injection pressures.

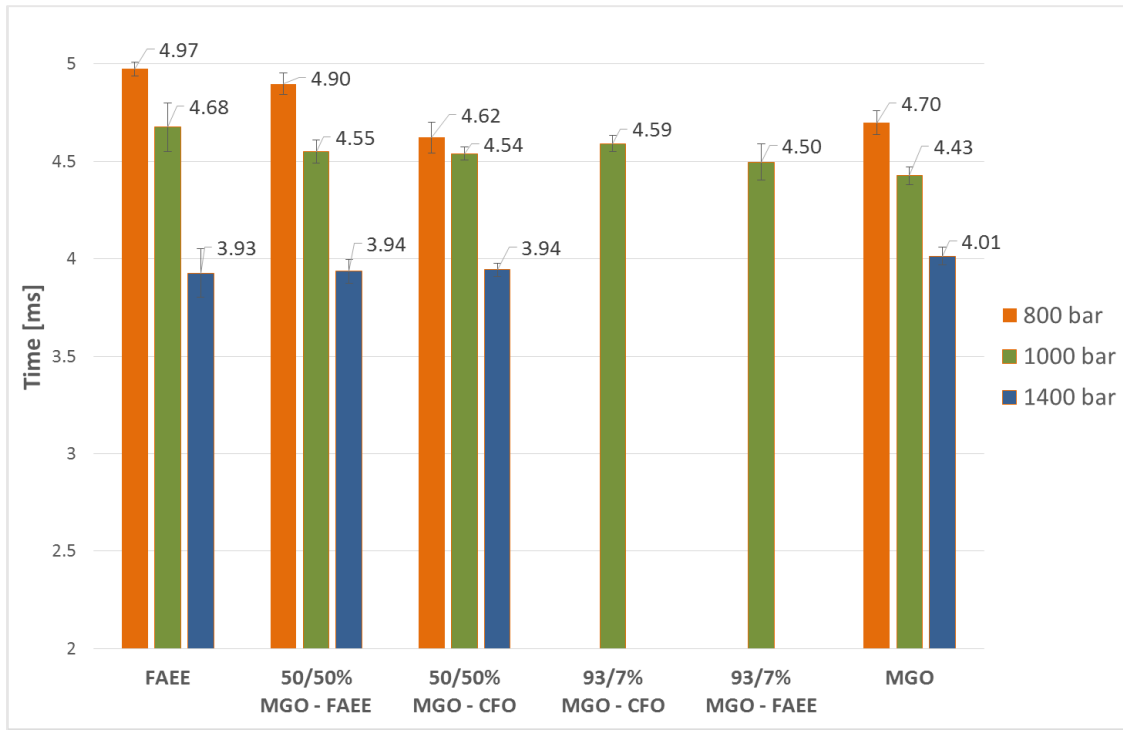


Figure 50: Combustion Phasing MFB 50%

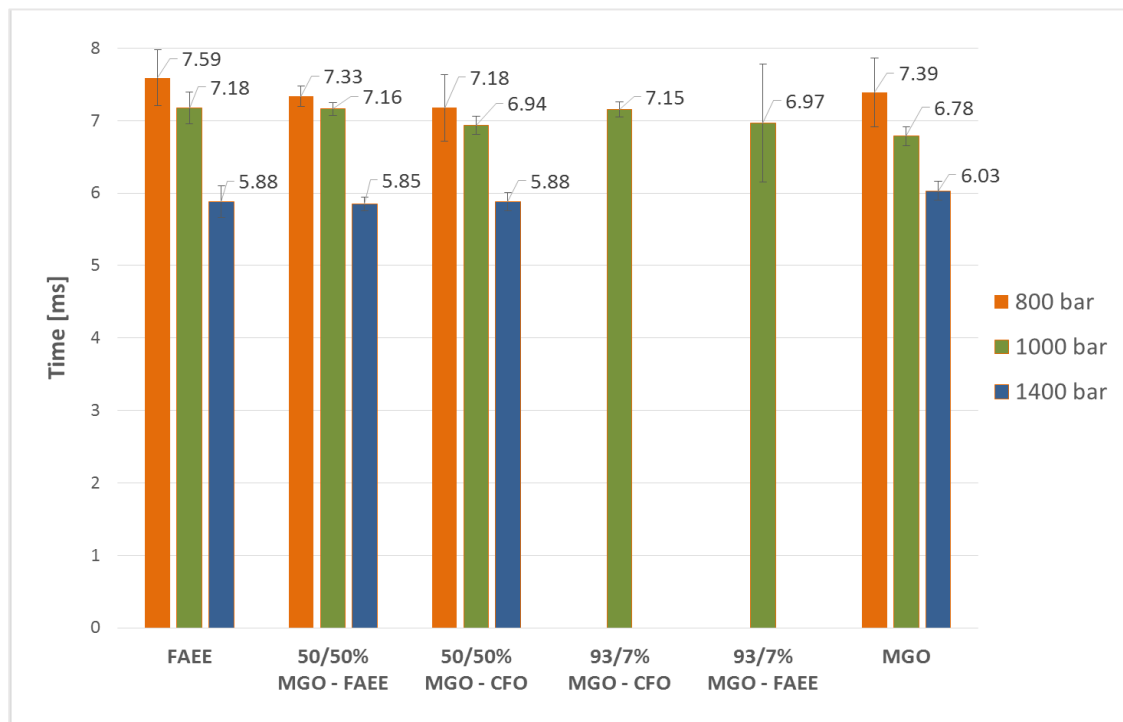


Figure 51: Combustion Duration MFB 90%

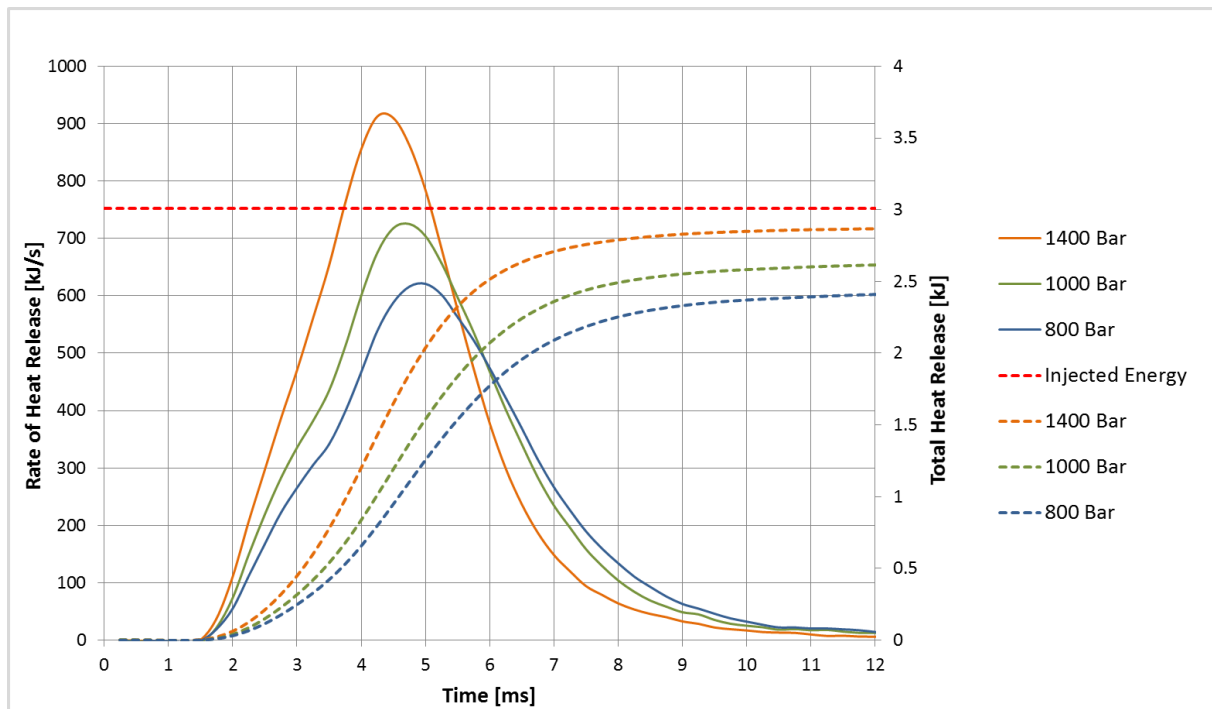


Figure 52: Rate of Heat Release for MGO at Different Injection Pressures

Figure 52 show the heat release for MGO at different injection pressures. It can be seen that the injection pressure has a big impact on the heat release. As the injection pressure increases, the curves are left-shifted corresponding to decreasing combustion phasing and combustion duration. At the same time, the peak heat release is increasing due to higher combustion efficiency. The trend is the same for all fuels and the better atomization at higher injection pressure once again show its significance in combustion performance.



### 6.2.4 Ignition Delay

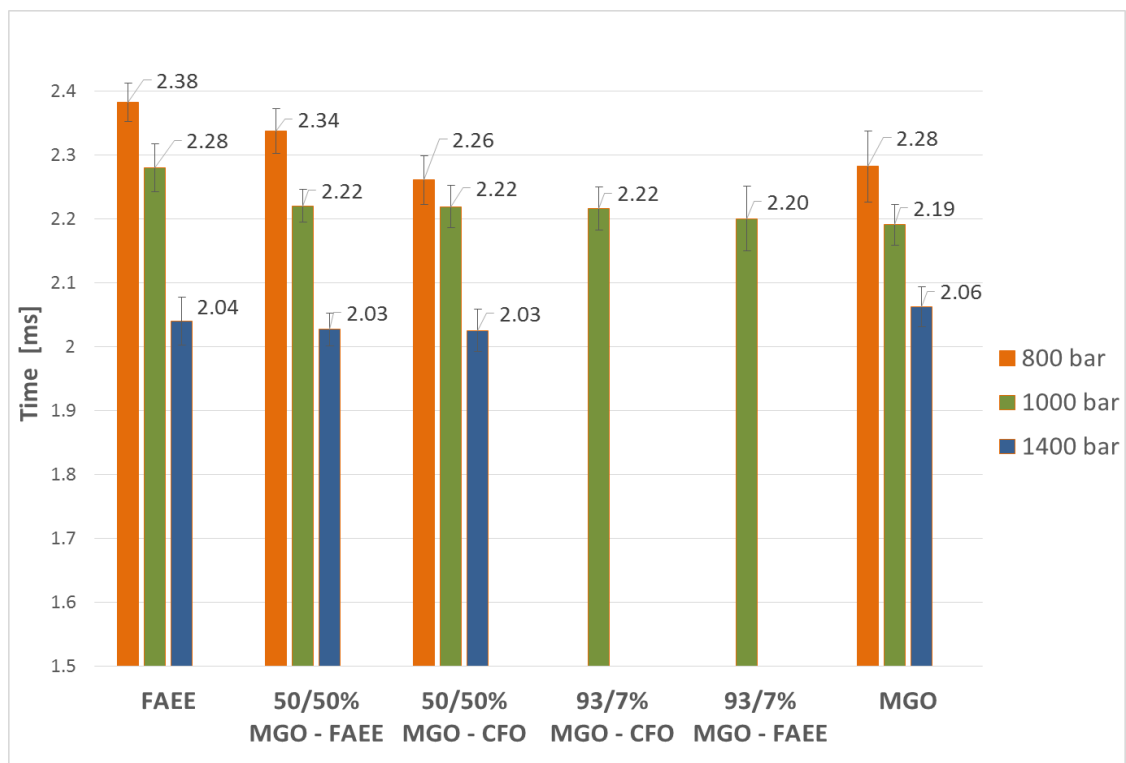


Figure 53: Ignition Delay MFB 5%

Figure 53 shows the ignition delay for all fuels at the different injection pressures. It is an obvious relation showing a decreasing ignition delay with increasing injection pressure and this correlates well with expectations. Between the fuels at the same injection pressures there are basically no difference and the small differences that can be observed are for the most part within the error of the test. The reason for the identical ignition delays are the temperature environment the fuel is injected in to. It would be interesting to inject the fuel in a temperature environment closer to the limit of the auto ignition temperature of the fuel. In this way, the ignition quality of the fuels would be tested and the differences in the fuels individual ignition delay would become clearer. There are a delay period from when the injection signal is sent to the injector and to the first fuel is leaving the nozzle. This delay period is called the hydraulic delay and is sometimes subtracted from the point of ignition to form the ignition delay. This is important if the hydraulic delay is different for the different fuels. There are some small variations in hydraulic delay, but when averaged over the eight injections per fuel, the hydraulic delay is identical for all fuels and is hence included in the ignition delay found in Figure 53.



# Chapter 7

## Conclusion

### 7.1 Conclusion

The focus of this study was to look at spray and combustion characteristics of the two fish based bio oils, CFO and FAEE. By testing different blends and comparing the results to pure MGO, the aim was to answer the question of whether CFO and FAEE can be used as an alternative to MGO for compression ignition engines.

FAEE and its blends with MGO performed for the most part very well and according to expectations. This bio oil resembles MGO in fuel characteristics and has earlier been proven to work well as engine fuel, with cleaner combustion and less emissions. One obvious problem with this fuel is its oxidation stability. A colour change was observed during testing and it is unclear if this has affected the results. It has to be prepared to satisfy the EN14241 biodiesel specification and further tested before a commercialisation will be possible. The most prominent result of this study is the strong reduction in soot formation for pure FAEE. Based on the results from this study, it is nothing indicating that FAEE cannot be used as a fuel for compression ignition engines in the future.

CFO and its blends with MGO also performed satisfactory. However, the high viscosity and density of this bio oil is believed to have affected the results in one way or another. It is unclear how homogeneous the fuel blends were after sitting in the fuel tank for some time, though periodic stirring was done. No clear indications of anything wrong can be referred to, but the laboratory performing the analysis of the fuel characteristics reported strange behaviour during their testing and it is not unthinkable that this strange behaviour has affected the combustion processes in this study. Even though the results from this study are promising there are too much uncertainty surrounding this bio oil at this point. It is in the author's opinion no doubt that this product can be further processed to a point where it will be an excellent fuel, and due to its oxygen content it has the same potential for emission reduction as FAEE. This makes it an interesting product for further combustion research. Based on the results of this study, CFO is absolutely not ruled out as a fuel and the author is recommending further research in closer cooperation with the producer. This will determine what they can do to enhance the fuel quality and if they are willing to do so.

## 7.2 Concluding Remarks

FAEE show strong reduction in soot emissions and in times of increasing environmental awareness, this is a strong argument for further investigating the feasibility and long-term effects of its use. If CFO are to be used as fuel it has to be further processed and the manufacturer must look into the economic viability of increasing production cost. None of these bio oils will solve the increasing demand for energy, but they may contribute in a positive way. Due to the food vs fuel argument the scale of production will be low, but it is realistic to see their use in small scale by ships linked to the industry.

## 7.3 Suggestions for Further Work

Even though the combustion rig was improved before this study, there are still some upgrades that can be done to allow for a deeper understanding of the combustion process. At this point, the CVCC is not equipped with tools to study microscopic spray characteristics. Laser diffraction is a widely used method to measure droplet size distribution and based on this, the Sauter mean diameter can be calculated. Investigation of the fuels surface tension will also be useful. A better understanding of the microscopic spray characteristics will provide valuable information for injection nozzle design. An injection nozzle that is designed with a special fuels flow characteristics in mind will greatly improve the atomization process and hence the performance of the fuel.

It will be interesting to perform non-reactive test in a hot environment. For this, the rig must be equipped with a heating system. It will also be possible to ignite a gas mixture that leaves no excess oxygen for the main combustion. These tests will show spray development that includes the vaporization effect on the spray development. This will give an understanding of the actual spray development without the turbulence created by the temperature differences in a combusting spray.

At this point, the pressure limitations of the CVCC makes the simulation of realistic load conditions impossible. In future studies, the load condition should be raised and to do this it will be necessary to ignite a leaner gas mixture. The current ignition system is not powerful enough to deliver the necessary spark energy and the rig must be equipped with a more powerful ignition system.

The temperature conditions used in this study was realistic compared to an actual engine, but it would be interesting to inject the fuels in a temperature environment closer to auto ignition limit of the fuels. This will test the ignition quality of the fuels and it will be possible to detect differences in ignition delay.

For further studies of macroscopic fuel characteristics, it will be advantageous to acquire an injection nozzle with smaller orifice diameter. This will shorten the penetration of the fuel sprays so that they are confined within the diameter of the window.

# References

- [1] S. Ushakov, H. Valland and V. Æsøy, "Combustion and emissions characteristics of fish oil fuel in a heavy-duty diesel engine," Science Direct, Trondheim, 2012.
- [2] V. Krivopolianskii, "Bio-Diesel Testing in a Constant Volum Combustion Chamber," Ålesund, 2014.
- [3] Mitsubishi Heavy Industries, "History of Fossil Fuel Usage since the Industrial Revolution," [Online]. Available: <https://www.mhi-global.com/discover/earth/issue/history/history.html>. [Accessed 3 November 2014].
- [4] ExxonMobil, "The Outlook for Energy: A view to 2040," ExxonMobil, Texas, 2014.
- [5] C. Chryssakis, O. Balland, H. A. Tvette and A. Brandsæter, "Alternative Fuels for Shipping," DNV-GL, OSLO, 2014.
- [6] L. Tangley, "Bird Habitats Threatened by Oil Spill," National Wildlife Federation, 6 June 2010. [Online]. Available: <http://www.nwf.org/News-and-Magazines/National-Wildlife/Birds/Archives/2010/Oil-Spill-Birds.aspx>. [Accessed 13 November 2014].
- [7] Biofuel, "Biofuels, The fuel of the future," 2010. [Online]. Available: <http://biofuel.org.uk/>.
- [8] K. J. Drapkin, "BP Oil spill four years later: Return to Barataria Bay and Cat Island," New Orleans, Louisiana Local News, 18 April 2014. [Online]. Available: [http://www.nola.com/environment/index.ssf/2014/04/bp\\_oil\\_spill\\_four\\_years\\_later.html](http://www.nola.com/environment/index.ssf/2014/04/bp_oil_spill_four_years_later.html).
- [9] EPA, "Overview of Greenhouse Gases," United States Environmental Protection Agency, 15 May 2014. [Online]. Available: <http://www.epa.gov/climatechange/ghgemissions/gases.html>. [Accessed 20 November 2014].
- [10] IPCC - Working Group 3, "Climate Change 2014: Mitigation of Climate Change," Intergovernmental Panel on Climate Change, Geneva, 2014.
- [11] European Commission, "Time for international action on CO2 emissions from shipping," European Commission, Brussels, 2013.
- [12] H. Riebeek, "Changes in the Carbon Cycle," NASA, 16 June 2011. [Online]. Available: <http://earthobservatory.nasa.gov/Features/CarbonCycle/page1.php>. [Accessed 20 November 2014].

- [13] L. J. Martin, "Biofuels - A Way To Reduce Your Carbon Footprint," Carbon Neutral Earth, 21 November 2014. [Online]. Available: <http://www.carbonneutralearth.com/biofuels.php>. [Accessed 21 Nov 2014].
- [14] British Petroleum, "BP Statistical Review of World Energy 63rd edition," BP, London, 2014.
- [15] CIA, "World Factbook," CIA, Washington D.C., 2014.
- [16] Full Circle Fuels, "Why Alternative Fuels," Full Circle Fuels, 2014. [Online]. Available: <http://www.fullcirclefuels.com/?page=why>. [Accessed 20 November 2014].
- [17] L. El-Katiri, B. Fattouh and R. Mallinson, "The Arab Uprising and MENA Political Instability: Implications for Oil & Gas Markets," The Oxford Institute For Energy Studies, Oxford, 2014.
- [18] UN, "Action Areas / Summit Announcements," UN, 2014. [Online]. Available: <http://www.un.org/climatechange/summit/action-areas/>. [Accessed 21 November 2014].
- [19] Sustainable Energy For All, "Our Vision," Sustainable Energy For All, 2013. [Online]. Available: <http://www.se4all.org/our-vision/>. [Accessed 21 November 2014].
- [20] T. Wallner and S. A. Miers, "Alternative Fuels for Internal Combustion Engines," Encyclopedia of Sustainability and Technology, Houghton, 2012.
- [21] Pasific Biodiesel, "History of biodiesel fuel," 2014. [Online]. Available: <http://www.biodiesel.com/biodiesel/history/>.
- [22] U.S. Department Of Energy, "Alternative Fuel Basics," 19 August 2013. [Online]. Available: <http://energy.gov/eere/energybasics/articles/alternative-fuel-basics>.
- [23] United Nations, "Sustainable Bioenergy: A Framework for Decision Makers," FAO, 2007.
- [24] D. B. A. Ladislao, T. Mallan and A. Walker, "Generations of Biofuels," [Online]. Available: <http://energyfromwasteandwood.weebly.com/generations-of-biofuels.html>.
- [25] E. Adlam, "LCA of Transportation Biofuels," NTNU, Trondheim, 2007.
- [26] J. Eichberger, "Supply, Marketing, Distribution, Transportation & Logistics News & Information," 2014. [Online]. Available: <http://fuelmarketernews.com/know-alternatives/>. [Accessed 31 October 2014].
- [27] Seaweed Energy Solution AS, "Seaweed," 2009. [Online]. Available: <http://www.seaweedenergysolutions.com/>. [Accessed 31 October 2014].

- [28] Y. Chisti, "Biodiesel from microalgae," Science Direct, Palmerston North, 2007.
- [29] United States Environmental Protection Agency, EPA, "Carbon Dioxide Capture and Sequestration," 2013. [Online]. Available: <http://www.epa.gov/climatechange/ccs/>. [Accessed 31 10 2014].
- [30] European Commission, "Biofuels and other renewable energy in the transport sector," European Commission, [Online]. Available: [http://ec.europa.eu/energy/renewables/biofuels/biofuels\\_en.htm](http://ec.europa.eu/energy/renewables/biofuels/biofuels_en.htm). [Accessed 22 November 2014].
- [31] European Commission, "An EU Strategy for Biofuels," 8 February 2006. [Online]. Available: [http://eur-lex.europa.eu/legal-content/EN/ALL/?ELX\\_SESSIONID=IH12JwYhfJTHTd5gk2mLbzbNhjmjrHZQjdh2dJsxvV3q2LM2ZLdx!-1545270827?uri=CELEX:52006DC0034](http://eur-lex.europa.eu/legal-content/EN/ALL/?ELX_SESSIONID=IH12JwYhfJTHTd5gk2mLbzbNhjmjrHZQjdh2dJsxvV3q2LM2ZLdx!-1545270827?uri=CELEX:52006DC0034). [Accessed 22 November 2014].
- [32] C. McLaughlin, "Joint Position ACEA/FuelsEurope on the intention of France to introduce B8 diesel," European Automobile Manufacturers Association, 30 September 2014. [Online]. Available: <http://www.acea.be/news/article/joint-acea-fuelseurope-position-on-b8-diesel>. [Accessed 8 Desember 2014].
- [33] U.S. Department of Energy, "Alternative Fuels Data Center," U.S. Department of Energy, 9 April 2013. [Online]. Available: [http://www.afdc.energy.gov/fuels/biodiesel\\_blends.html](http://www.afdc.energy.gov/fuels/biodiesel_blends.html). [Accessed 22 November 2014].
- [34] Statens vegvesen, "Biodiesel," Statens vegvesen, 10 November 2010. [Online]. Available: <http://www.vegvesen.no/Kjoretoy/Fakta+og+statistikk/Kjoretoy+og+drivstoff/Biodiesel>. [Accessed 22 November 2014].
- [35] Neste Oil, "Demand for biofuel increasing," Neste Oil, 16 July 2014. [Online]. Available: <http://www.nesteoil.com/default.asp?path=1,41,537,2455,8529,12421>. [Accessed 23 November 2014].
- [36] Soybean & Corn Advisor, "Higher Ethanol Blend in Brazil (27.5%) Passes Preliminary Tests," Soybean & Corn Advisor, 30 October 2014. [Online]. Available: [http://www.soybeansandcorn.com/news/Oct30\\_14-Higher-Ethanol-Blend-in-Brazil-Passes-Preliminary-Tests](http://www.soybeansandcorn.com/news/Oct30_14-Higher-Ethanol-Blend-in-Brazil-Passes-Preliminary-Tests). [Accessed 23 November 2014].
- [37] Shipping efficiency, "Shippers & Charterers," Shipping efficiency, [Online]. Available: <http://www.shippingefficiency.org/shippers-and-charterers>. [Accessed 24 November 2014].
- [38] CIMAC, "Guideline for the Operation of Marine Engines on Low Sulphur Fuel," The International Council on Combustion Engines, Frankfurt, 2013.

- [39] National Biodiesel Board, "Materials Compatibility," 2004. [Online]. Available: [http://www.biodiesel.org/docs/ffs-performace\\_usage/materials-compatibility.pdf?sfvrsn=4](http://www.biodiesel.org/docs/ffs-performace_usage/materials-compatibility.pdf?sfvrsn=4). [Accessed 24 November 2014].
- [40] Filter Manufacturers Council, "The Effect of Biodiesel on Fuel Filters," October 2011. [Online]. Available: <http://www.aftermarketsuppliers.org/Councils/Filter-Manufacturers-Council/TSBs-2/English/06-1.pdf>. [Accessed 24 November 2014].
- [41] University of Strathclyde, "Engine modifications," University of Strathclyde, [Online]. Available: [http://www.esru.strath.ac.uk/EandE/Web\\_sites/02-03/biofuels/perf\\_mods.htm](http://www.esru.strath.ac.uk/EandE/Web_sites/02-03/biofuels/perf_mods.htm). [Accessed 2014 November 2014].
- [42] A. A. Refaat, "Correlation between the chemical structure of biodiesel and its physical properties," *International Journal of Environmental Science and Technology*, vol. 6, no. 4, pp. 677-694, 2009.
- [43] "Standards and Publications," ASTM International, [Online]. Available: <http://www.astm.org/Standard/standards-and-publications.html>. [Accessed 06 April 2015].
- [44] M. J. Pratas, S. Freitas, M. B. Oliveira, S. C. Monteiro, A. S. Lima and J. A. P. Coutinho, "Densities and Viscosities of Fatty Acid Methyl and Ethyl Esters," *Journal of Chemical & Engineering Data*, vol. 55, no. 9, pp. 3983-3990, 2010.
- [45] M. E. Tat and J. H. Van Gerpen, "The Specific Gravity of Biodiesel and Its Blends with Diesel Fuel," Springer, Iowa, 2000.
- [46] A. Sarin, *Biodiesel - Production and Properties*, Cambridge: The Royal Society of Chemistry, 2012.
- [47] J. B. Heywood, *Internal Combustion Engine Fundamentals*, Singapore: McGraw-Hill Book Company, 1988.
- [48] G. Knothe, "'Designer' Biodiesel: Optimizing Fatty Ester Composition to Improve Fuel Properties," *Energy and Fuels*, vol. 22, no. 2, pp. 1358-1364, 2008.
- [49] G. Knothe, A. C. Matheus and T. W. Ryan III, "Cetane numbers of branched and straight-chain fatty esters determined in an ignition quality tester," Science Direct, Peoria, 2002.
- [50] "Standard Test Method for Calculated Cetane Index by Four Variable Equation," ASTM, [Online]. Available: <http://www.astm.org/Standards/D4737.htm>. [Accessed 15 April 2015].
- [51] M. S. Graboski and R. L. McCormick, "Combustion of Fat and Vegetable Oil Derived Fuels in Diesel Engines," Pergamon, Golden, 1998.



- [52] U.S. Department of Energy, "Biodiesel Handling and Use Guidelines," October 2004. [Online]. Available: <http://www.biofuels.coop/archive/HandlingAndUse2004.pdf>. [Accessed 16 April 2015].
- [53] M. Lapuerta, J. Rodriguez-Fernandez and O. Armas, "Correlation for the estimation of the density of fatty acid esters and its implications. A proposed Biodiesel Cetane Index," *Chemistry and Physics of Lipids*, vol. 163, pp. 720 - 727, 2010.
- [54] J. Pullen and K. Saeed, "An overview of biodiesel oxidation stability," *Renewable and Sustainable Energy Reviews*, no. 16, pp. 5924 - 5950, 2012.
- [55] R. Farhoosh and S. Mohammad Reza Moosavi, "Rancimat Test for the Assessment of Used Frying Oils Quality," Mashhad, 2006.
- [56] Petro Industry News, "Determining the Oxidation Stability of Biodiesel According to EN 14112," 10 January 2008. [Online]. Available: [http://www.petro-online.com/news/analytical-instrumentation/11/metrohm/determining\\_the\\_oxidation\\_stability\\_of\\_biodiesel\\_according\\_to\\_en\\_14112/3218/](http://www.petro-online.com/news/analytical-instrumentation/11/metrohm/determining_the_oxidation_stability_of_biodiesel_according_to_en_14112/3218/). [Accessed 17 April 2015].
- [57] U. D. o. Energy, "Characterization of Biodiesel Oxidation and Oxidation Products," Golden, 2005.
- [58] G. Knothe and R. O. Dunn, "Dependence of Oil Stability Index of Fatty Compounds on Their Structure and Concentration and Presence of Metals," *Journal of the American Oil Chemists' Society*, vol. 80, pp. 1021 - 1026, 2003.
- [59] U.S Department of Energy, "Characterization of Biodiesel Oxidation and Oxidation Products," Golden, 2005.
- [60] Noria Corporation, "A Comprehensive Look At the Acid Number Test," *Machinery Lubrication Magazine*, no. 7, 2007.
- [61] ASTM International, "Standard Test Method for Acid and Base Number by Color-Indicator Titration," 2014. [Online]. Available: <http://www.astm.org/Standards/D974.htm>. [Accessed 18 April 2015].
- [62] Ö. O. Taskiran and M. Ergeneman, "Experimental Study on Diesel Spray Characteristics and Autoignition Process," *Journal of Combustion*, vol. 2011, p. 20, 2011.
- [63] C. Baumgarten, *Mixture Formation in Internal Combustion Engines*, Berlin: Springer, 2006.
- [64] H. Hiroyasu, "Diesel Engine Combustion and Its Modeling," Hiroshima, 1985.
- [65] A. Urlaub and F. Chmela, "High-Speed, Multifuel Engine: L9204 FMV," SAE, 1974.

- [66] J. Galle, S. Defruyt, C. Van de Maele, R. P. Rodriguez, Q. Denon, A. Verliefe and S. Verhelst, "Experimental investigation concerning the influence of fuel type and properties on the injection and atomization of liquid biofuels in an optical combustion chamber," Science Direct, 2013.
- [67] A. K. Agarwal and V. H. Chaudhury, "Spray characteristics of biodiesel blends in a high-pressure constant volume spray chamber," Science Direct, Kanpur, 2012.
- [68] C. Arcoumanis and T. Kamimoto, *Flow and Combustion in Reciprocating Engines*, Springer, 2009.
- [69] D. L. Siebers and B. S. Higgins, "Effects of Injector Conditions on the Flame Lift-Off Length of DI Diesel Sprays," Sandia National Laboratories, Albuquerque, 2000.
- [70] H. Zhao and N. Ladommatos, "Optical Diagnostics for Soot and Temperature Measurement in Diesel Engines," Pergamon, Uxbridge, 1998.
- [71] R. Pittermann, "Spectroscopic Analysis of the Combustion in Diesel and Gas Engines," MTZ Worldwide eMagazine, 2008.
- [72] M. Planck, "The Theory of Heat Radiation," P. Blakiston's Son & Co, Philadelphia, 1913.
- [73] P. A. Lakshminarayanan and Y. V. Aghav, *Modelling Diesel Combustion*, Springer, 2009.
- [74] K. J. Laidler, "The Development of the Arrhenius Equation," *Journal of Chemical Education*, vol. 61, no. 6, 1984.
- [75] M. M. PhD Candidate, "The Combustion Rig as a Basic Investigation Tool for Alternative Fuels and Injection Systems on Marine Diesel Engines," Trondheim, 2014.
- [76] G. S. Settles, *Schlieren and Shadowgraph Techniques*, Berlin: Springer, 2001.
- [77] *Gas Dynamics Lecture 47*. [Film]. Indian Institute of Technology Madras, <http://freevideolectures.com/Course/3215/Gas-Dynamics/47>.
- [78] U.S. Environmental Protection Agency, "In-Use Marine Diesel Fuel," August 1999. [Online]. Available: <http://www.epa.gov/otaq/regs/nonroad/marine/ci/fr/dfuelrpt.pdf>. [Accessed 20 April 2015].
- [79] MAN, "Quality of Diesel Fuel (MGO,MDO)," October 2008. [Online]. Available: quality requirements for operating supplies. [Accessed 2015 April 20].
- [80] Australian Institute of Petroleum, "Refining of Petroleum," [Online]. Available: [http://www.aip.com.au/industry/fact\\_refine.htm](http://www.aip.com.au/industry/fact_refine.htm). [Accessed 20 April 2015].

- [81] U.S. Energy Information Administration, "Crude oil distillation and the definition of refinery capacity," 12 July 2012. [Online]. Available: <http://www.eia.gov/todayinenergy/detail.cfm?id=6970>. [Accessed 20 April 20].
- [82] Food and Agriculture Organization of the United Nations, "The production of fish meal and oil," Fisheries and Aquaculture Department , [Online]. Available: <http://www.fao.org/docrep/003/x6899e/X6899E04.htm>. [Accessed 17 December 2014].
- [83] R. E. Armenta, M. Vinatoru, A. M. Burja, J. A. Kralovec and C. J. Barrow, "Transesterification of Fish Oil to Produce Fatty Acid Ethyl Esters Using Ultrasonic Energy," AOCS, McKinney, 2007.
- [84] D. K. Ramesha, P. M. Gowda, N. Manjunath, R. Simhasan and K. T. Rajiv, "Performance, Combustion and Emission Evaluation of Fish and Corn Oil substitute fuel in Direct Injection C.I. Engine," AMAE, Bangalore, 2013.
- [85] ChmlTech Ltd., "Changing the world into biodiesel," ChmlTech, 2012. [Online]. Available: <http://www.chmltech.com/biodieseltch.htm>.
- [86] R. D. Reitz and F. V. Bracco, "Mechanism of Atomization of a Liquid Jet," *AIP - Physics of Fluids*, vol. 25, no. 10, pp. 1730 - 1742, 1982.
- [87] J. Dernette, C. Hespel, S. Houille, F. Foucher and C. Mounaim-Rousselle, "Influence of Fuel Properties on the Diesel Injection Process in Nonvaporizing Conditions," *Atomization and Sprays*, vol. 22, no. 6, pp. 461 - 492, 2012.
- [88] R. Payri, F. J. Salvador, J. Gimeno and R. Novella, "Flow regime effects on non-cavitating injection nozzles over spray behaviour," *International Journal of Heat and Fluid Flow*, vol. 32, pp. 273 - 284, 2011.
- [89] M. Xiao, H. Liu, X. Bi, H. Wang and C.-f. F. Lee, "Experimental and Numerical Investigation on Soot Behavior of Soybean Biodiesel under Ambient Oxygen Dilution in Conventional and Low-Temperature Flames," *American Chemical Society*, vol. 28, pp. 2663 - 2676, 2014.
- [90] D. K. Ramesha, R. K. Thimmannachar, R. Simhasan, M. Naqappa and P. M. Gowda, "A Study on Performance, Combustion and Emmission Characteristics of Compression Ignition Engine Using Fish Oil Biodiesel Blends," Springer, Bangalore, 2012.
- [91] J. Zhang, W. Jing, W. L. Roberts and T. Fang, "Soot temperature and KL factor for biodiesel and diesel spray combustion in a constant volume combustion chamber," Science Direct, 2012.



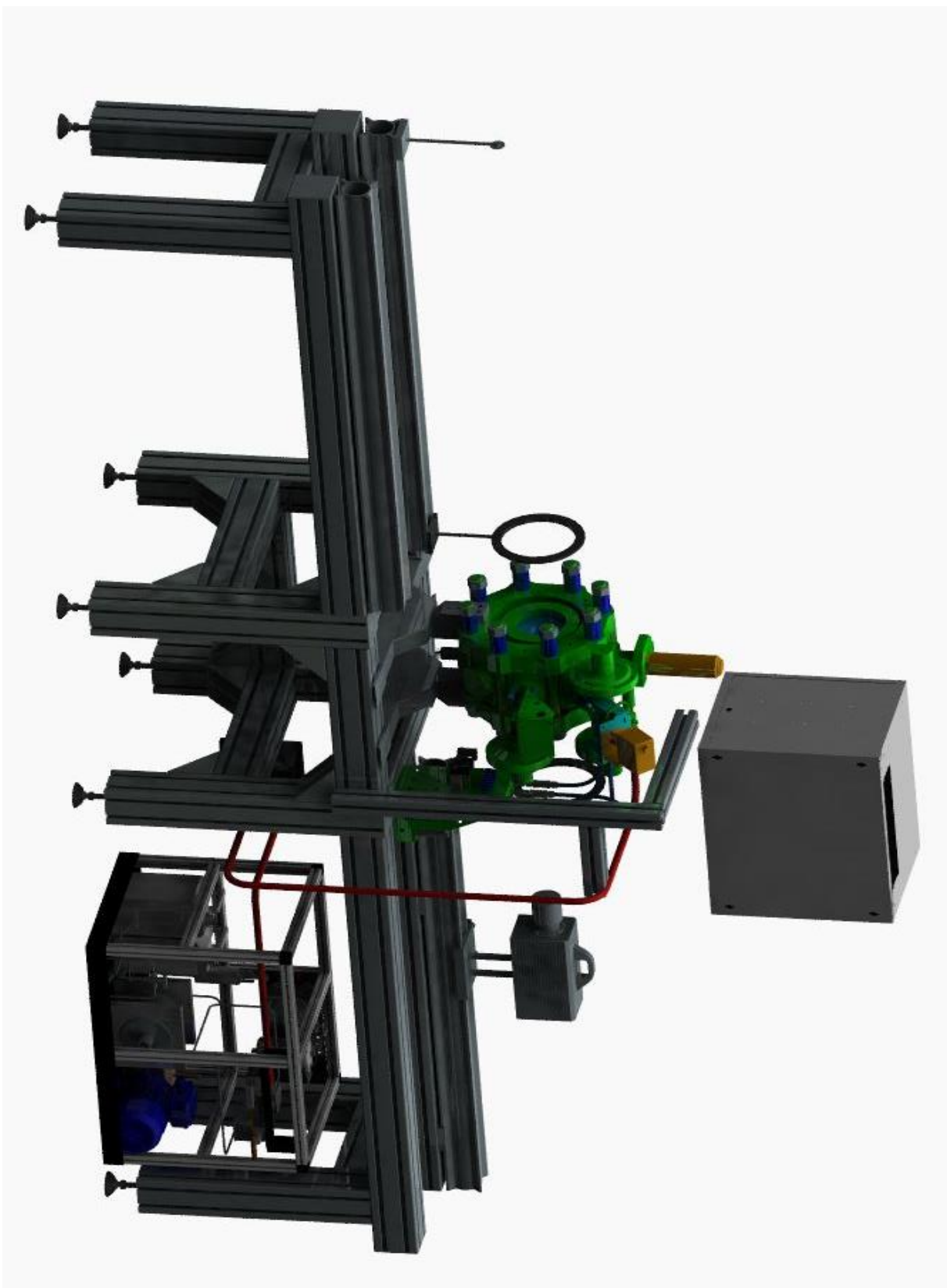
# Appendix A

## Summary of Important Fuel Standards

Property	Unit	Petroleum Diesel		MGO		Biodiesel		
		EN 590	ASTM D975	ISO 8217 - DMA	EN 14214	ASTM D6751		
	Limit	Test	Limit	Test	Limit	Test	Limit	Test
Density	kg/m <sup>3</sup>	820 - 845	-	890	860-900	-	-	-
Kinematic Viscosity	mm <sup>2</sup> /s	2.0 – 4.5	1.9 – 4.1	2.0 – 6.0	3.5 – 5.0	1.9 – 6.0	-	D-445
Flash Point, min	°C	60	52	60	120	130	-	D-93
Cetane Number, min	-	51	40	40	51	47	-	D-613
Oxidation stability, min	Hours	-	-	-	8	8	-	EN 14112
Oxidation stability, max	g/m <sup>3</sup>	25	-	25	-	-	-	-
Ash, max	Weight %	0.01	0.01	0.01	-	-	-	-
Water, max	mg/kg	200	-	200	500	-	-	-
Acid Value, max	mg KOH/g	-	-	0.5	0.5	0.5	-	D-664

# Appendix B

CAD drawing of the test bed



# Appendix C

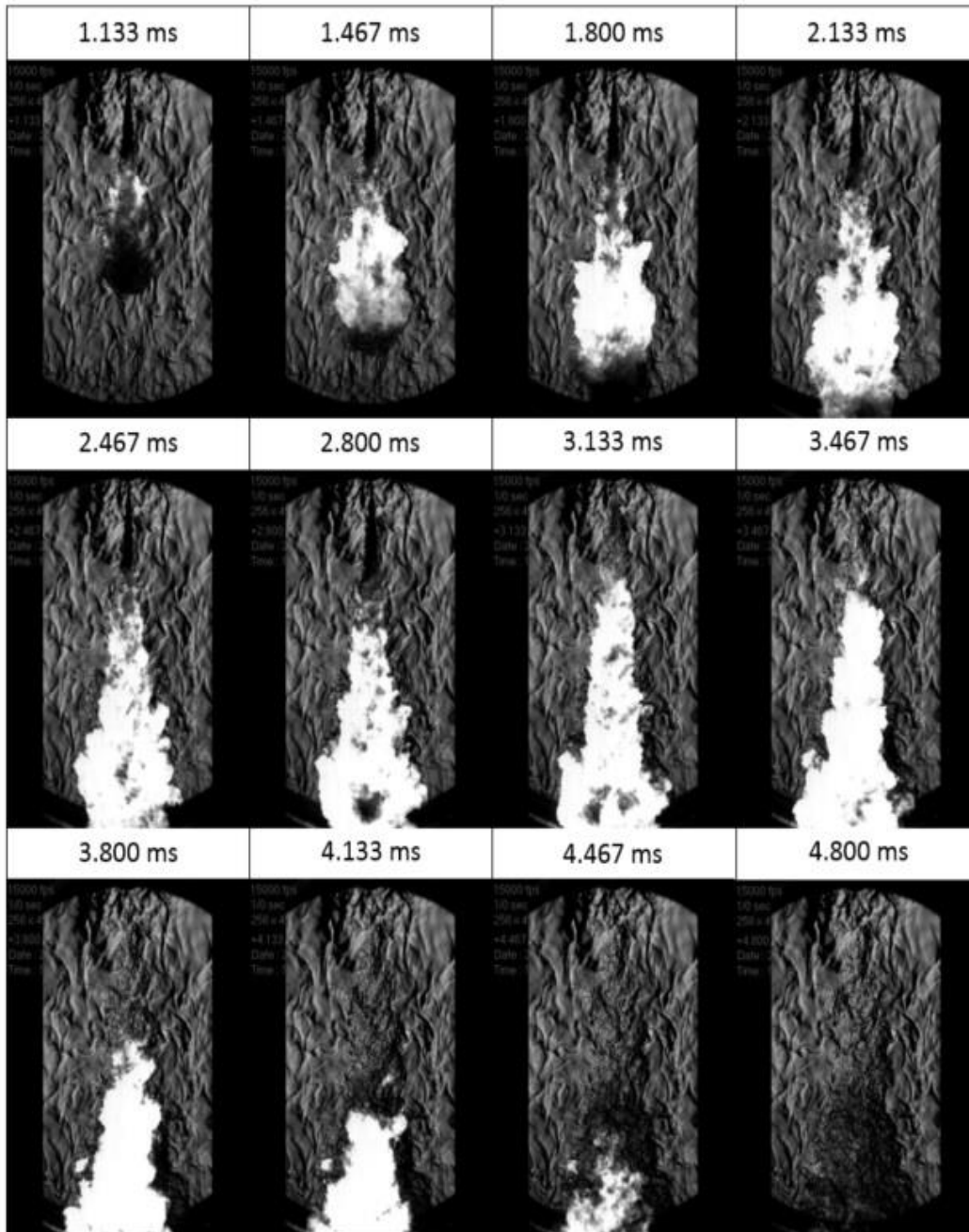
## Example of Measurement Protocol

Measure Protocol #70								Reference	
Keyword		MGO cold shot							
Protocol number								Spark plug position bottom	
Injector		L'Orange VUO-G298uV120							
Nozzle		Single hole							
Injector number		-							
Q100		-	[ml/min]	Lens opening		5.6	[-]		
Nozzle Diameter		0.35	[mm]	Full load quantity		-	[mm <sup>3</sup> ]		
Number of holes		1	[-]	Injection Temp		-	[°C]		
Spray angle		-	[°]	Calc. Injection time		-	[s]		
Room temp.		22	[°C]	Shutter time		1/50000	[s]		
Fuel Density		849	[kg/dm <sup>3</sup> ]	Pictures		120	[-]		
Fuel Pressure		800-1400	bar	fan start		10	[s]		
Frame Rate		15000	p/s	fan stop		10	[s]		
Resolution		256x496	[-]						
Point	Rig load	Injector opening	Pressure	Injected volume	optic	filter	shutter		
[-]	[bar]	[μs]	[bar]	[mm <sup>3</sup> ]	[-]	[-]	[s]	[-]	[s]
1	10.00	560.00	1000	83.41	Schadow	YES	1/50000	256x496	3
2	10.00	560.00	1000	83.41	Schadow	YES	1/50000	256x496	3
3	10.00	560.00	1000	83.41	Schadow	YES	1/50000	256x496	3
4	10.00	560.00	1000	83.41	Schadow	YES	1/50000	256x496	3
5	10.00	560.00	1000	83.41	Schadow	YES	1/50000	256x496	3
6	10.00	560.00	1000	83.41	Schadow	YES	1/50000	256x496	3
7	10.00	560.00	1000	83.41	Schadow	YES	1/50000	256x496	3
8	10.00	560.00	1000	83.41	Schadow	YES	1/50000	256x496	3
9	10.00	400.00	1400	82.90	Schadow	YES	1/50000	256x496	3
10	10.00	400.00	1400	82.90	Schadow	YES	1/50000	256x496	3
11	10.00	400.00	1400	82.90	Schadow	YES	1/50000	256x496	3
12	10.00	400.00	1400	82.90	Schadow	YES	1/50000	256x496	3
13	10.00	400.00	1400	82.90	Schadow	YES	1/50000	256x496	3
14	10.00	400.00	1400	82.90	Schadow	YES	1/50000	256x496	3
15	10.00	400.00	1400	82.90	Schadow	YES	1/50000	256x496	3
16	10.00	400.00	1400	82.90	Schadow	YES	1/50000	256x496	3
17	10.00	760.00	800	83.22	Schadow	YES	1/50000	256x496	3
18	10.00	760.00	800	83.22	Schadow	YES	1/50000	256x496	3
19	10.00	760.00	800	83.22	Schadow	YES	1/50000	256x496	3
20	10.00	760.00	800	83.22	Schadow	YES	1/50000	256x496	3
21	10.00	760.00	800	83.22	Schadow	YES	1/50000	256x496	3
22	10.00	760.00	800	83.22	Schadow	YES	1/50000	256x496	3
23	10.00	760.00	800	83.22	Schadow	YES	1/50000	256x496	3
24	10.00	760.00	800	83.22	Schadow	YES	1/50000	256x496	3
25									
Comments									
Operator		Malin;Vladimir Krivopolianskii; Bjørn Rygh							

# Appendix D

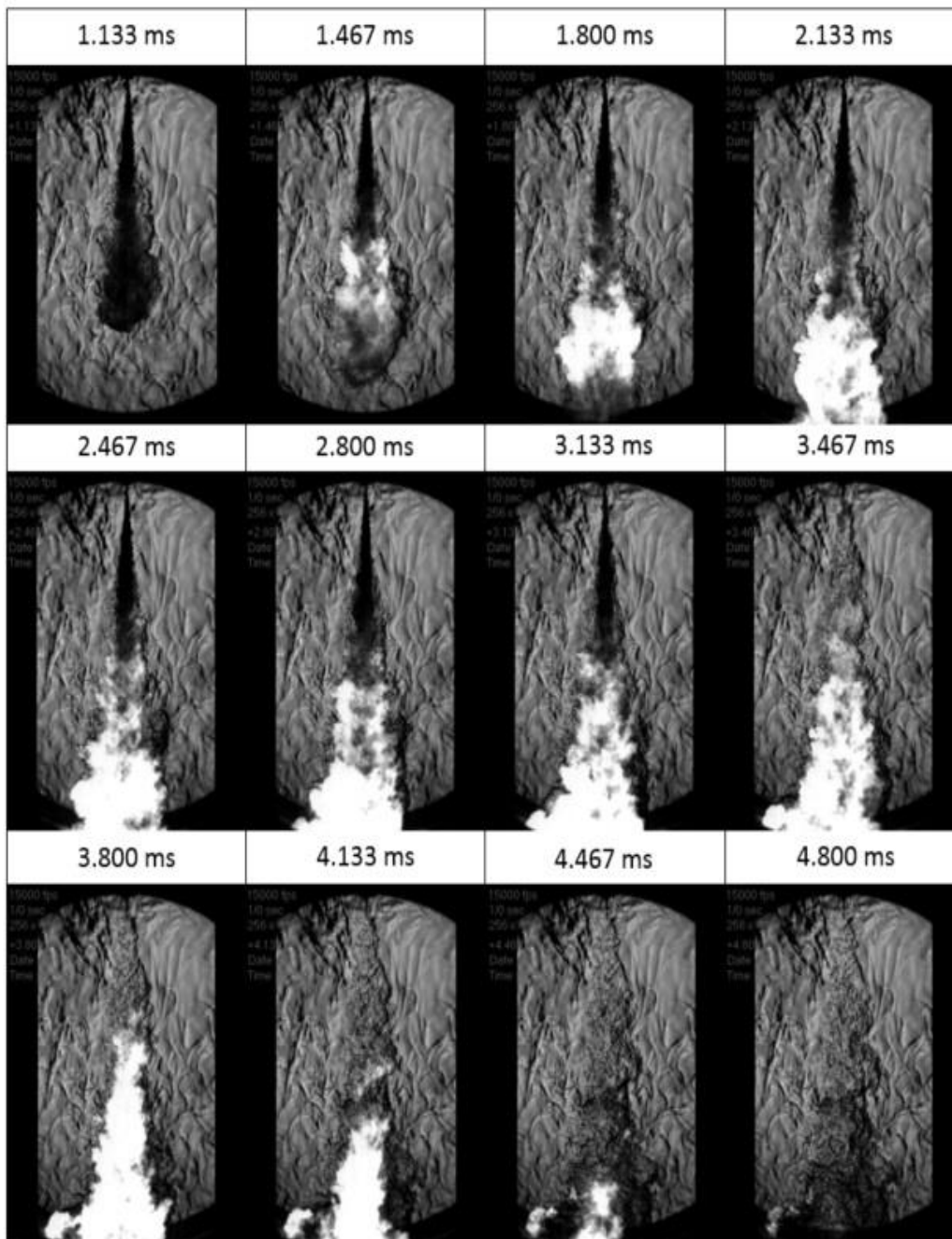
Spray development of different fuels at 1000 bar injection pressure

## MGO – 1000 Bar

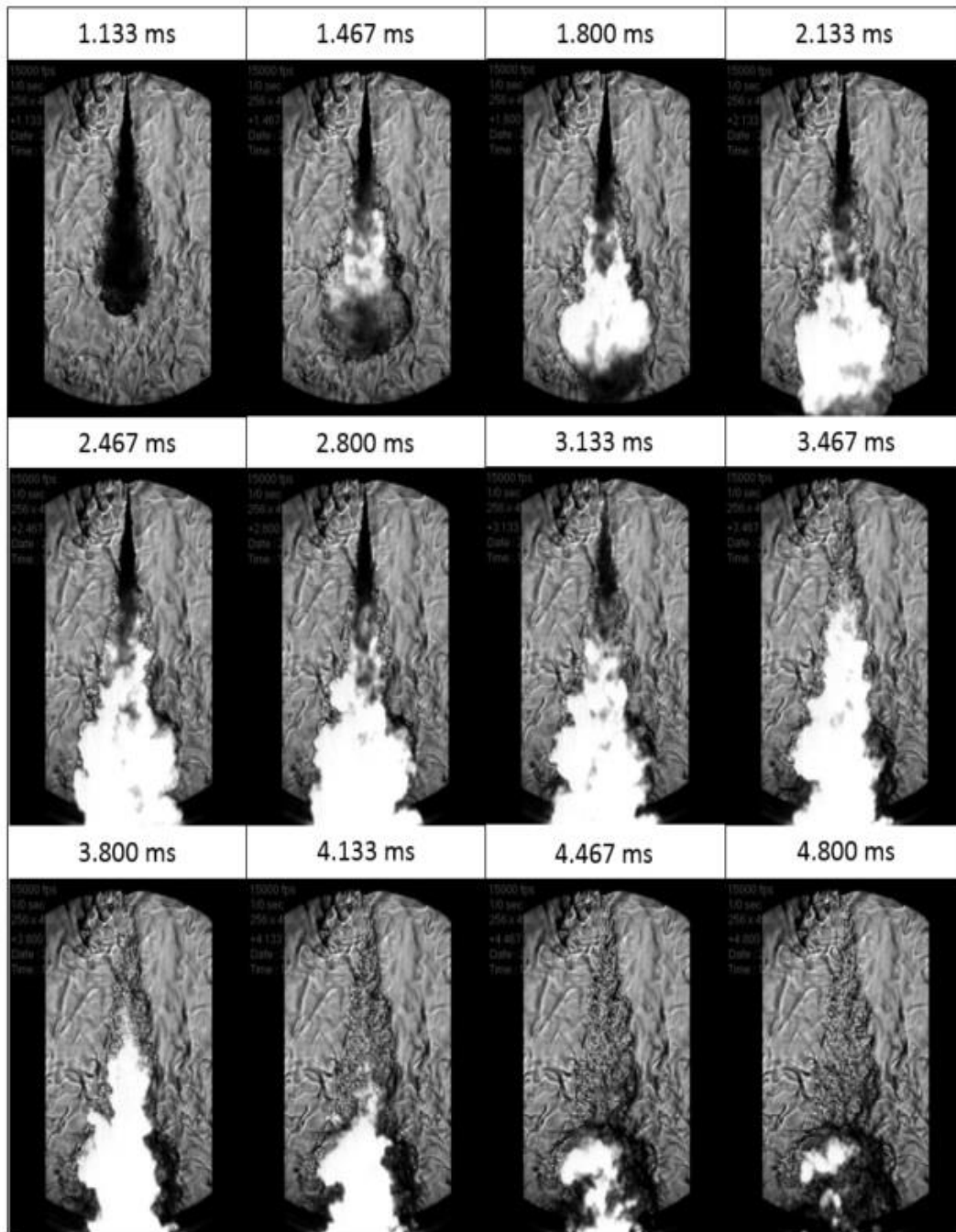




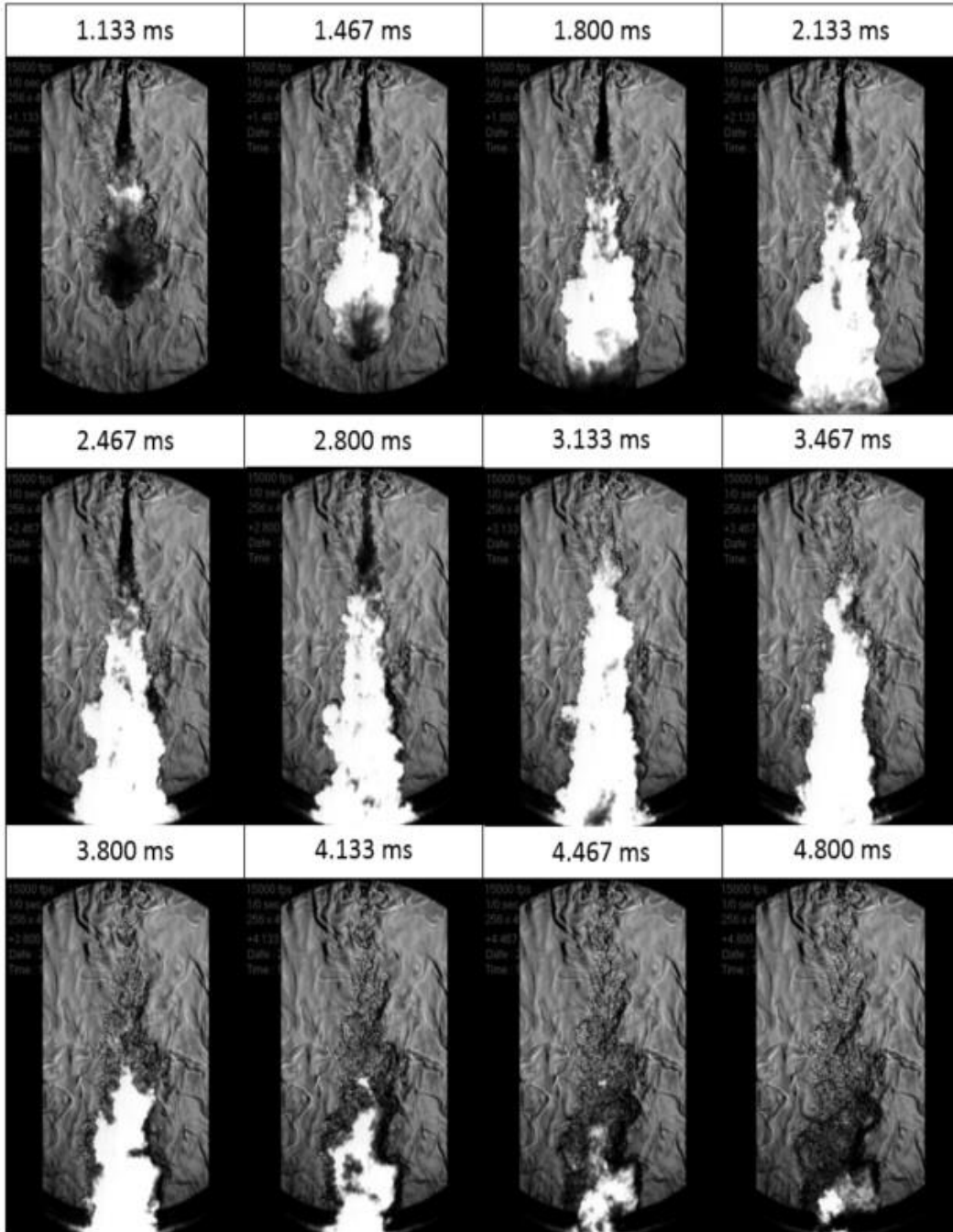
# FAEE – 1000 Bar



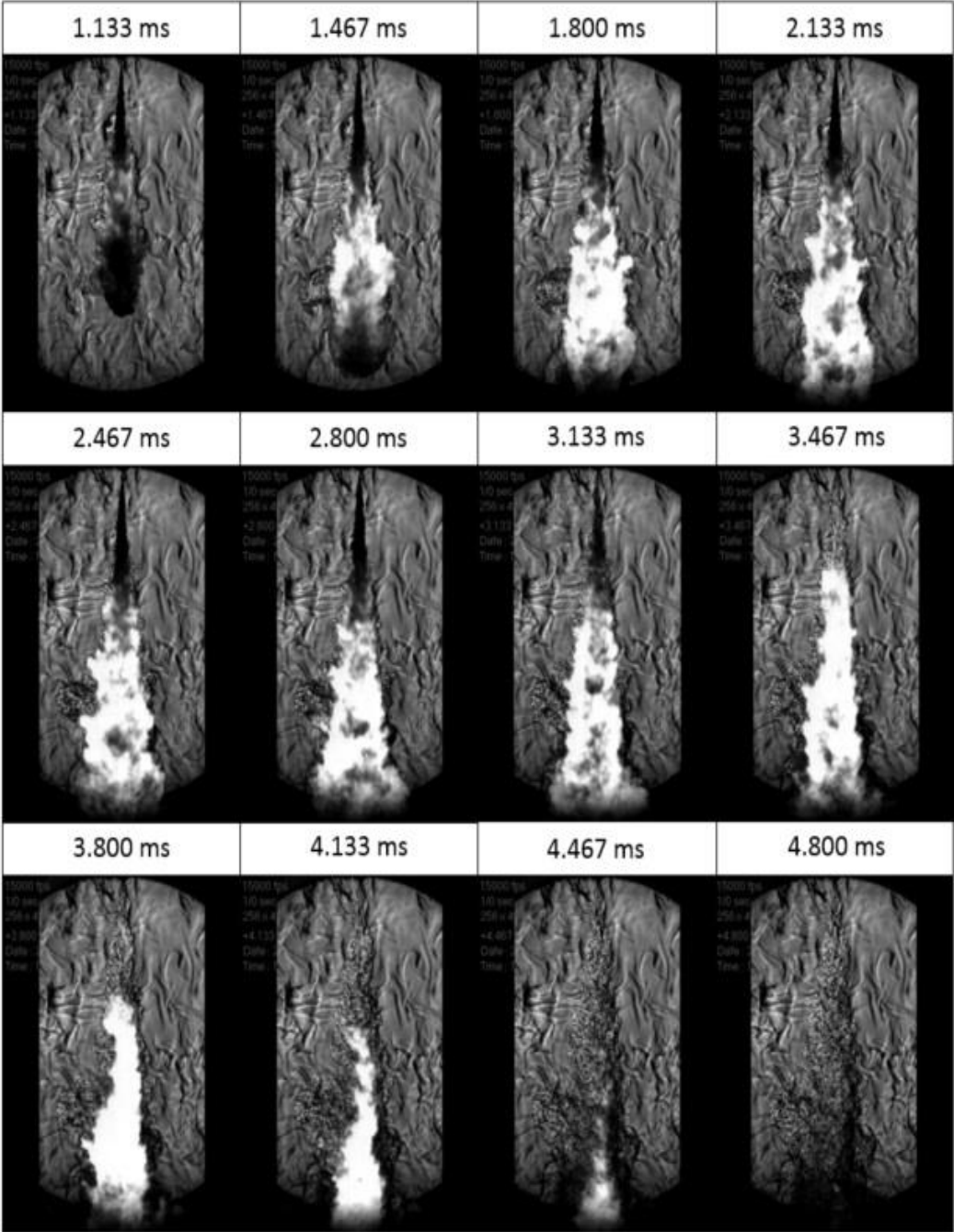
# 50/50% MGO - FAEE – 1000 Bar



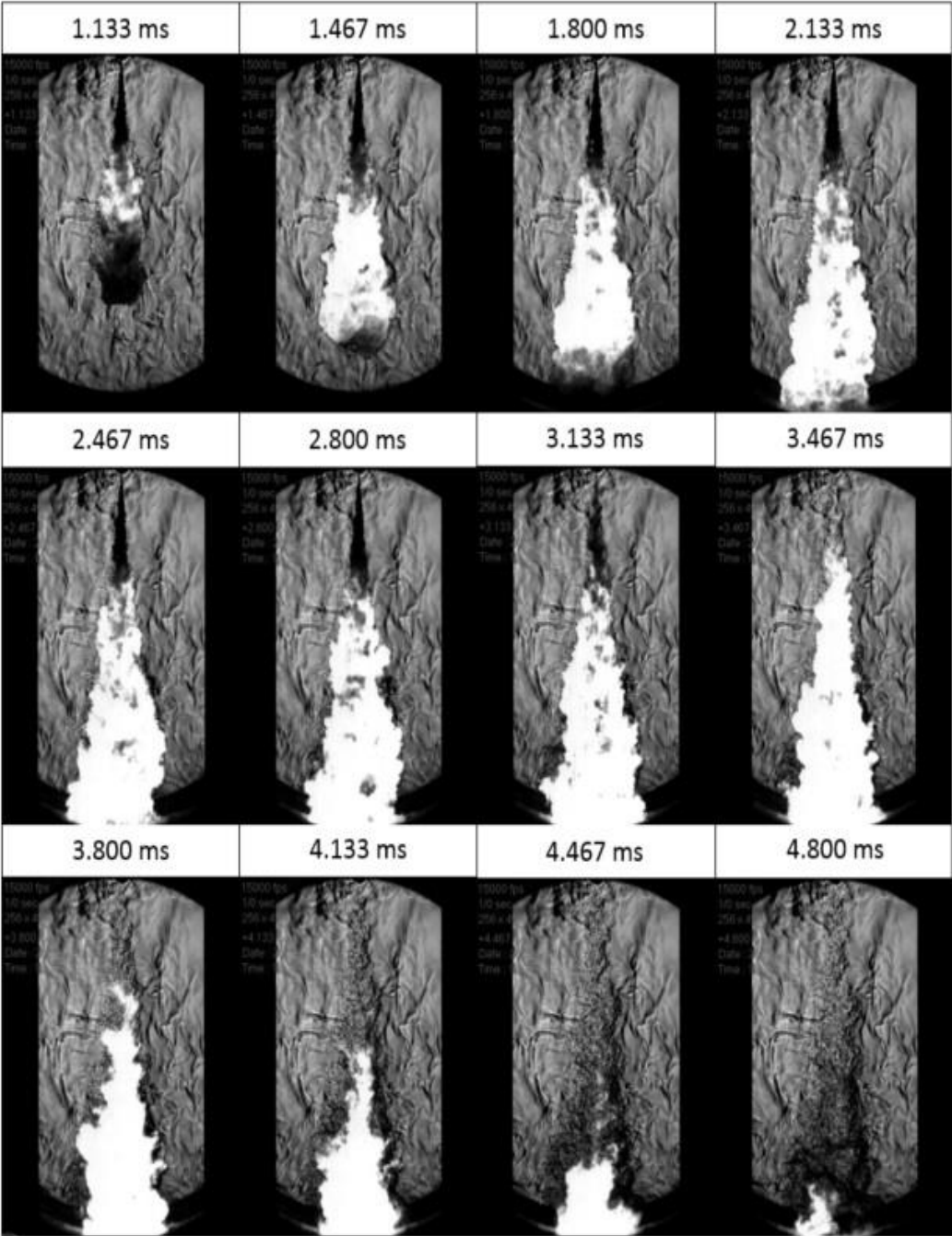
# 93/7% MGO - FAEE – 1000 Bar



# 50/50% MGO - CFO – 1000 Bar

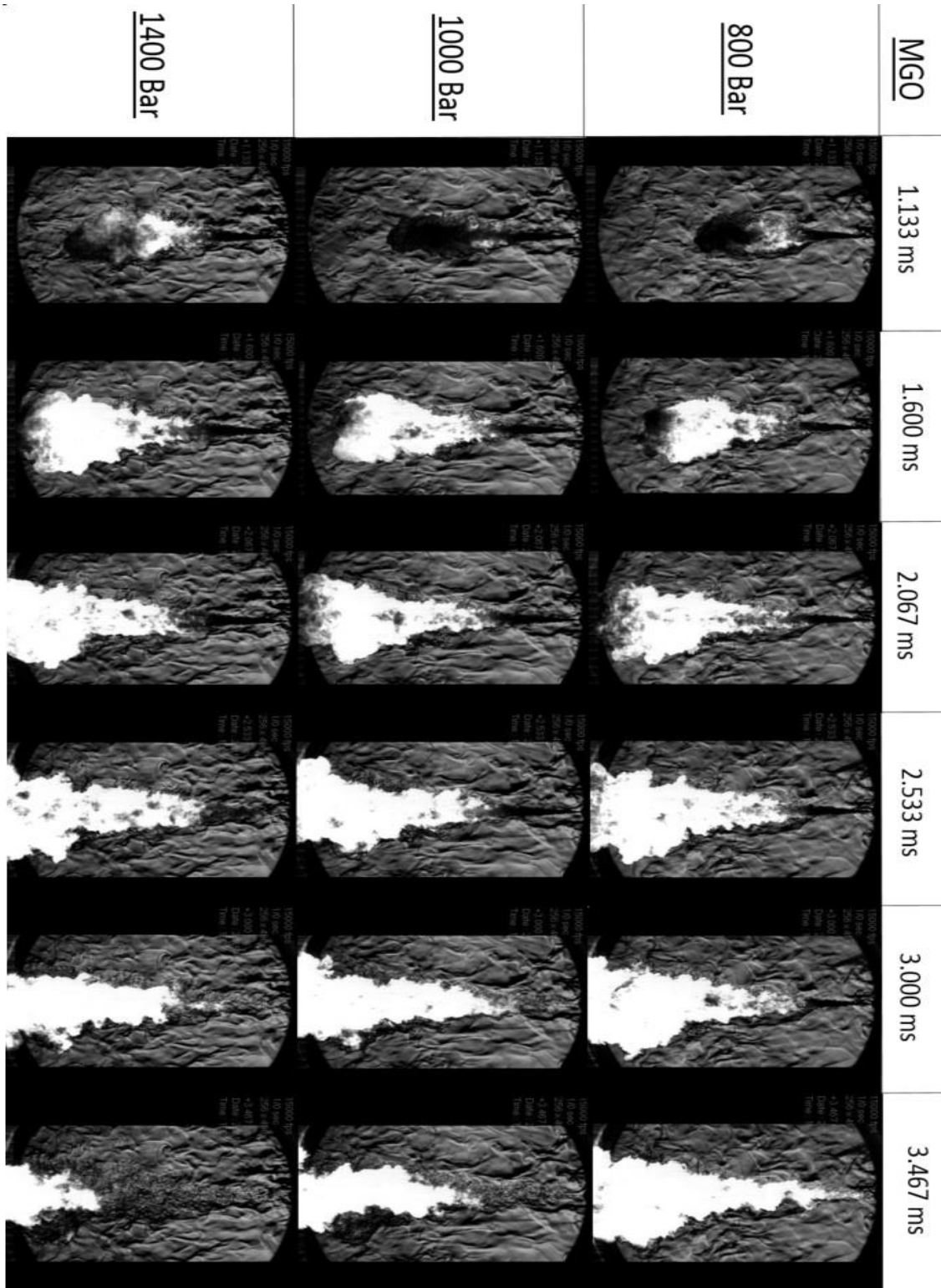


# 93/7% MGO - CFO – 1000 Bar



# Appendix E

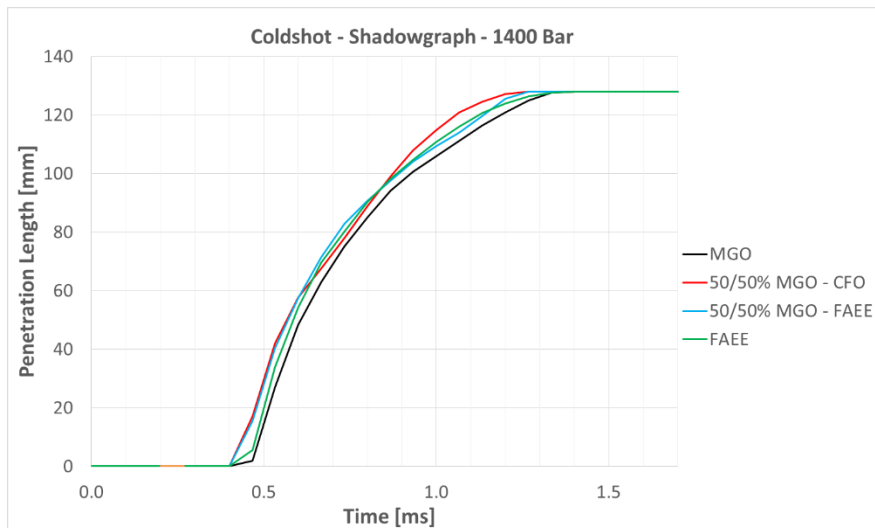
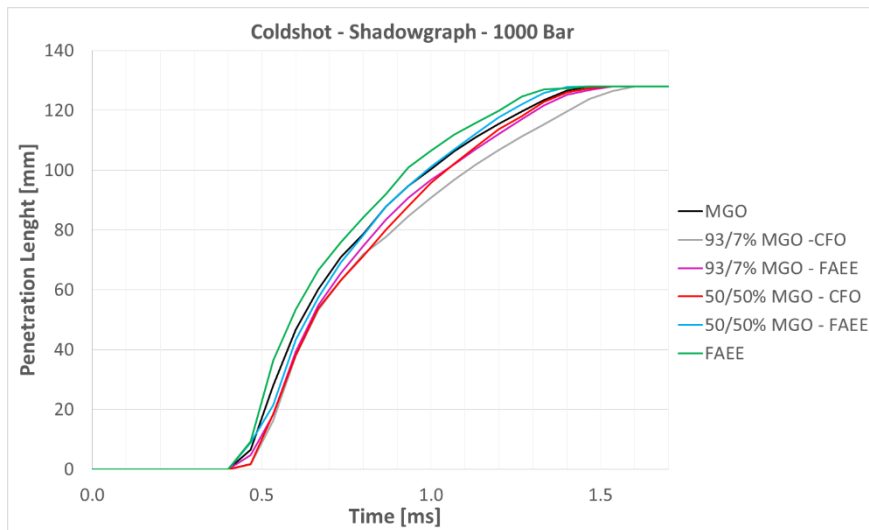
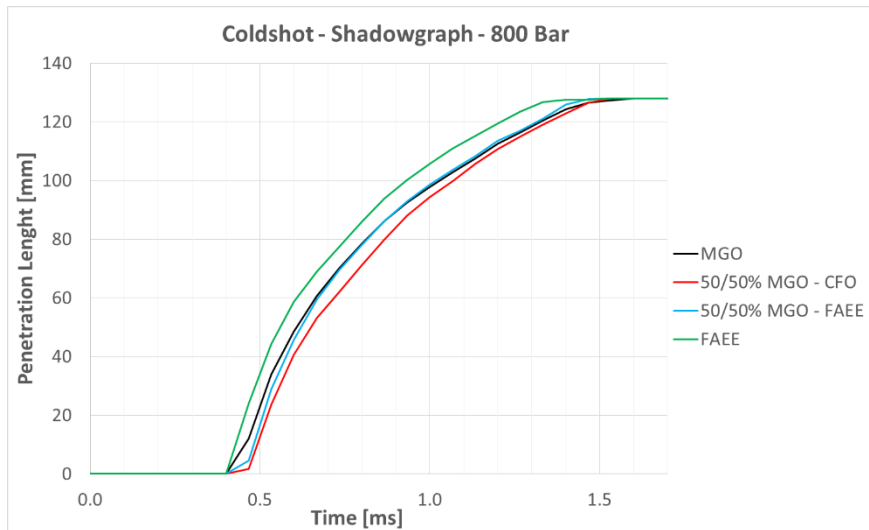
Spray Development of MGO at different injection pressures

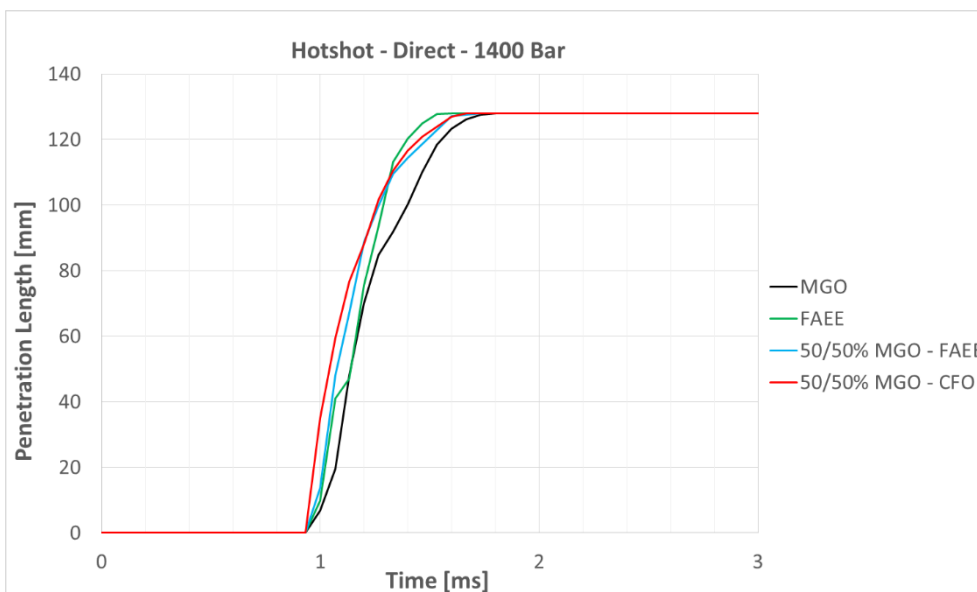
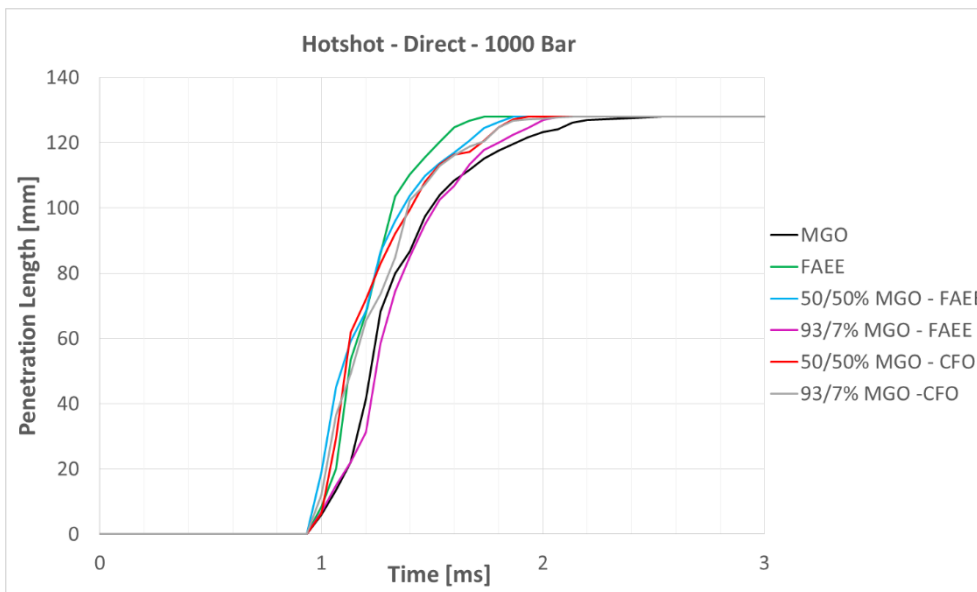
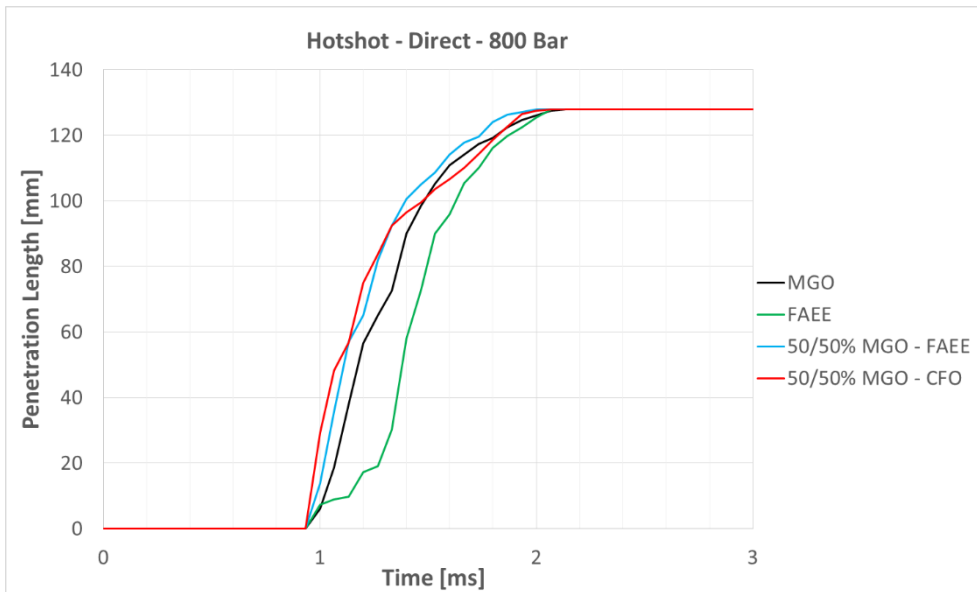


# Appendix F

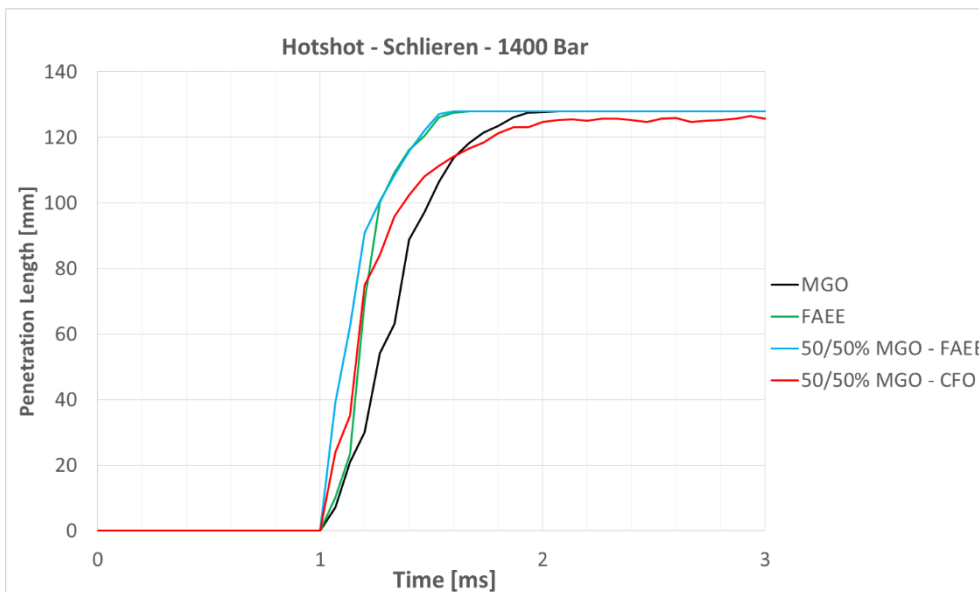
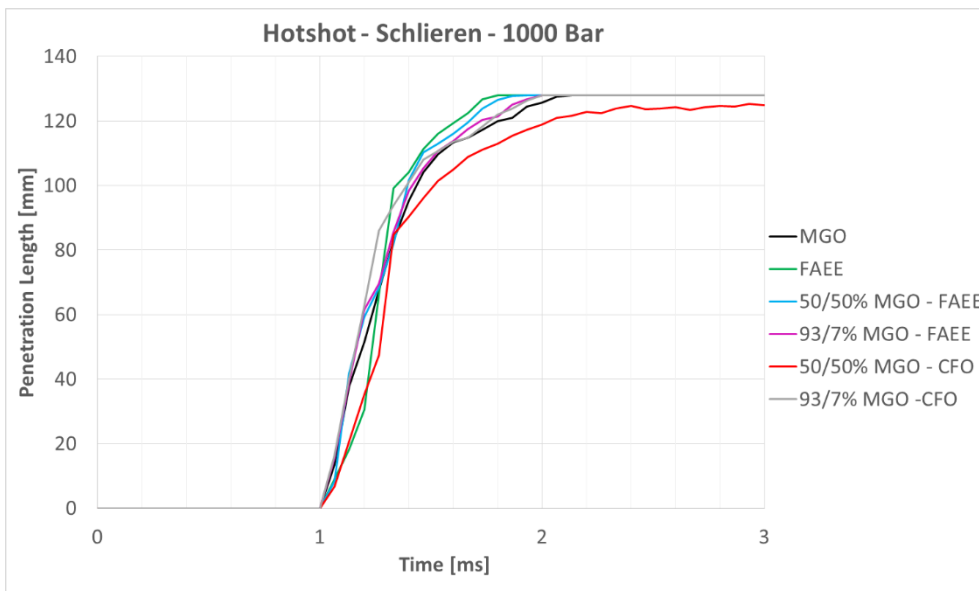
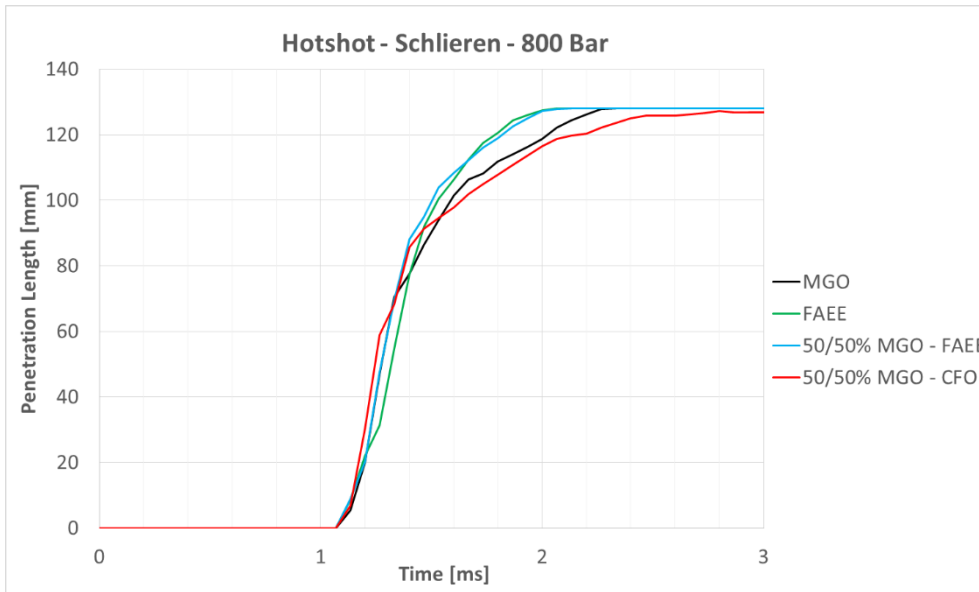
## Additional Results from Image Analysis

### Penetration Length

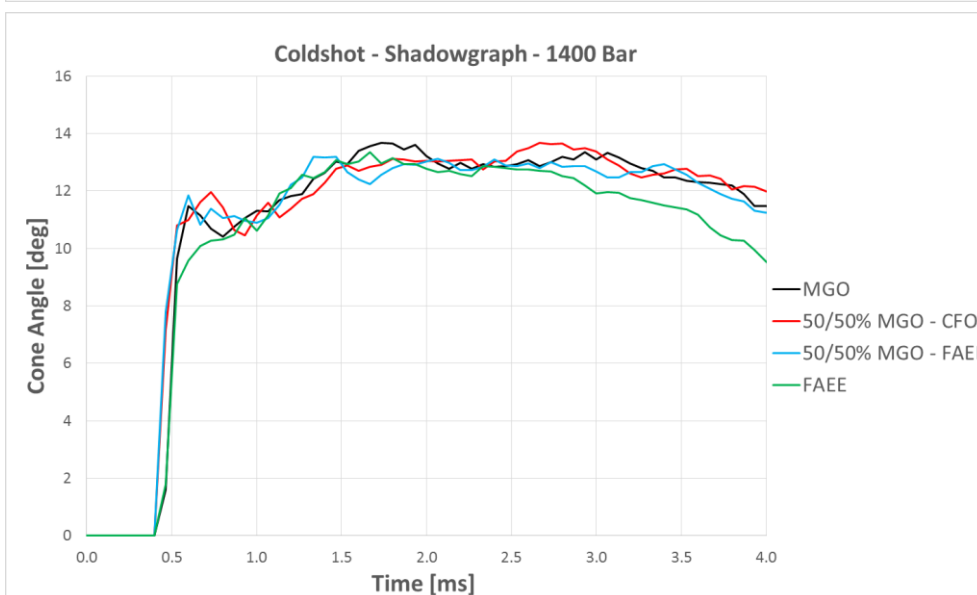
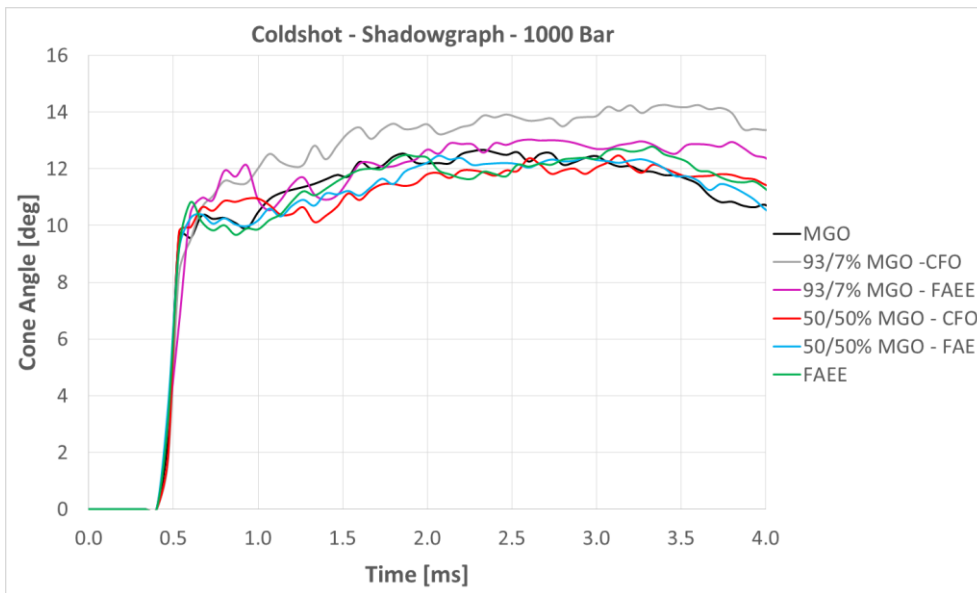
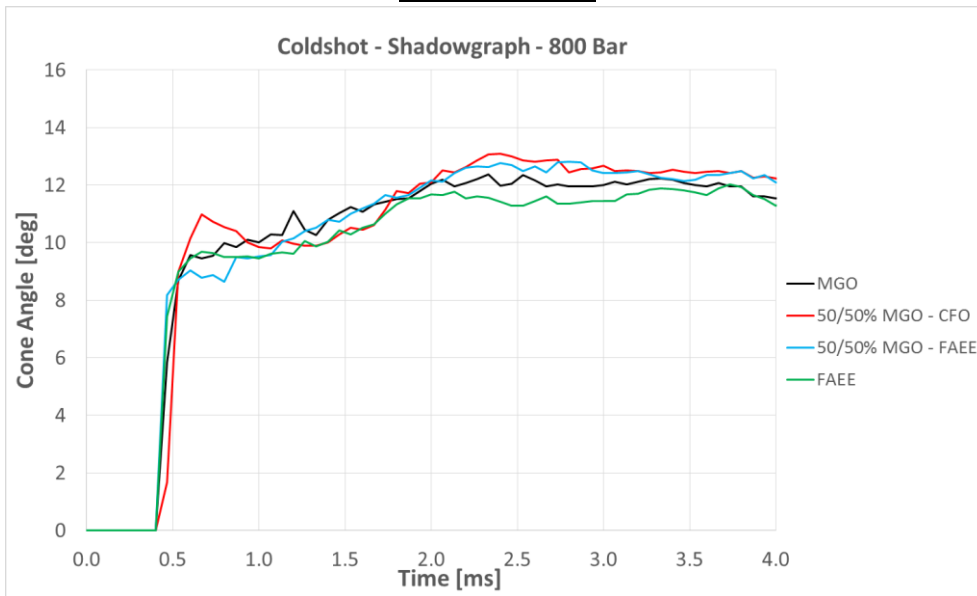


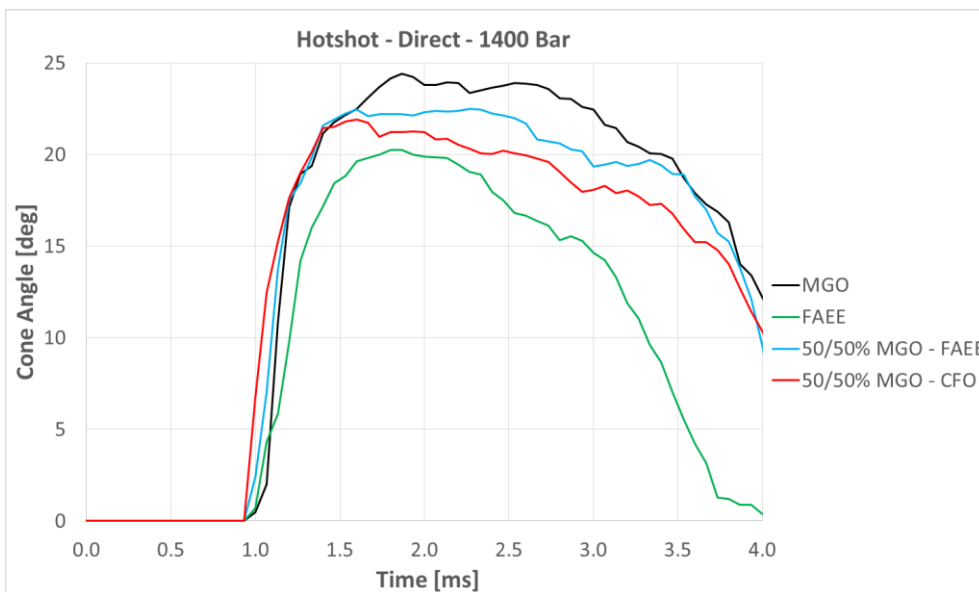
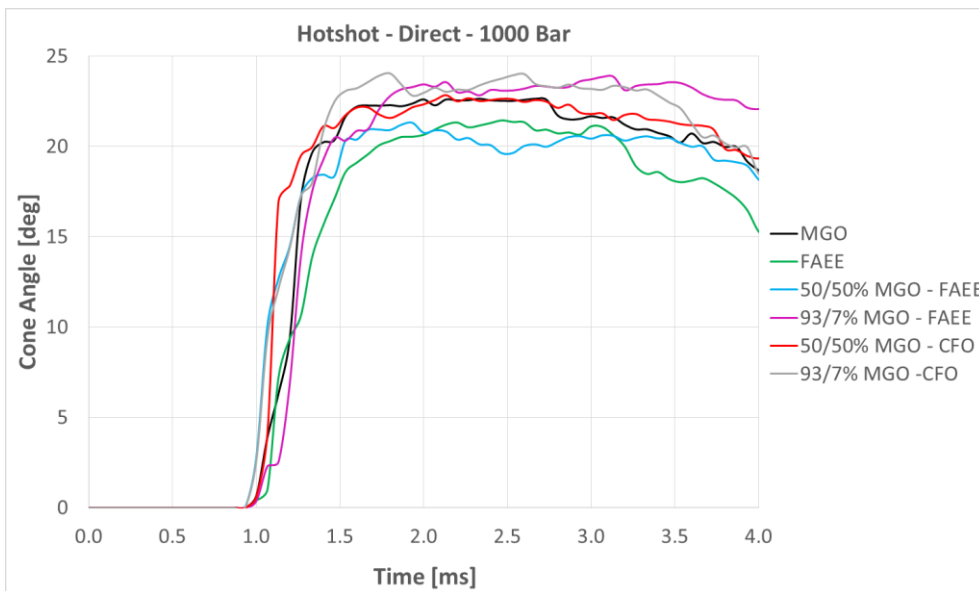
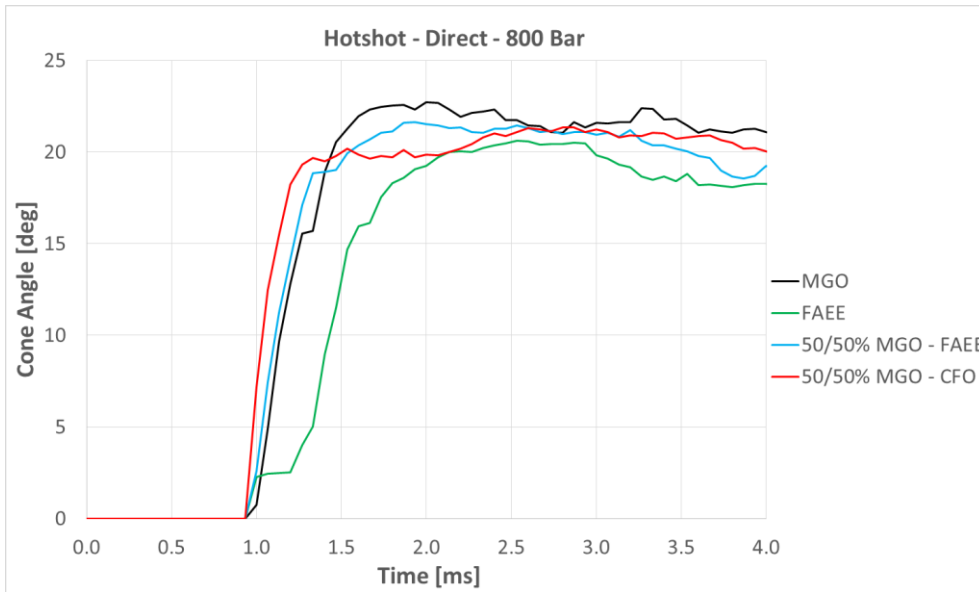


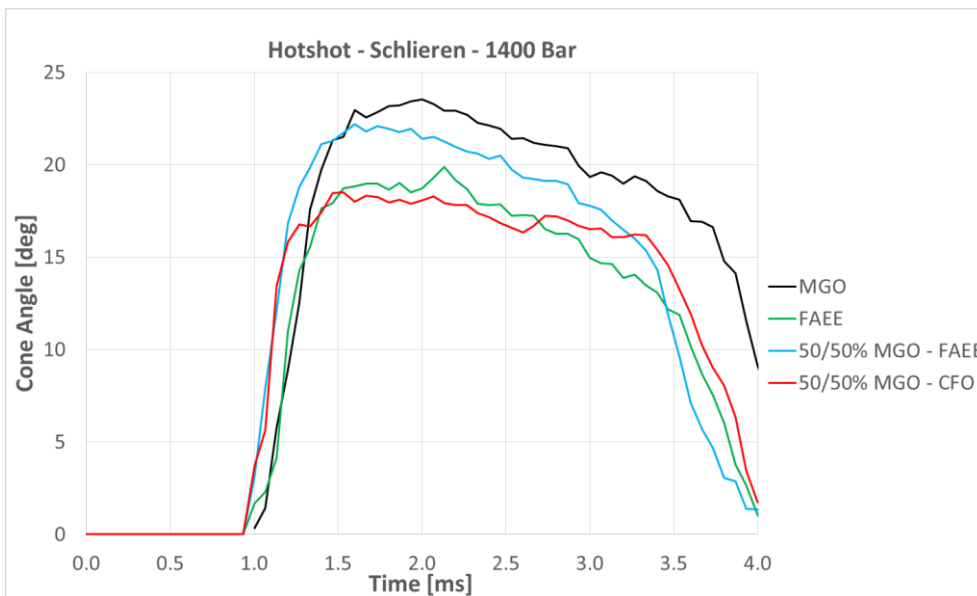
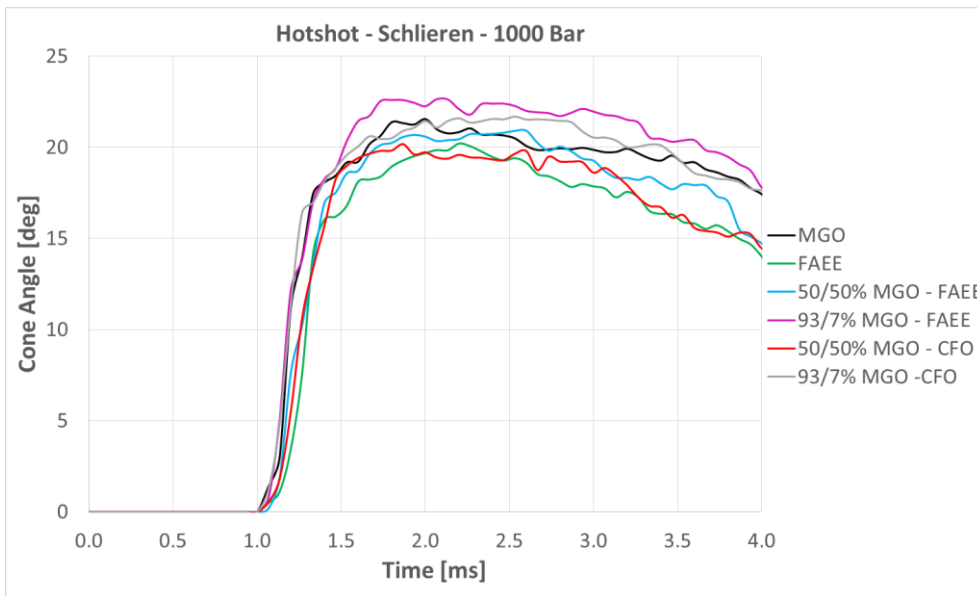
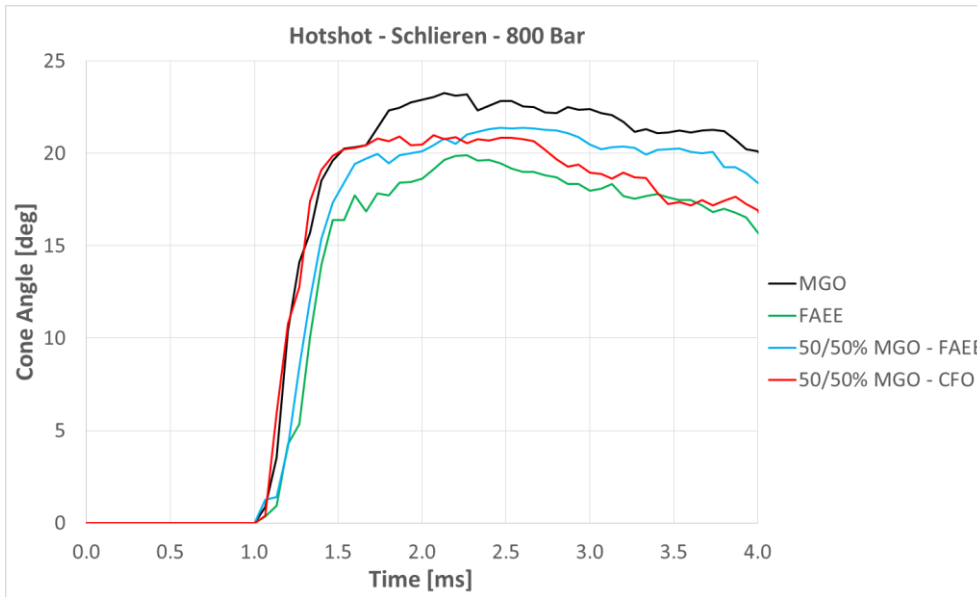




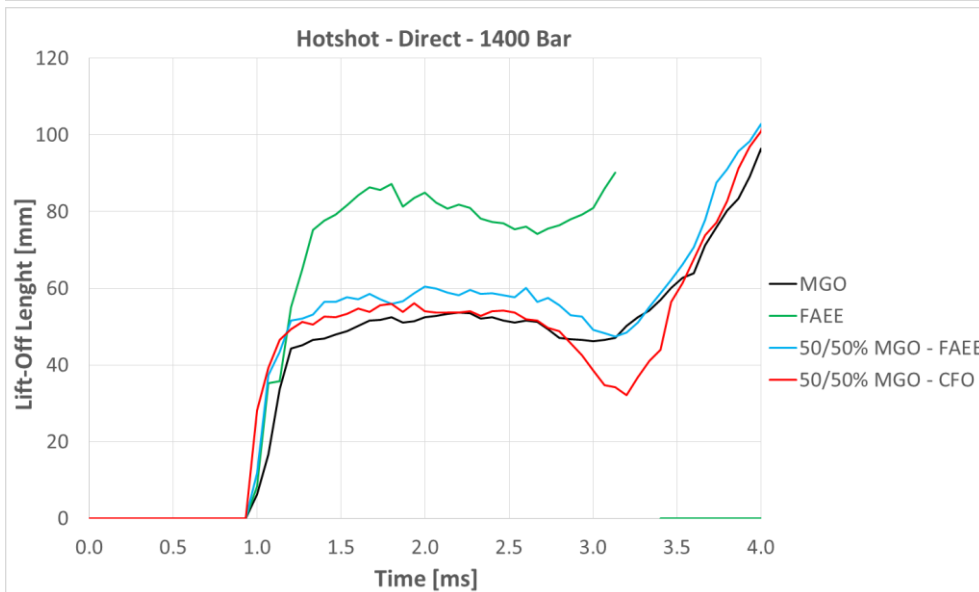
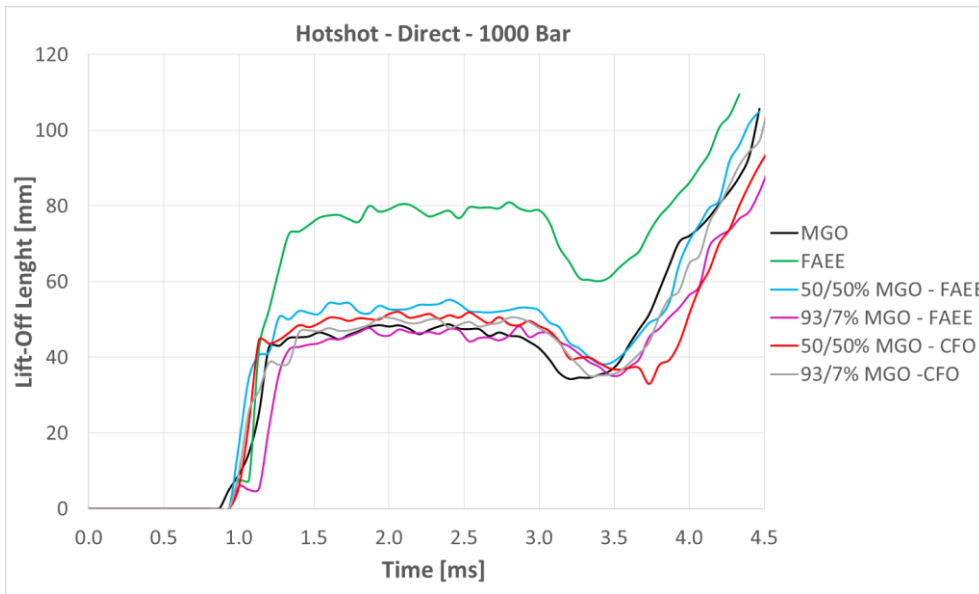
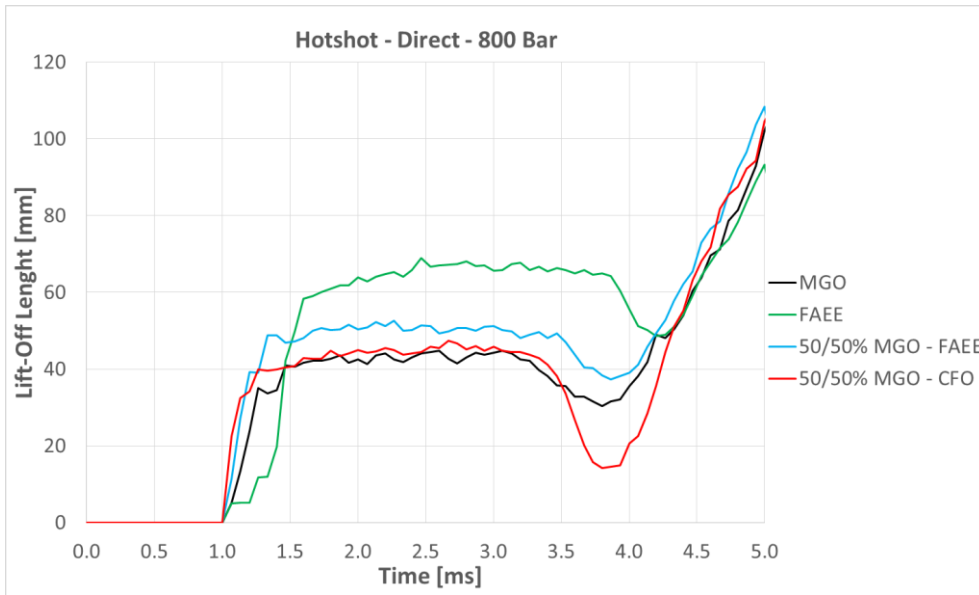
# Cone Angle

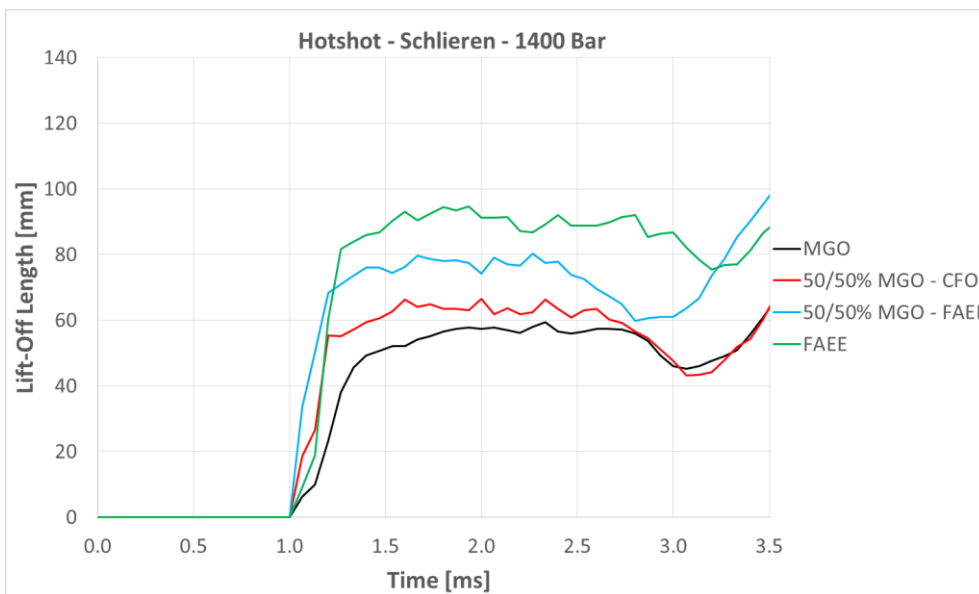
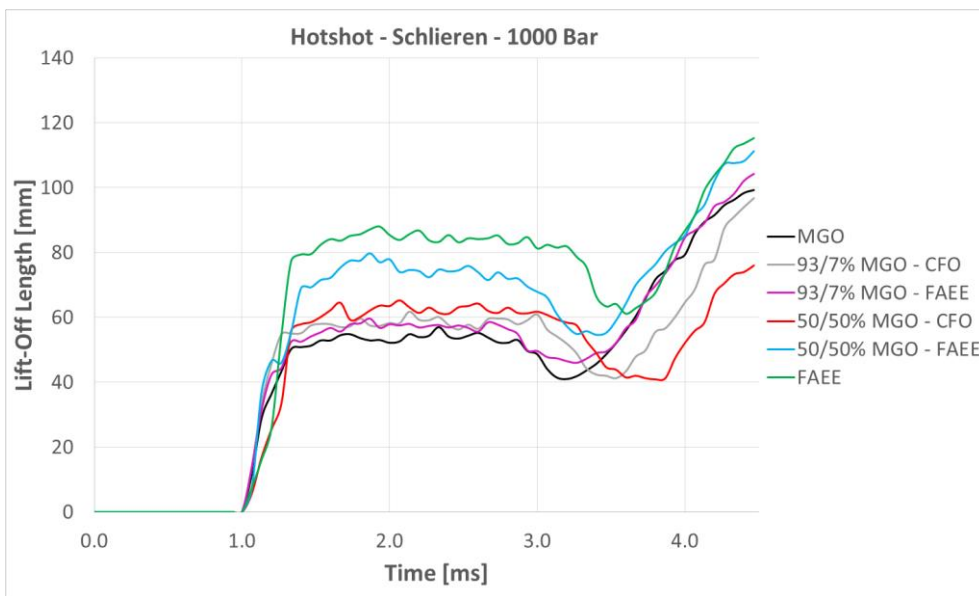
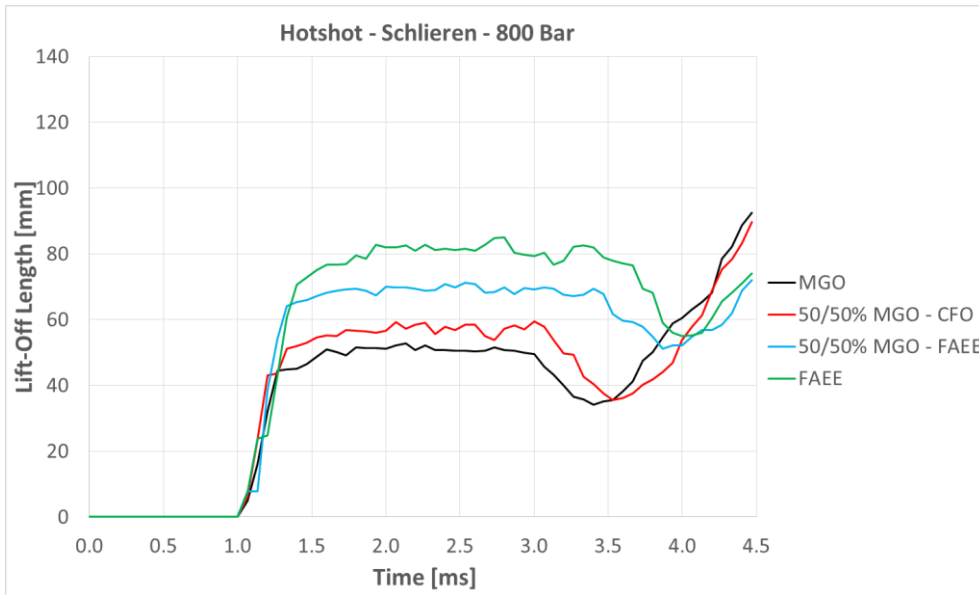






# Lift-Off Length





# Intensity

